Alma Mater Studiorum – Università di Bologna

DOTTORATO DI RICERCA IN

Meccanica e scienze avanzate dell'ingegneria

Ciclo XXXI

Settore Concorsuale: 09-C1

Settore Scientifico Disciplinare: ING-IND/08

ANALYSIS, MODELING AND CONTROL OF STANDARD AND ALTERNATIVE COMBUSTION STRATEGIES IN A DIESEL ENGINE

Presentata da: Ing. Filippo Carra

Coordinatore Dottorato	**Supervisore**
Prof. Marco Carricato	**Prof. Fabrizio Ponti**

Esame finale anno 2019

ABSTRACT

Research on compression ignited engines from combustion control point of view assumes an important role since this technology is being demonstrated lacks in the accomplishment of the evolving emissions standards to more stringent targets. The nature of combustion, in particular, seems not to be able to overcome some crucial trade-offs in emission and efficiency management. This work is aimed at investigating some key points on the way a diesel engine is conventionally run, such as noise control, nitrogen oxides modeling and closed loop methodologies to handle combustion. At the same time a great effort is spent in understanding the most important aspects of reactivity-controlled compression ignition (RCCI) combustion, which in the scenario of low temperature combustions is the one, theoretically speaking, to provide the most extended applicability throughout the engine operating field. Investigation on RCCI combustion has the main objective to offer a work-around to the previously cited trade-offs. Since literature provides several examples of how this kind of injection strategy is advantageous to the predetermined goals, this work tries to focus on how it can be controlled, because combustion stability remains the most critical issue.

CONTENTS

FIGURES INDEX

INTRODUCTION

The theme of combustion analysis applied to compression-ignited (CI) piston engines is dealt with, in the present work, in order to discuss effective algorithms and control-oriented modeling to improve engine management when run with several injection strategies. Recent years regulations are placing ordinary diesel engines in a difficult position because of their intrinsic tendency in producing pollutant species hardly manageable with an economically convenient exhaust gases aftertreatment system. Although this kind of internal combustion engine architecture is nowadays the one globally providing the best performances in terms of energy conversion efficiency, it is widely known that issues arise if exhaust pipeline emissions are taken into account. In contrast with a spark-ignited engine, where mixture characteristics allow a proper air-fuel ratio control to be able to manage efficiently a three-way catalyst, the globally lean environment existing in a diesel engine discourages nitrogen oxides (NOx) reduction reactions and makes the same solution impossible to be adopted. Moreover, while operating at high loads with an insufficient amount of air (load steps, high amount of gas recirculation), fuel oxidation may occur incompletely leading to particulate matter (PM) nucleation mode initiation, and consequently, to soot emissions. The causes of this pollutant species production have to be sought in the way combustion takes place: comparing angle resolved heat release rates between a conventional diesel engine and a gasoline one, an important difference is present in how combustion develops. Even if modern diesel engines control system allows a fine control over heat release "shape", the characteristic diffusive "tail", generally considered responsible of PM generation, is hard to be avoided without a negative impact on other undesired phenomena. In addition, self-ignition of diesel, in the small chamber areas where mixture can be considered premixed, generates local temperature peaks, which, together with the abundance of oxygen, are the responsible of NOx production according to thermal NOx formation mechanism proposed by Zel'dovich.

From the combustion control point of view, the briefly depicted scenario implies a great calibration effort because even if a modern diesel engine is plenty of control levers (both on the

fuel and air side), PM and NOx minimization are two tasks that cannot be accomplished at the same time since their formation reasons are in contrast to each other. Thus, the pollutant emission abatement is mainly demanded to the aftertreatment system, which is gaining in both complexity and cost.

This work focuses on engine-out emissions (every value reported from now on concerning experimental tests has to be interpreted as neither catalyst nor filter are present between the engine and the probe), and aims at two main objectives, synthetically reported below:

- *Investigation on unconventional injection strategies*: as a way to change combustion physics in nature, in order to overcome the typical trade-off problem between PM and NOx while keeping a CI-engine like efficiency. Particular attention is paid to how the tested combustions could be controlled.

- *Combustion remote sensing techniques*: several ways to process production engines compatible sensors signals are examined, to obtain key combustion indices leading to injection pattern optimization in terms of efficiency, pollutant and acoustic emissions.

In this context, the topics that have been faced have been numerous, since several ways a CI engine could be run have been tested. The following list provides the most relevant aspects discussed in the present thesis grouped by the specific "type of combustion" adopted:

- *Conventional diesel combustion (CDC)*:
  o noise analysis and control,
  o combustion indices based on engine speed fluctuations, on-line estimation and closed loop control,
  o engine-out NOx concentration model based on in-cylinder pressure trace.

- *Reactivity controlled compression ignition (RCCI)*:
  o experimental setup design,
  o emission and efficiency sensitivity with respect to control parameters variation,
  o closed loop combustion phase control strategies,
  o control-oriented ignition mechanism analysis.

This order in discussing the subject is maintained throughout the present work itself.

The whole activity has been carried on at the University of Bologna mechanics and propulsion laboratories, located in Forlì, where a 1.3-liter, four cylinders CI engine has been adapted to research purposes.

The first chapter describes the test cell environment to highlight engine features and how the successively discussed algorithms can be effectively be actuated.

The second chapter deals with every topic lying in the field of conventional diesel combustion sharing the objective to highlight control levers and algorithm to handle pollutant emissions, efficiency and noise radiation.

The third chapter regards a discussion on RCCI combustion as a way to combine homogenous charge advantages with compression ignition efficiency. A significant part of this section focuses on the methodologies which can be adopted to control combustion.

1. ENGINE AND TEST BED SYSTEMS

In this chapter, the test bed layout adopted for the whole activity is described, in order to clarify the environment in which the experimental data discussed in the following sections have been obtained. Every experimental facility is briefly depicted, but a more detailed presentation is provided concerning the rapid control prototyping system since it has been one of the main development areas during the whole PhD course.

The Engine

The engine used for each topic discussed in this work is a 1.3-liter multijet engine equipped with almost stock hardware in Euro V configuration. Modification concerns intake system, since an air-water intercooler has been fit, exhaust system, catalyst and DPF have been removed, and injection system as it will be shown later. Thus, no change has been performed on the shape of neither the combustion chamber nor piston. An optical encoder (180 – 2 wheel) is tightened to the fly-wheel and serves as high resolution phasing signal to both the RCP and indicating systems. Glow plugs have been substituted with four piezoelectric in-cylinder pressure sensors (AVL GH14P) through proper adaptors (AVL AG04.63). In Table 1.1, the main engine features are reported.

Displacement	1.248 liters
Architecture	L4, firing order 1-3-4-2
Maximum Power	70 kW @ 3800 rpm
Maximum Torque	200 Nm @ 1500 rpm
Compression Ratio	16.8:1
Number of valves	4 per cylinder
Injection system	Common Rail, Multijet
Intake system	Turbocharged with variable geometry turbine, HP, liquid cooled EGR

Table 1.1: Engine parameters

The injection system requires a more detailed treatment since several investigated combustion strategies required the injection of an additional fuel (gasoline). To accomplish this task, firstly, a set of port fuel injectors have been installed in the intake manifold (Figure 1.1) which favor a proper fuel brake up. Difficulties arise in controlling the amount of fuel entering into each cylinder, since the main flow, coursing from left to right in the figure, tends to increase the amount of fuel introduced in farther cylinders from the throttle body.
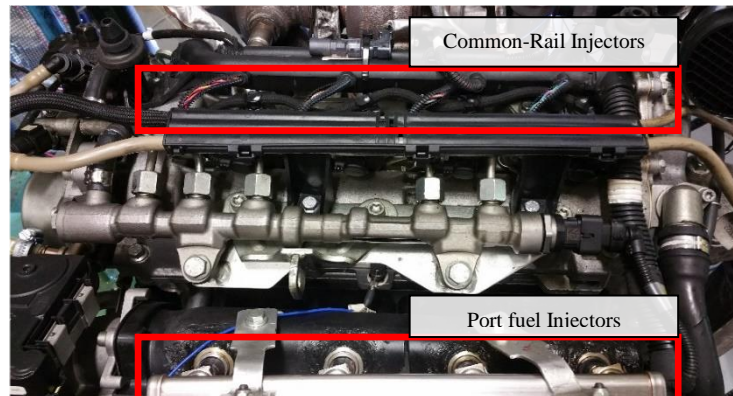
Figure 1.1: Manifold port fuel injectors installation

Secondly, to overcome this uncertainty, a component to house one more set of port injectors has been designed and carved out from aluminum. This kind of "spacer", which replicates intake runners allowing a proper connection between the runners themselves and the injectors tip, has been fit in between the intake manifold and the engine head (Figure 1.2). Such an approach obviously modifies the ducts driving air into the cylinders, but since the engine is turbocharged and it is tested in primarily steady-state conditions the effects of extending runners has been considered negligible. It has to be noticed that each cylinder is fed by two runners, for swirling purposes, having a limited cross section, thus even if the injector inclination is optimized a complete wall impingement-free behavior cannot be ensured. Moreover, the latter solution has
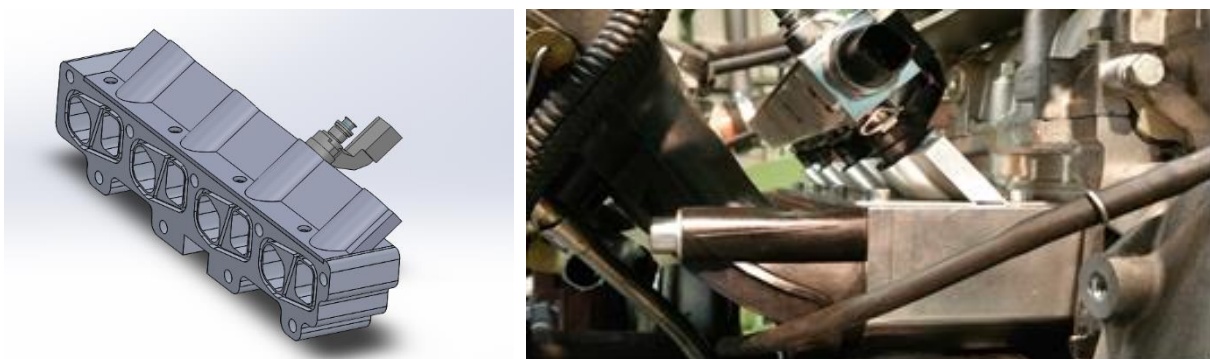
Figure 1.2: Intake runners port fuel injectors installation

16

been designed to withstand a higher rail pressure (up to 20bar) and to be compatible with either gasoline or water. Both injection systems are mounted and usable according to the specific needs.

Test bed control system

The global management of an engine test cell is usually assigned to a processing unit named "test bed control system". In our application, its tasks are mainly:

- provide signals to engine ECU in order to properly manage engine load
- remotely control eddy-current brake driving unit to set the desired engine speed
- manage engine temperature and intake air temperature by regulating the pneumatic-valves varying the cold water mass flow rate passing through the water-water heat exchanger and air-water intercooler respectively
- acquire dyno signals: torque and speed
- acquire environment conditions: pressure, temperature, humidity
- acquire signals of pressure and temperature transducers mounted on the engine: compressor intake, compressor outlet, intercooler outlet, intake manifold, exhaust manifold, turbine outlet, exhaust pipe
- acquire additional signals: rail pressure, air mass flow rate, turbo speed, …
- manage fueling system and monitor consumption by communicating with fuel balances, AVL 733s (RS-232)
- obtain information on pollutant-emission by dialoguing with a Continental NOx sensor for on-board application (CAN BUS) and AVL 415s smoke meter (RS232)
- manage power on slave ECUs
- provide logging utilities
- guarantee test bed and engine integrity by triggering recovery procedures when anomalies are detected
- provide test automation utilities.

Every listed feature is guaranteed by the hardware structure sketched in Figure 1.3 where a real-time PC serves a coordination unit for several slave chassis. Some of them, such as the FPGA unit, can be programmed in order to make it able to perform some low-level signal conditioning, filtering for instance. The software platform on which the whole structure is based, is NI-VERISTAND, which allows a reliable structure for basic functionalities such as National Instruments hardware discovery and communication, alarms and recovery procedures definition and test automation programming. At the same time, it includes the possibility to completely customize specific functions, by integrating a compiled Labview or Simulink model and linking

it to physical or virtual channels, for instance. The primary loop is set to run at 500Hz, which is also the logging frequency. Concerning the interfaces to the other systems, the test bed control system is able to interact with both the RCP and the indicating system via the same CAN-bus, and with INCA software through ASAM/ASAP protocol.
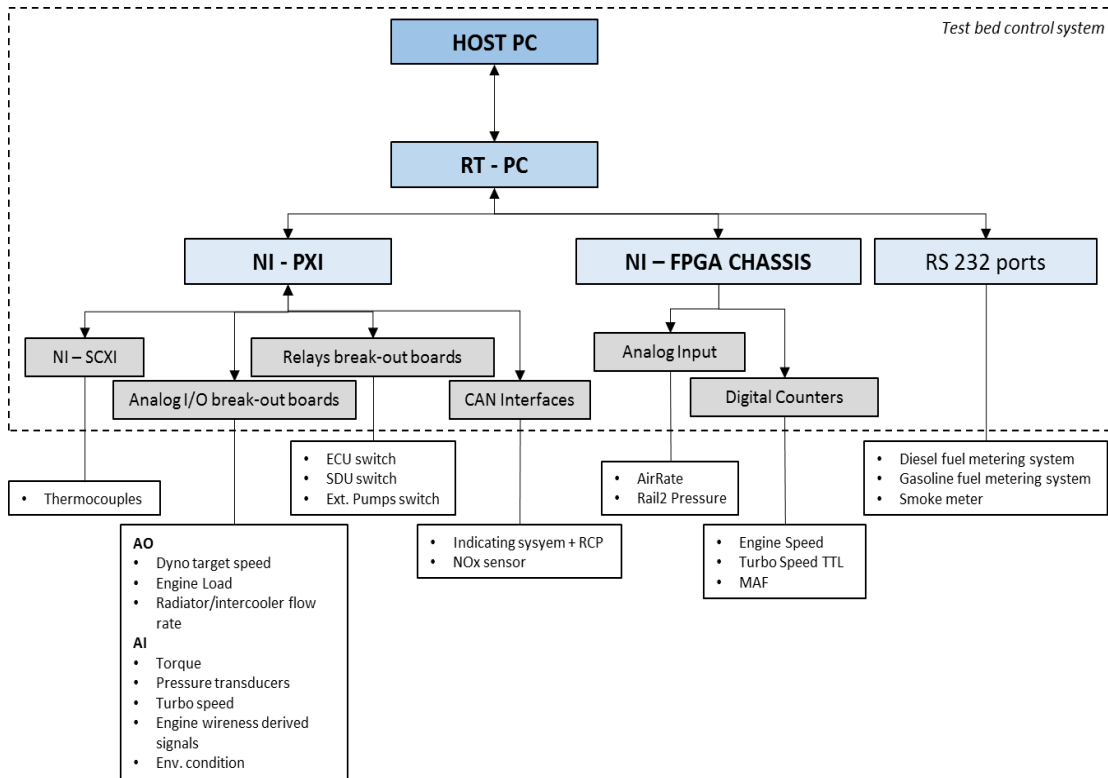
Figure 1.3: Test Bed Control System Layout

Automations are programmable via text-scripts where every channel (physical or virtual) can be read and manipulated. Scripts structure resembles ordinary scripting languages, since structures as for/while loop and conditional statements can be included.

Indicating system

In order to investigate properly the way combustion takes place and potentially set up a closed loop control, a system that real-time processes in cylinder pressure sensor signals is fundamental. During the whole experimental activity OBI (On-Board Indicating), by Alma-Automotive, has been used, together with mASTRO charge amplifier. The latter hardware includes a high cut-off frequency low pass filter (for noise attenuation purposes) and a dynamic drift compensation. For sake of completeness, it must be specified that in some cases four piezoelectric in-cylinder pressure sensors are not used, but on three cylinders, piezo-resistive BERU PSG (pressure sensor glow-plugs) have been installed. This configuration has been chosen when a detailed rate-of-heat-release (ROHR) analysis is not needed and the only requirement is to obtain consistent IMEP and

MFB50 indications, which even piezo-resistive sensors are able to guarantee. In this manner, life of more expensive piezoelectric sensors can be preserved, glow plugs functionality is available, and the behavior of production-compatible sensors is tested. Table 1.2, Figure 1.4 and Figure 1.5 illustrate the distinctive features of the adopted sensors with particular focus on how the piezoelectric sensor is fit in the glow plug slot.

	AVL GH14P	BERU PSG003
Measuring Range	0 – 250bar	0 – 200bar
Sensitivity	15 pC/bar	50 bar/V (dependent on the adopted voltage supply)
Accuracy	±0.3% Full-scale output (linearity)	±2%
Bandwidth	n.a.	0 -5 kHz
Natural Frequency	130 kHz	n.a.
Acceleration sensitivity	≤0.001 bar/g	n.a.

Table 1.2: In-cylinder pressure sensors specifications

Figure 1.4: In-cylinder pressure sensors: (a) AVL GH14P (b) BERU PSG003
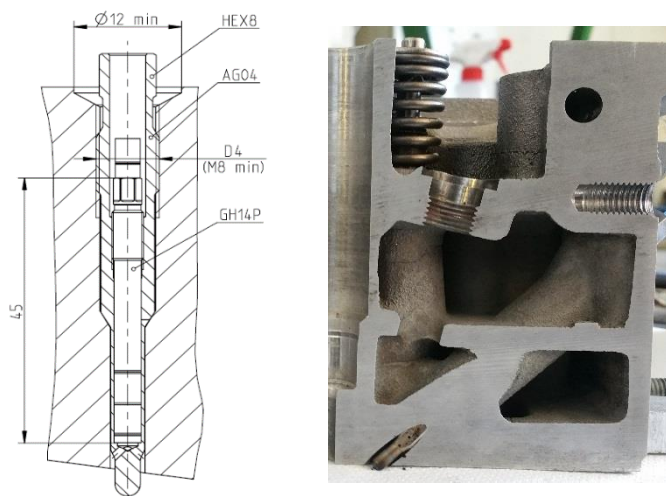
Figure 1.5: AVL GH14P installation through AG04 adaptor

The fundamental features provided by the indicating system needed for the following analysis are firstly the real-time publishing of the synthetic combustion indices (IMEP, MFB50, PPRR, MAPO, …) on CAN-bus, independently for each cylinder, allowing a next-cycle combustion control, secondly, the 200kHz time domain raw export of 12 analog input channels (4 cylinder pressures, MAP, accelerometers, microphones). Starting from the raw signal is often necessary to test several processing techniques and not to be influenced by the ordinary way to treat indicating signals.

Engine ECU

From the ECU software point of view, a specific release based on a commercial Euro V structure has been loaded with some extended features. The electronic hardware is an ordinary combination allowing the operator to monitor engine sensor measures and set calibrations through ETAS INCA software, thus a host PC is present, linked to the development engine ECU via ETK + ES modules. Regarding the extended SW capabilities, it has to be stated that every limitation present on injection pattern definition on both the start and injection dwell time has been removed in order to be able to actuate very early injection on one hand and to "squeeze" a multi-injection pattern up to 20us dwell between the injectors command on the other.

In addition, the most remarkable feature is that by setting some Boolean flags it is possible to make the ECU to completely ignore the engine control system output in terms of injectors control, providing the possibility to overwrite injection parameters through CAN communication. Nevertheless, the ECU keeps on publishing on the same CAN bus its reference actuations values. The whole list of the variables which can be read and written is reported in Table 1.3. Using this information an external ECU can understand what the standard engine control system would do when operating in a determined condition and potentially force the injection pattern independently for each cylinder. This concept is fundamental when in some following examples the engine is run by CDC on three cylinders while the fourth one is used for experimentation.

Concerning the option to override the nominal air path related actuations (mainly EGR, VGT, TVA) it is possible to operate manually on INCA user-interface. Nevertheless, for automation purposes, a work-around has been set up which make use of the communication that has been defined between the test bed control system and INCA through the ASAM/ASAP3 protocol. More in detail, every measure and calibration present on INCA experiment can be seen and written respectively by the test bed control system at a 100Hz rate, which in our case is sufficient to maintain air-quantities at their setpoints with a satisfying dynamic. This functionality is particularly useful when the engine control system does not offer a closed loop control of both the fresh air mass flow rate and boost pressure since it would not be compatible to on-vehicle

applications due to dynamic coupling effects. But in a test-cell experimental campaign aimed to understand the main effects that these variables have on combustion, it is crucial to keep every single quantity uncoupled and at its target value. All these things considered, when the automatic control is enabled, the test bed control system specifies to INCA an AirQ target and a VGT position. This choice has been made since the ECU SW privileges the AirQ closed loop control by moving the EGR valve position, thus the boost pressure is consequently adjusted by forcing a VGT position calculated by a customized PI regulator running on the TBCS RT-PC and comparing the measured manifold pressure to a user-defined target. Finally, these two fundamental targets could be mapped directly to variables coming from the RCP system via CAN-BUS in order to let it control every key parameter of engine functioning.

From ECU	To ECU
Pilot required quantity	ET main cyl1
Pre required quantity	ET main cyl2
Engine speed	ET main cyl3
Total required quantity (load)	ET main cyl4
Main injection energizing time	SOI main cyl1
Required rail pressure	SOI main cyl2
Required VGT position	SOI main cyl3
SOI main	SOI main cyl4
Air mass flow rate target	ET Pilot cyl1
Current cylinder	ET Pilot cyl2
	ET Pilot cyl3
	ET Pilot cyl4
	ET Pre cyl1
	ET Pre cyl2
	ET Pre cyl3
	ET Pre cyl4
	Rail pressure target

Table 1.3: ECU CAN database

Rapid Control Prototyping system

If the organization of every task related to the test bed functionalities and automation is managed by the test bed control system, from the engine control point of view, the whole test cell configuration is aimed to provide to the RCP system the master privileges in controlling the main actuations. As hardware platform, a National Instruments cRIO 9082 has been used. It includes a reconfigurable low-level FPGA and a real-time controller in an embedded chassis, to whom several input/output modules can be inserted. The adopted configuration is reported in Figure 1.6 where all the used features are highlighted.

RT - controller	FPGA
Control Tasks	Phasing-algorithm, signal acquisition, low level injection driving unit
	NI 9401 Digital I/O: Encoder wheel
Ethernet Connection to HOST	**NI 9862 Hi-Speed CAN:** ECU comm
RS 232 Connection with aux. balance	**NI 9464 Digital Output**: PFI injectors logic commands
	NI 9215 Analog Input: pcyl (phasing), accelerometers, microphones
	NI 9862 Hi-Speed CAN: TBCS + OBI comm

Figure 1.6: cRIO configuration

In order to clarify briefly, which are the duties demanded at every sub-structure it has to be specified that the FPGA module allows the system to be phased by processing the square wave signal coming from the optical encoder and a cylinder pressure raw signal used as cycle trigger instead of camshaft sensor. This task is fundamental for injection management for obvious reasons, but also, having a synchronized engine speed vector within the engine cycle, allows some angle resolved signal processing of both the engine speed itself and an accelerometer signal, feeding the combustion indices estimation algorithms described in the following sections.

Whereas the direct injectors drivers are located inside the standard engine ECU, port fuel injectors are managed directly by the RCP system. A digital output module is used to emulate port fuel injection commands, the logical signal is acquired by an external hardware, a smart driving unit (SDU), converting it in a power signal. It can be either low-side or peak-and-hold, depending on which set of port fuel injectors is used.

A four-channels simultaneous sampling differential analog input device is used to acquire a cylinder pressure (for phasing purposes, as stated above), and accelerometers/microphone signals. The sampling rate can be ideally set up to 100kS/s.

Finally, two high-speed CAN interfaces are present connected with two different buses: one communicating exclusively with the engine ECU and the other one interacting with the indicating system and the test bed control system. This differentiation has to be made because the two lines work at a different baud-rate and the risk of overload of the RCP to ECU bus must be avoided for safety reasons.

The global test cell interconnection diagram is reported below.
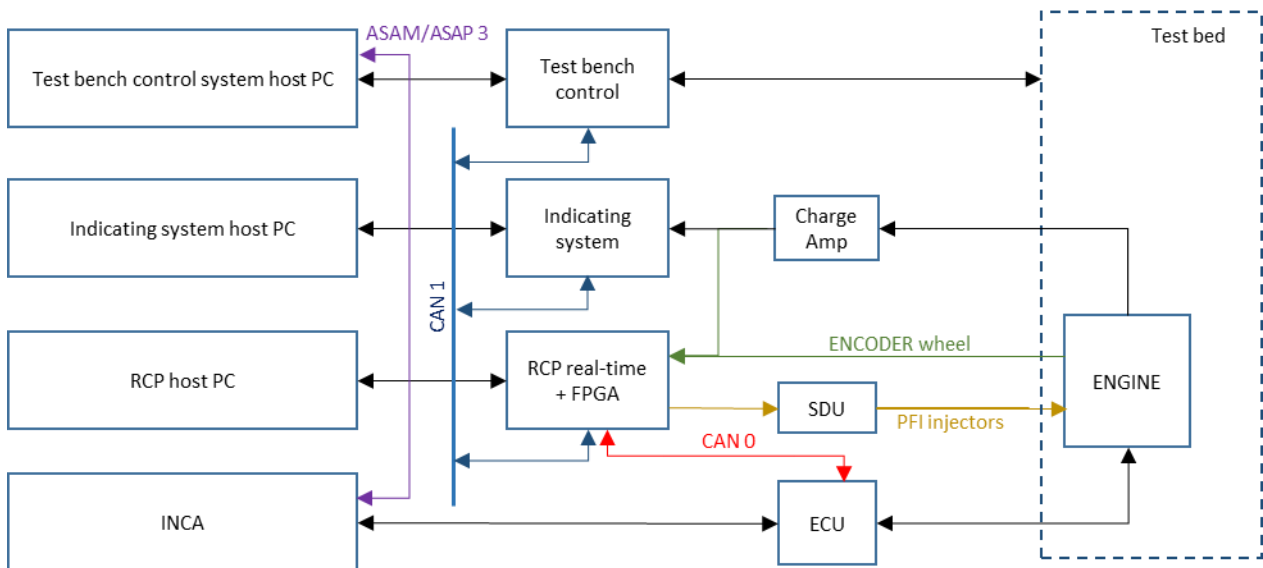
Figure 1.7: Test cell systems layout

The final thing, which is worthy to highlight in this section, is the basic structure of the code lying inside the real-time controller. Even if not any reference on the specific developed algorithms is made here it is important to depict how the different tasks communicates with each other. The whole framework is written in Labview language (since it is run on NI platform), some functions are built Simulink models imported and executed with the Model Interface Toolkit (MIT).

The key issue in making the previously described system layout work, is understand how the several sub-systems deliver and receive the information travelling throughout the network (here mainly the CAN buses) in terms of which cycle they refer to. This is because the RCP has to coordinate cycle-based data coming from three different devices: the indicating system, the engine

ECU and its own phasing unit. In the following scheme (Figure 1.8), the various loops (i.e. tasks) are sketched.
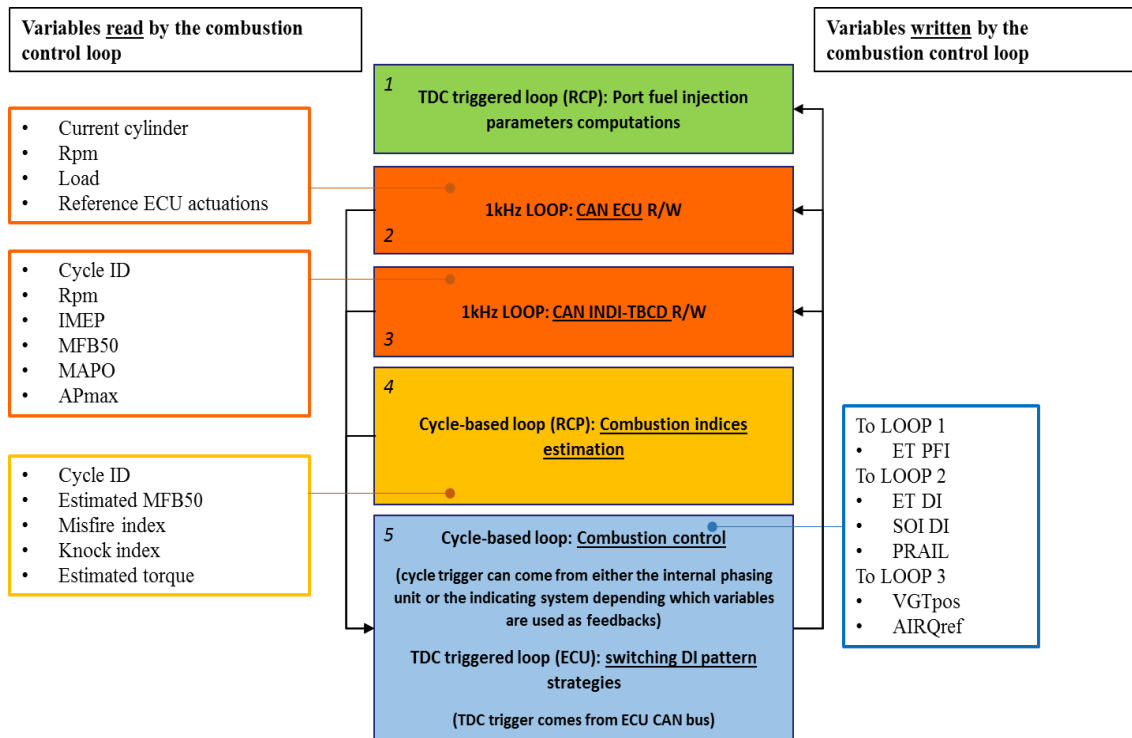
Figure 1.8: RCP RT SW structure

To summarize synthetically what the above scheme tells, the essential thing is that a master loop exists (No. 5) whose computations can be triggered by the three different phasing units according to which strategy is actuated. For instance:

- if the closed loop control is running based on the indices coming from the indicating system, then its trigger is used;
- if estimated indices are exploited, the internal phasing algorithms is used;
- if, once more, the data affecting DI injection pattern have to keep on switching between two values in two consecutive cycles it is fundamental to be sure that the variables travelling on CAN is updated as soon as its reference cylinder has ended burning;
- if mixed functioning is performed the loop has to wait that every trigger related to the used variables is detected.

CAN communications have thus to be fast enough to guarantee that not any cycle is skipped and as soon as a variable is updated it is sent to its address.

To summarize all the possible control levers used for real-time control purposes by the RCP system, Table 1.4 is included. It is fundamental to recall that every calibration which do not belong

24

to Table 1.4 can either be adjusted manually or added to the low speed variables set (compatibly with buses load).

PARAMETERS CONTROLLED DIRECTLY BY RCP SYSTEM	
TDC triggered computation	
ET PFI injectors [ms] (cyls controlled individually)	
SOI PFI injectors [degBTDC] (cyls controlled individually)	
PARAMETERS CONTROLLED THROUGH DRIVERS INCLUDED IN ECU	
High Speed CAN	**Low Speed CAN-ASAM/ASAP communication**
Direct RCP-ECU connection	Variables travel from RCP to TBCS via CAN bus, then are sent to INCA via ASAM/ASAP protocol
1ms write period	**100ms update rate**
ETmain [µs] (cyls controlled individually)	VGT position [%]
SOImain [degBTDC] (cyls controlled individually)	AirQ target [mg/str]
ETpil [µs] (cyls controlled individually)	
ETpre [µs] (cyls controlled individually)	
DI rail pressure [bar]	

Table 1.4: Control levers available for real-time combustion control

2. CONVENTIONAL DIESEL COMBUSTION

In this chapter every topic and analysis related to conventional diesel combustion are discussed. They are various in nature but shares the same objective which is an improvement in emission (acoustic and pollutant) control. Three main research categories are identified: the first one is focused on the combustion noise, being traditionally a key point of investigation in diesel engines; the second one is an application of research group previous work concerning combustion indices estimation based on fly-wheel speed fluctuations, here intended as a way to feed a closed loop combustion controller; finally an engine-out nitrogen oxides concentration model, based on in-cylinder pressure is described.

Combustion noise analysis and control

In this section, the influence that the injection pattern has on combustion noise is studied and used for control purposes. As a first step the sensitivity noise and pollutant emission demonstrate with respect to dwell time is reported at low load operating condition for both two injection patterns and three injection ones. Some interesting and unexpected aspects are highlighted. Secondly, an unconventional way in controlling noise emission is shown which is based on a "switching" pattern, aimed at keeping noise at a target value (ideally set by regulations) while maximizing efficiency by limiting the worsening effect due to pilot injections.

Noise emission sensitivity with respect to pilot injections dwell time

Modern diesel engines injection system technology allows a fine control over the injection timing, as quite close and short commands are translated in reasonably precise effective energizing time. Most of the commercial calibrations make use of a multi-injection pattern where a main injection (namely the one to deliver torque) is preceded and followed by other smaller ones. In general, every injection following the main one is performed to properly manage the aftertreatment devices, while the two or three events (pilots) happening before the main one serve as charge preconditioner [1,2,3], to mainly control the amount of fuel burning in a "premixed" way when

entering the combustion chamber during the main injection. It is well known that the premixed combustion mode in a diesel engine is the main responsible of noise radiation, here noise and pollutant emissions are correlated to the number and distance of pilot events in a low load operating condition: 2000rpm, 3bar BMEP [4].

The injection pattern is generally defined by both the energizing time associated to every event and the crank angular position at which they occur. In this work, the whole pattern is referenced to the start of main injection (SOImain) since to express the delay between the several pilot events the time passed between the end of one injection and the beginning of the successive is used (dwell time - DT). For convention, if a two-injection pattern is actuated the nomenclature adopted is Pilot + Main, if the third event is added it modifies in Pilot + Pre + Main.

Noise calculation is performed in different ways as both in-cylinder pressure sensors and a microphone facing the engine block are used. In cylinder pressure is processed as many works in literature suggest [5], which is a similar way used by some commercial devices. The raw signal is brought to the frequency domain through a Fourier transform, a specific attenuation function is applied (still in frequency domain) representing ideally the effect of the engine block, then the resulting spectrum is A-weighted to emulate human earing response and then integrated. Finally, it is normalized by the reference sound pressure level of 20uPa to provide combustion noise in dB(A). If the microphone signal is used the procedure still involves a Fourier transform over a predetermined buffer and an A-weighting function, then the resulting spectrum, squared to obtain a power, is integrated from the first Fourier harmonic to the Nyquist frequency. Once again, it is compared to the same sound pressure level to obtain dB.

The last thing to highlight before starting result discussion is how the several tests have been performed. As previously anticipated, the operating condition is kept stationary and fixed in terms of speed, load and every other parameter not affecting injection pattern definition. Then both two and three injection strategies are analyzed, where pilot injection quantity target is 1.5mm^3/str for both Pilot and Pre. For the first investigated pattern (2 injections), a dwell time sweep is done, and the optimal value is found according to criteria involving the amount of emitted noise. Successively, this value is maintained constant and the third injection is introduced, again a Pilot-Pre dwell-time sweep is actuated recording noise and pollutant species behavior. Finally, the two obtained best points are compared with the reference calibration. A quite relevant issue while varying the injections distance is the effect on the effectively injected quantity if the energizing time is kept fixed, that because of the rail pressure instantaneous value which is affected by non-negligible oscillations when the injectors stem closes (pressure waves). To overcome this problem, a closed loop combustion controller has been programmed in the RCP control loop aiming at keeping constant the delivered torque (IMEP) and combustion phase (MFB50) adjusting main injection ET and SOI. This is done because it can be assumed that if the combustion

efficiency is function of the MFB50, then it is possible to state that equal MFB50 means equal efficiency, and if it is maintained constant, the same torque means the same injected mass.

The latter expression could be in a way "forced", thus it has been verified using the fuel metering system as shown in the following figures. Two tests are reported: in Figure 2.1 the closed loop controller is deactivated and the consumption is measured, in Figure 2.2 it is shown how the closed loop controller behaves when dwell time is moved in order to keep IMEP and MFB50 at their target values 4bar and 9degATDC respectively. It is clear how the curve representing consumption and the one showing the ETmain the closed loop controller actuates are mirrored.
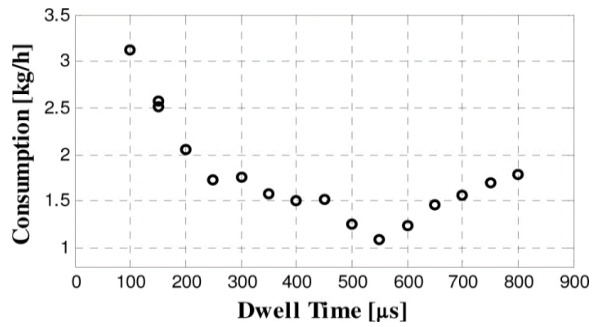
Figure 2.1: Fuel consumption vs dwell time (Pilot+Main pattern) – Closed loop control inactive
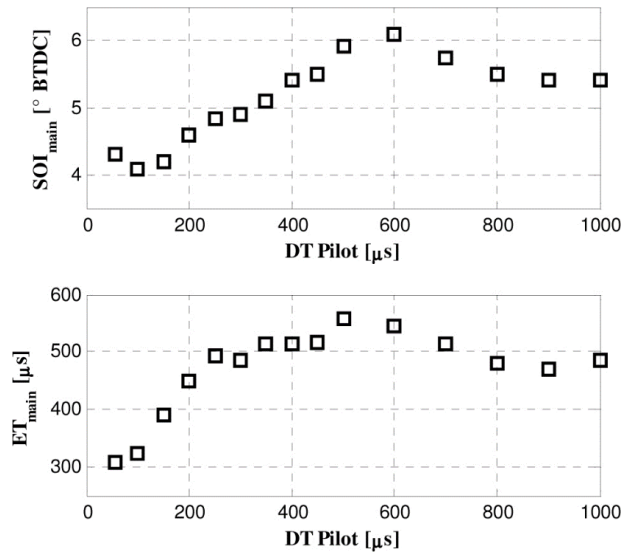
Figure 2.2: Closed loop effect on Main injection parameters to keep IMEP and MFB50 at their target values

This kind of considerations can be done only if a two-injection pattern is adopted, because, if a third injection is present, another degree of freedom appears, being the uncertainty in the Pre injection. When operating in this condition the closed loop has been still kept active to adjust main injection parameters, while the Pre energizing time is actuated on the basis of previously

learnt look-up table. The learning procedure has been possible since it has been based once again on a two injections pattern.

Figure 2.3 reports the actuated injection pattern when three injections are present. It is just useful to recall that when a three-injections pattern is actuated, the Pre-Main dwell is kept at its optimal value determined in the two-injections sweep.
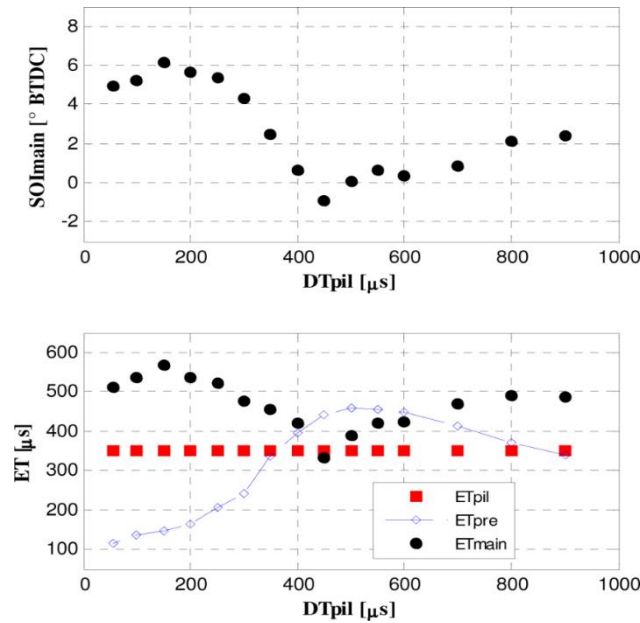
Figure 2.3: SOImain and ET of the three injection to IMEP and MFB50 at their target values

The closed-loop combustion controller is, in this case, constituted by two PIDs regulators working in parallel adjusting the ECU reference actuations related to the main injection (SOImain, ETmain), taken as feed forward contributions. One PID corrects SOImain according to the difference that exists between the measured MFB50 and the target one, the other one varies ETmain to match a target IMEP value. This simple structure is 4-times replicated to control each cylinder independently. The two PIDs can work in parallel in reasonably satisfying way because the cross dependencies are weak in this engine. Torque is very poorly influenced by the combustion phase if the latter value is kept in an ordinary range and the energizing time affects MFB50 just because the more fuel is injected, the more heat is released and the position at which it is half burnt retards. According to these considerations, when a step is performed on the target value of one (or both) the regulators, the path to reach the desired condition cannot be optimal, but it is close to, and the simplicity of the depicted structure, makes it robust (Figure 2.4).
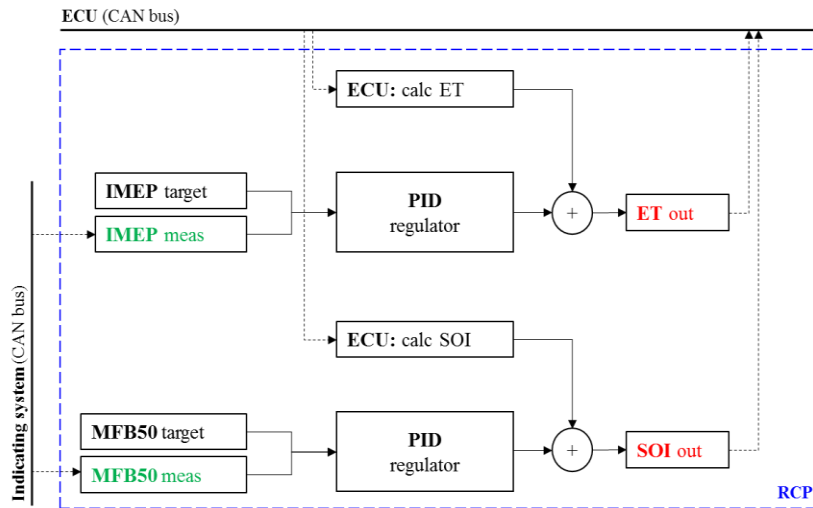
Figure 2.4: Closed loop controller

Moving to results analysis, the influence the distance between the injections has on the acoustic emissions is firstly reported (Figure 2.5) when adopting a two events pattern.
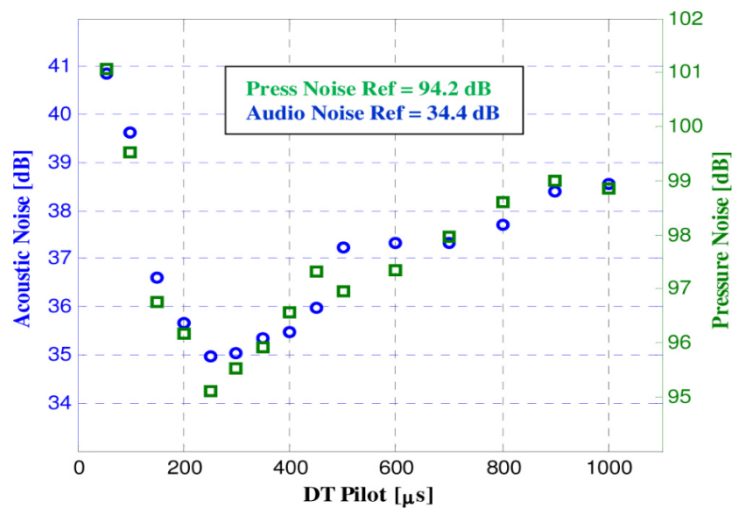
Figure 2.5: Combustion noise vs Pilot dwell (2-injections pattern)

In the above figures, the blue dots represent the combustion noise computed using the in-cylinder pressure signal as described before, while the green ones denote the same quantity obtained from the microphone signal. It can be noticed that both ways agree. The legend reports the values acquired when operating the engine adopting the base calibration, that is to say three injections are present separated by approximately 800us dwell. The graph shows, though, that if the events are kept closer to each other (250us dwell time) in a two injections pattern the cost that has to be paid to the reference noise value is minimal, but with one injection less and all the implications it has on the pollutant emissions, shown below (Figure 2.6).

Nitrogen oxides and FSN behavior while dwell time is varied is reported, all values are normalized with respect to the base calibration measure. Theoretically speaking, making the rate
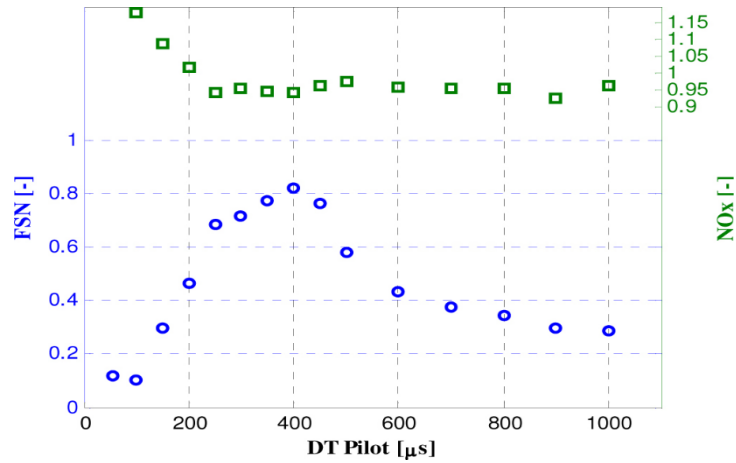
Figure 2.6: FSN and NOx vs dwell time (2-injections pattern), normalized with respect to base calibration value

of heat release gentler should decrease the amount of emitted noise while encouraging the soot formation, this trend is confirmed, taking into account that the FSN measure can be affected by precision error when low load conditions are examined. Nevertheless, it has to be noticed that saving an injection is always better from the FSN point of view. NOx seem to be hardly affected by dwell time, with exception of the extreme left region in the figures: very close injection command leads to a dramatic increase of this kind of pollutant specie. It is also worthy to notice how ETmain behaves when dwell time is moved toward values smaller than 250us: the linear decreasing tendency suggests that the injectors are not able to reflect electrical commands in actual opening/closing actions. In particular, in this case, the injector does not manage to close properly within the dwell time, reducing the zero-offset time of the main injection. The better performances in terms of radiated noise occur just before this condition is reached.
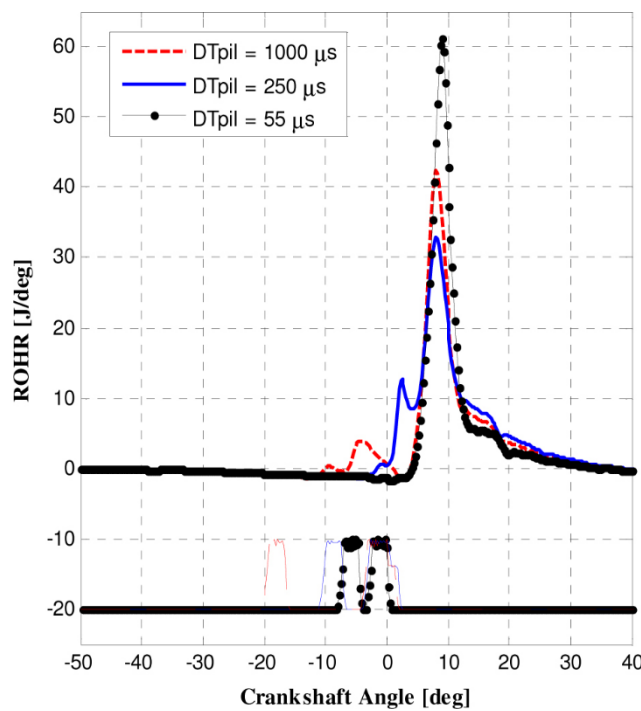
Figure 2.7: ROHR at different dwell time (2-injections pattern)

32

To complete the analysis of the two injections pattern, relevant heat-release curves are shown (Figure 2.7), averaged over 150 cycles.

Figure 2.7 confirms the correlation existing between the shape of rate of heat release and emitted noise and pollutant species. Here, once again it has to be noticed that the peak of the ROHR curve can be reduced by actuating closer injection commands until the point in which the two injections begin to "fuse" with each other.

The last step of the analysis concerning dwell time influence on emissions is a similar discussion with respect to the one just reported, where a two injections pattern is adopted, but moving to a three-injections one. The middle event (Pre) is kept at the optimal distance to the main one according to the previously shown results: 250us dwell-time. The first injection (Pil) is then progressively brought near Pre, starting from 950us dwell-time and ending up to 55us. Result are sketched in the following figures (Figure 2.8, Figure 2.9).
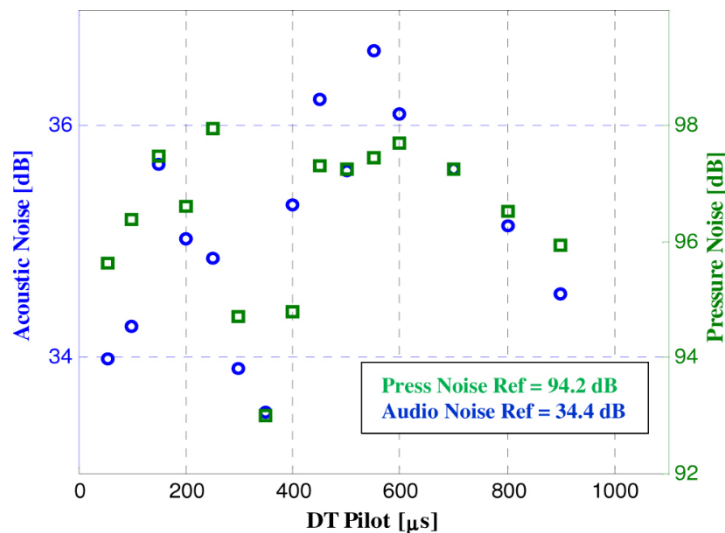
Figure 2.8: Combustion noise vs Pilot dwell (3-injections pattern)
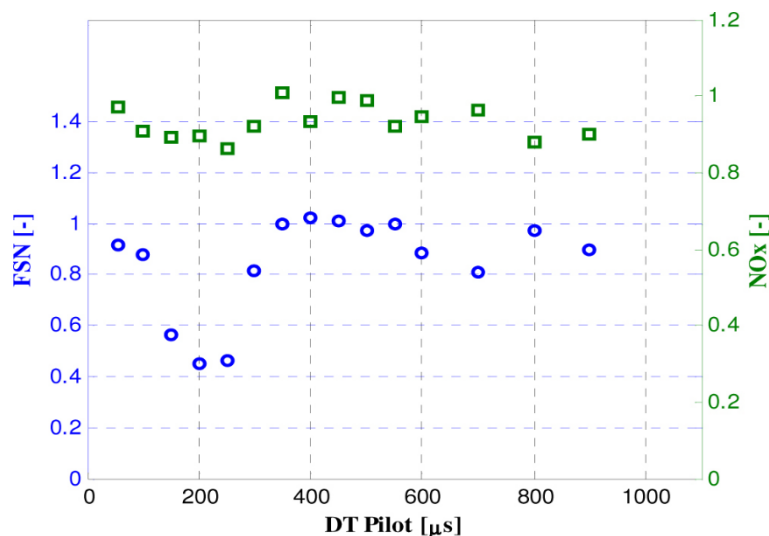
Figure 2.9: FSN and NOx vs dwell time (3-injections pattern), normalized
with respect to base calibration value

Some considerations made for the previous case can be further applied, such as the presence of an optimal DTpilot where acoustic emissions are minimized (350us), this effect is put in evidence by both the microphone and in-cylinder pressure signals. Moreover, the influence on NOx is once again found to be minimal. On the contrary, some differences due to the mutual injections interactions are present: when Pilot approaches Pre, no increase on either acoustic or NOx emission is observed, that because it is like to actuate a single Pilot injection providing the sum of Pilot + Pre amount of fuel, but Main injection remains unaffected. Finally, a drop on measured FSN is found at DTpilot equal to 200-250us. Best point is chosen where radiated noise is found to be minimal.

In Figure 2.10 the optimal identified conditions are compared to the standard base calibration.
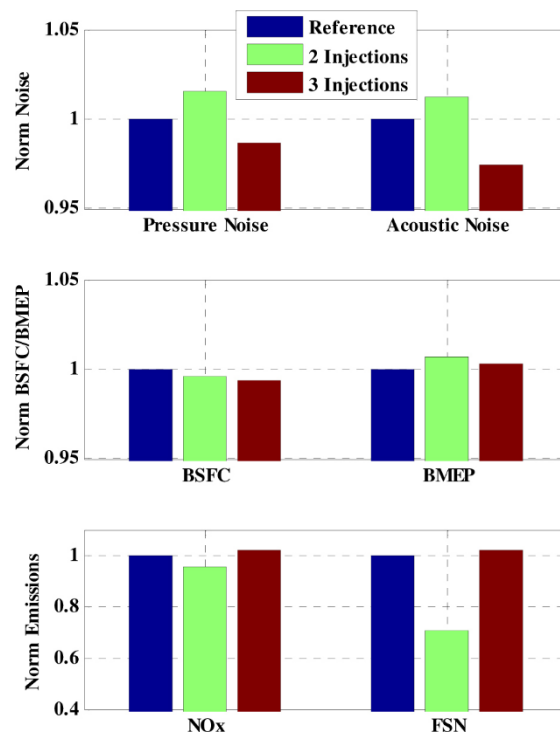
Figure 2.10: Best points comparison

In both cases, when operating in low-load condition, making the injections closer to each other seems to be worthy. If a Pil + Main pattern is adopted a little worsening effect is paid to the noise emission, but a huge gain is observed on FSN. If a three injections pattern is alternatively used, pollutant emissions are maintained almost constant while an advantage on noise is detected. Both the investigated strategies have also shown a slight improvement on the measured brake efficiency. The activity on this thematic area has finally shown how the rate of heat release can be modified by just varying injection dwell-time, the optimal condition for a two-injections pattern has found to be just before the (solenoid) injectors cannot behave as they are commanded. Investigation would be necessary when more technologically advanced components are used (piezo-injectors, for instance).

Closed-Loop combustion noise control strategy

A different approach is discussed in this section, aimed at a diesel-engine combustion noise control. Several examples are present in literature where both feed-forward and closed loop structures are used to handle noise radiation [6,7,8]. The proposed procedure is based on an on-line processing of a microphone signal in order to meet a target emitted radiation. Such a methodology finds its application if noise abatement limits engine performances when an ordinary open-loop strategy is applied. Assuming that, in order to make noise regulations compliant, a three injections pattern is used in most of the engine operating field, theoretically speaking, it could worsen combustion efficiency since a well-known trade-off arises: concentrating the delivered heat in a single event is thermodynamically better as soon as the increased wall heat losses make the exploitable energy lower. Moreover, since noise is highly correlated with diesel characteristic pollutant emissions when the injection pattern is varied, an efficient control on it makes possible to move consciously along the PM and NOx trade-off. The proposed algorithm makes use of a so-called "switching pattern", which means that the injection pattern changes on a single combustion basis, regardless of which cylinder is burning. A matrix is then used as calibration data in order to manage which is combustions succession. To clarify this aspect, Table 2.1 is reported below.

Lev1	0	0	0	0	0	0	0
Lev2	1	0	0	0	0	0	0
Lev3	1	0	0	1	0	0	0
Lev4	1	0	1	0	0	1	0
Lev5	1	0	1	0	1	0	1
Lev6	1	1	0	1	1	0	1
Lev7	1	1	1	0	1	1	1
Lev8	1	1	1	1	1	1	1

Table 2.1: Matrix defining combustion succession

The values present inside Table 2.1 represent which injection pattern has to be actuated, for instance, with "0" a Pilot + Pre + Main pattern can be identified, while "1" could be, symbolically, a main-only pattern. These two ways of performing fuel injection have to be calibrated in order to deliver the same torque, but, from the emitted noise point of view they are quite different since a single injection pattern namely produces a more impulsive combustion. Thus, each row of the table defines an average level of combustion noise. The differences in the way combustion takes place adopting the described injection patterns is shown in Figure 2.11 by means of in-cylinder pressure and ROHR curves in a low load condition.

As it can be noticed, the values inside the reported table are chosen to maximize switching frequency and not to actuate the same pattern on a determined cylinder in order to better "filter" the emitted oscillating noise, for this reason the switching combustions basis has been set to seven.
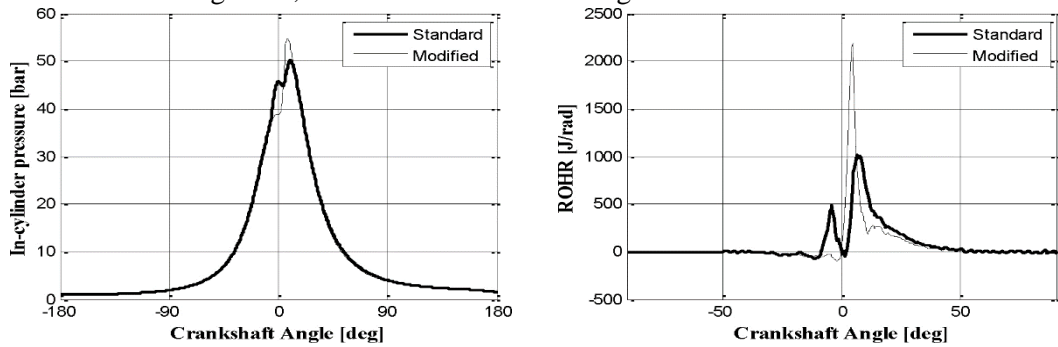
Figure 2.11: In-cylinder pressure and ROHR comparison between a three injections pattern (standard) and a single injection one (modified)

Figure 2.12 shows how Table 2.1 is translated to actuations, as the single injection pattern can be recognized through a steeper in-chamber pressure curve. With "levels" the fraction of type "1" combustions over the defined buffer is identified.

As anticipated before, the effect injection pattern has on both noise and pollutant emissions is
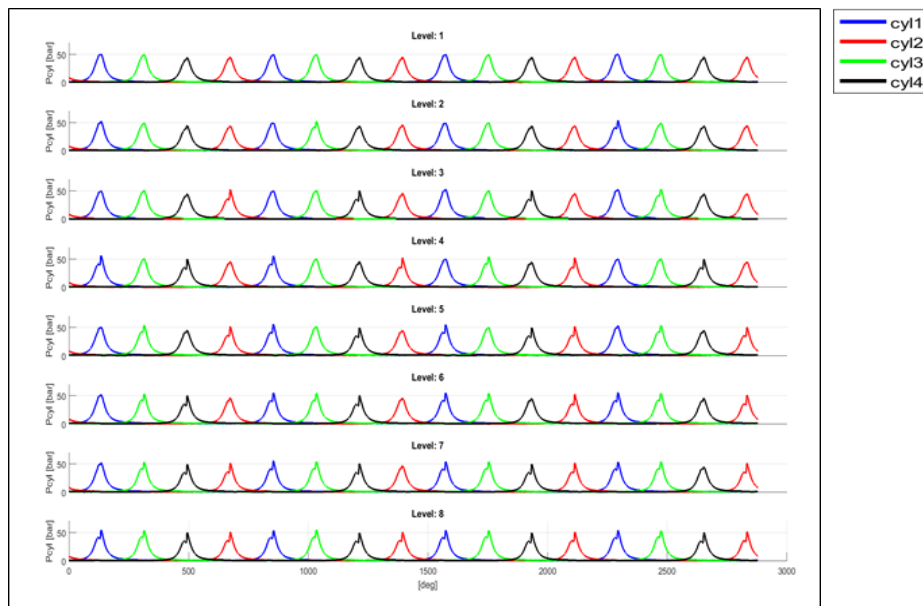
Figure 2.12: Combustion sequences

relevant. A single injection pattern is expected to be better than a three injections one concerning PM emission (higher temperature and ROHR peak imply a more complete fuel oxidation), while it is certainly worse from the noise (higher pressure derivative) and NOx (larger premixed portion, higher temperature) point of view. Figures below report how these quantities vary when different levels are actuated in a low load operating condition, demonstrating that noise could be effectively used as control input for pollutant emissions.

36

Figure 2.13 shows how the variables of interest behave, all trends are normalized with respect to the base calibration value which corresponds in this case to "Level 1". Noise increase linearly according to the frequency "Type 1" actuations are performed. NOx and FSN have an opposite trend, as expected, and even in this case it can be noticed how the functionality tends to be linear. A quite remarkable thing is that in the particular operating condition examined (2000rpm, 4bar IMEP), the effect on PM is huge, since it almost drops below smoke meter measuring sensitivity when "Type 1" combustions only are present. Concerning combustion efficiency, here reported as indicated specific fuel consumption (ISFC), a weak trend in improving the efficiency moving toward higher levels is present, but fuel balance precision error affects this result in a significant way. For sake of completeness, it must be stated that energizing time and injections phasing has been set to provide the same IMEP and MFB50 for both the adopted patterns.
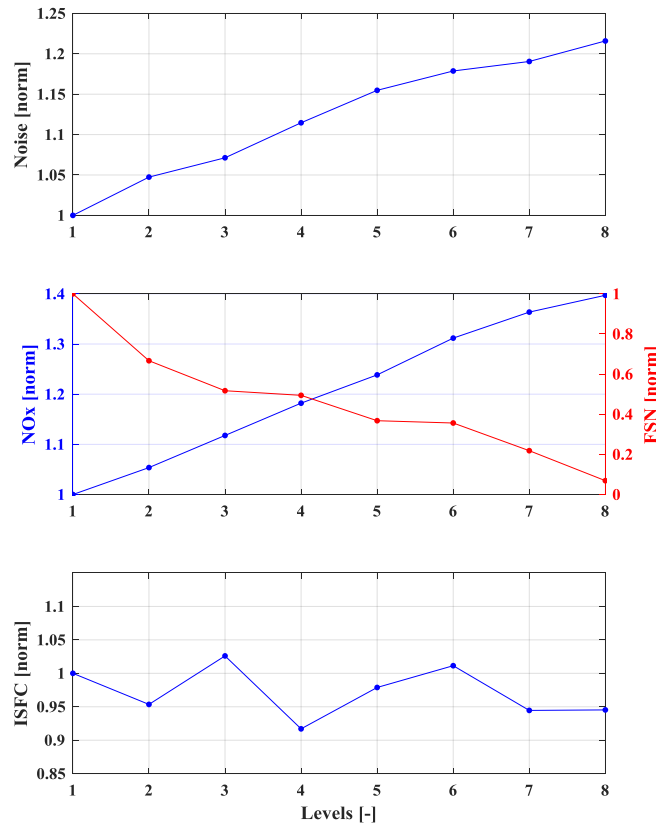
Figure 2.13: Emission and efficiency vs actuated level

In this context, a microphone (PCB Teds 378C01) is faced to engine block, its signal is processed in the same way described in the previous section by choosing Fourier transform buffers compatible with real-time processing (here 256 samples). The obtained measured noise values are used as feedback for a closed-loop controller, which selects which injection sequence has to be actuated in order to fulfill a calibrated requirement in terms of target acoustic emission. The closed loop controller, in this case is simply a PI regulator, with anti-windup feature, in case the

required level of noise is not reachable in a certain condition. The regulator output is then rounded to an integer value, used to properly index the previously defined matrix (Table 2.1) and get an injection sequence.
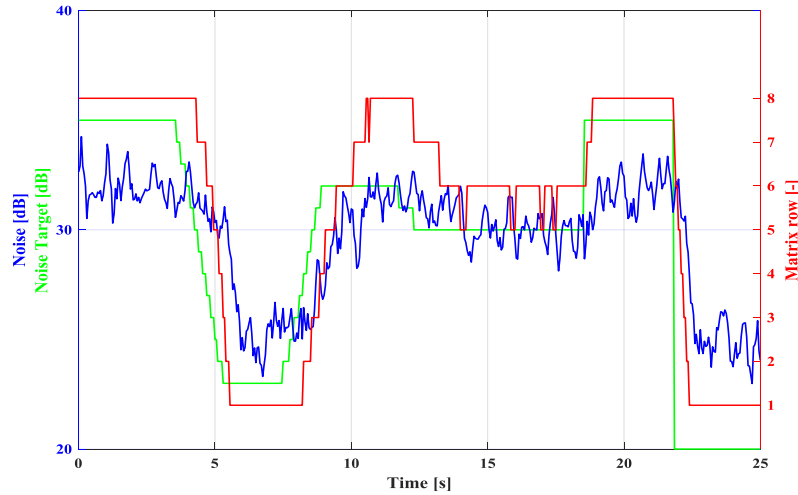
Figure 2.14: Noise controller response to target variations

In Figure 2.14 an example of PI regulator functioning is reported. The target (green line) undergoes some random variation while the controller tries to match the desired value by moving along the predetermined combustion sequences (red line). If the requested noise value falls outside the reachable limits, then the controller clips its output to either a full "type 0" or "type 1" injection sequences.

The possible applications of this kind of controller actually depends on the characteristics of each specific engine. In particular, the key factor in order to make it effectively useful, is that ordinary noise reduction strategies limits system performance in terms of efficiency or pollutant emissions. If this is true, combustion noise can be kept at the maximum value meeting regulations ranges. Moreover, in an ideal on-board application, microphone position and its signal processing must be optimized in order to filter environmental noise out. Finally, this kind of algorithm, even without closed loop contribution, can be used to appropriately manage the aftertreatment system, when either NOx or PM emission are critical, to improve DPF and SCR operation since it is possible to select intermediate levels in NOx-PM trade-off.

Closed loop torque and MFB50 control based on estimated combustion indices

Modern diesel engines are equipped with control systems that, concerning the fuel delivery, are based on fulfilling torque requests (driver, auxiliary systems, traction control, cruise control, …) regulating the amount of injected fuel, while injection pattern composition and timing is mainly a feed forward calibration aimed at optimizing other engine outputs such as efficiency, acoustic and pollutant emissions. In this context, it is widely known that injectors characterization is a critical issue since it is subjected to ageing and it could be influenced by surrounding conditions.

Although this consideration is quite simplistic because of the complexity reached by contemporary diesel engines control algorithms, the key thing that is wanted to be highlighted is that even if several strategies exist to on-line update the look up tables describing injectors behavior, no direct feedbacks on how combustion takes place is used.

In this section, previous work published by the research group, concerning combustion remote-sensing techniques, is inserted in a real-time application in order to develop a closed loop combustion control. The idea is to build up a simple on-line control loop quite similar to the one described in the previous section and sketched in Figure 2.4, but substituting the indicating system interface as the source of produced torque (IMEP) and center of combustion (MFB50) with a specific processing of the flywheel signal providing instantaneous engine speed [9].

Engine speed signal is used as the fundamental source of information since it is commonly available in on-board applications and it contains the fingerprint of combustion, if fluctuations are examined [10]. In this treatment, a 180-2 encoder wheel is used, but the same procedure can be applied to the standard production flywheels. Each detail of the torque and MFB50 estimation procedure can be found in [11,12,13,14], here are not reported rigorously since they are assumed to be the knowledge background on which the work shown in this report relies.

Every consideration from now on is based on the link existing between the torque delivered by each cylinder and the speed fluctuations readable at the end of crankshaft, where the speed sensor is installed. This "link" can be sought in the frequency domain and it is constituted by the frequency response function (FRF) of the driveline, representing torsional behavior. Ideally speaking the rotating part of the engine, as well as the load (i.e. the eddy-current brake), can be modeled as inertias whose interface is constituted of a spring/damper group, as it is sketched in Figure 2.15.
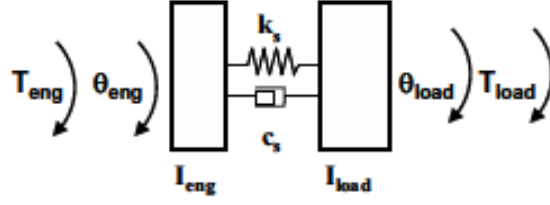
Figure 2.15: Driveline model

The elastic element (k_s) and the damping one (c_s) reported in the figure above, have to be imagined as connecting the engine and the load in a torsional way, thus the following relations apply:

$$\begin{cases} I_{eng}\ddot{\theta}_{eng} = T_{eng} - k_s(\theta_{eng} - \theta_{load}) - c_s(\dot{\theta}_{eng} - \dot{\theta}_{load}) \\ I_{load}\ddot{\theta}_{load} = T_{load} - k_s(\theta_{load} - \theta_{eng}) - c_s(\dot{\theta}_{load} - \dot{\theta}_{eng}) \end{cases} \qquad 2.1$$

Where the symbols I, T and θ are inertias, torque and angular position respectively, the subscripts "load" and "eng" identify which component T and I belong to, and the dot accent represent time derivative.

Moving to the frequency domain, by means of Fourier transform and rearranging the formulation taking into account T_{load} has a negligible dynamic with respect to T_{eng}, it is possible to come up with the expression below:

$$\dot{\theta}_{eng,i} = \frac{1}{\omega F(j\omega)} T_{eng,i} \qquad 2.2$$

Here, the subscript "i" indicates the "i[th]" Fourier transform coefficient (i.e. harmonic component). $F(j\omega)$ represent the frequency response function depending on inertias, stiffness and dampers modeling the system (the same approach can be applied to more complex cases than the one reported in Figure 2.15), ω is the pulsation.

Now it is clear how the engine speed fluctuations can be linked to torque fluctuations as long as $F(j\omega)$ is known. To determine it, two paths could be followed: the first one by using a complete CAD model while the second one by deducing it experimentally. The second techniques are preferable in our case, thus equation 2.2 is rearranged to explicit the frequency response function. Recalling that T_{eng} is the sum of all the torques components acting on the engine it can be expressed as the difference between the indicated torque (T_{ind}, which can be measured with in cylinder pressure sensors) and the reciprocating one (T_r, which can be a priori computed, in function of engine speed, if the masses undergoing alternate movement are known). Thus, equation 2.2 turns into 2.3:

$$F(j\omega) = \frac{T_{ind,i} - T_{r,i}}{\omega\dot{\theta}_{eng,i}} \qquad\qquad 2.3$$

However, the values of reciprocating masses may not be known with an acceptable precision thus the issue of canceling out reciprocating torque influenced terms can be overcome by adopting a formulation involving differences between a specific test and a reference one as equation 2.4 reports.

$$F(j\omega) = \frac{T_{ind,i} - T_{ind\,ref,i}}{\omega(\dot{\theta}_{eng,i} - \dot{\theta}_{eng\,ref,i})} \qquad\qquad 2.4$$

The reference test has usually to be chosen in order to maximize the numerator of equation 2.4, to obtain a signal to noise ratio as higher as possible, so an engine speed ramp in cut-offs (no injected fuel) condition is used. To clarify which are the signals involved in equation 2.4, Figure 2.16 shows which are denominator and numerator in crank angle domain. As reference conditions
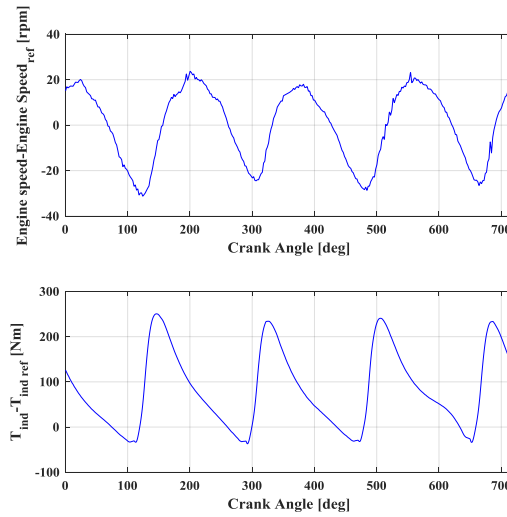
Figure 2.16: Engine speed and indicated torque depurated of their
respective reference value (2500 rpm)

cutoffs are used.

The following step is the selection of the harmonic order to be considered to the predetermined purpose. To quantify the average value of IMEP and MFB50 between the four cylinders, for an L4 architecture, it is worthy to investigate the fourth cycle harmonic, that is to say the second engine order, since it is the most excited one and signal to noise ratio is maximized.

Equation 2.4 can now be resolved explicitly to determine $F(j\omega)$, in characterization tests where in-cylinder pressure sensors are mounted. Results are shown in Figure 2.17, where three engine

speed ramps are displayed (every dot represents an engine cycle). The fact the three curves are overlapped confirms the linear behavior, not depending on torque itself.

The FRF has to be mapped in function of engine speed (or frequency), as well as the data obtained by the reference cutoffs (namely $T_{ind\,ref}$ and $\dot{\theta}_{eng\,ref}$). Once this information is stored in the ECU memory, equation 2.4 can be used to compute the indicated torque harmonic without needing in-cylinder pressure sensor measurement as shown in Figure 2.18 where the obtained calibrations are applied to an engine speed ramp not used to characterize the model.
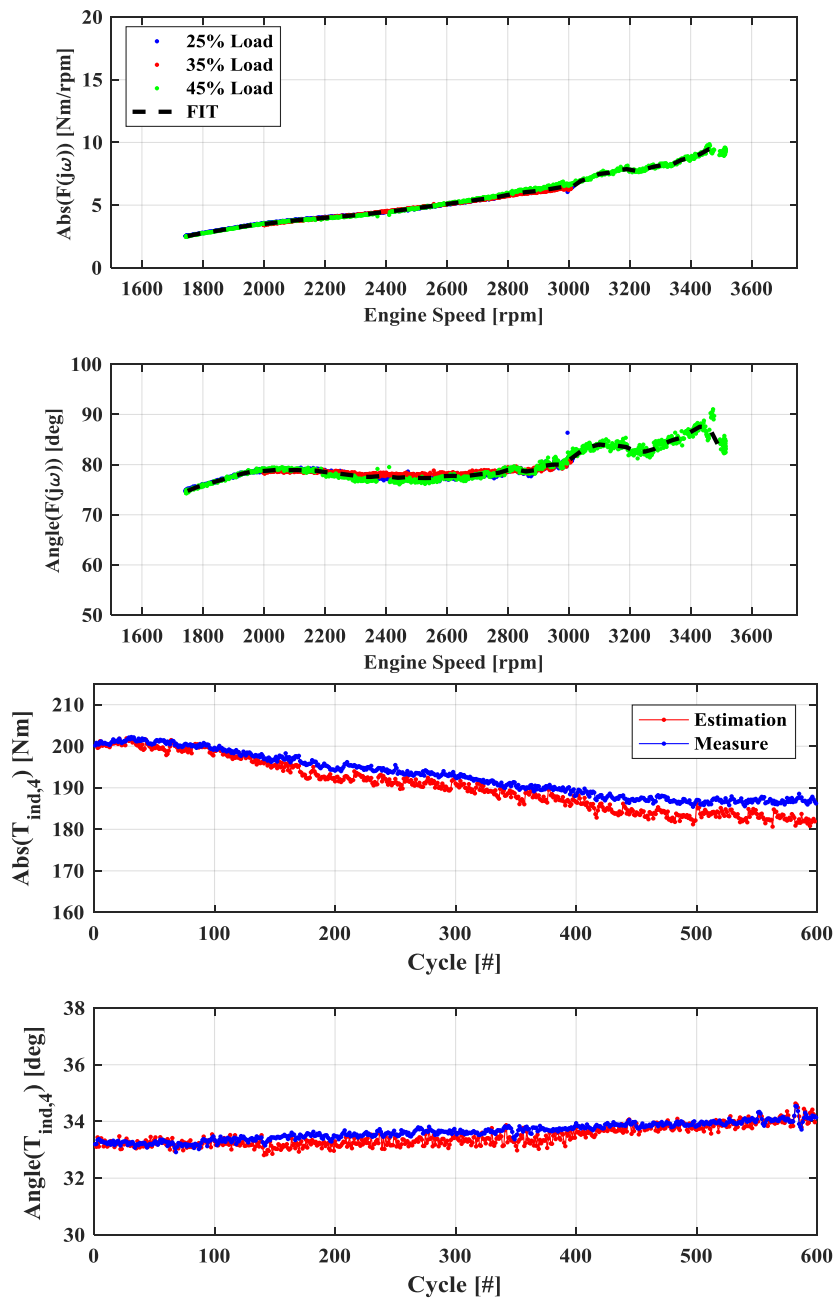
Figure 2.18: Indicated torque 4th harmonic estimation

42

At this point, the correlation between the indicated torque harmonic and the searched combustion indices has to be sought. In particular the amplitude of the fourth harmonic component is found to be correlated to IMEP, while the phase to MFB50. Boost pressure is also included in the dependencies, since trapped mass certainly affects the indicated torque. The calibrations to be comprised in order to complete the described torque and MFB50 estimation algorithm are the correlations sketched in relations 2.5, obtained as a linear regression of a model training dataset.

$$\begin{cases} T_{ind,est} = f\big(Abs(T_{ind\ est,4}), Boost\ Pressure, Engine\ Speed\big) \\ MFB50_{,est} = f\big(Angle(T_{ind\ est,4}), Boost\ Pressure, Engine\ Speed\big) \end{cases} \qquad 2.5$$

Figure 2.19 shows how the indicated torque averaged over an engine cycle and the center of combustion (mean value of the four cylinders) can be estimated over the same engine speed ramp shown in Figure 2.18 (from 1800rpm to 3500rpm at 40% load).
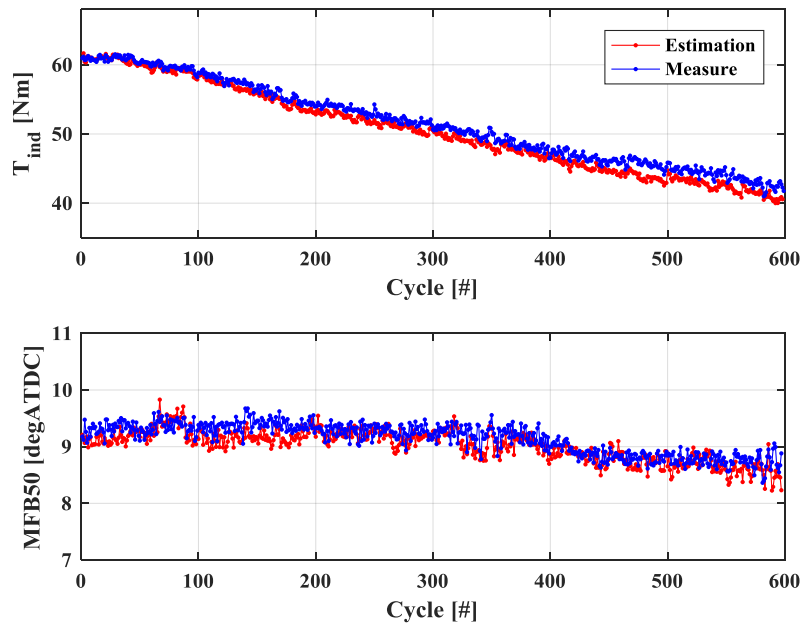
Figure 2.19: Indicated torque and MFB50 estimation

As previously stated, the objective of the present section is not to describe in details how the estimation algorithm works, but to show how it could feed a closed loop combustion controller able to fulfill specific targets in terms of indicated torque and combustion phase.

According to these purposes, a code section in the RCP system has been developed, whose structure is depicted in the following diagram, Figure 2.20.
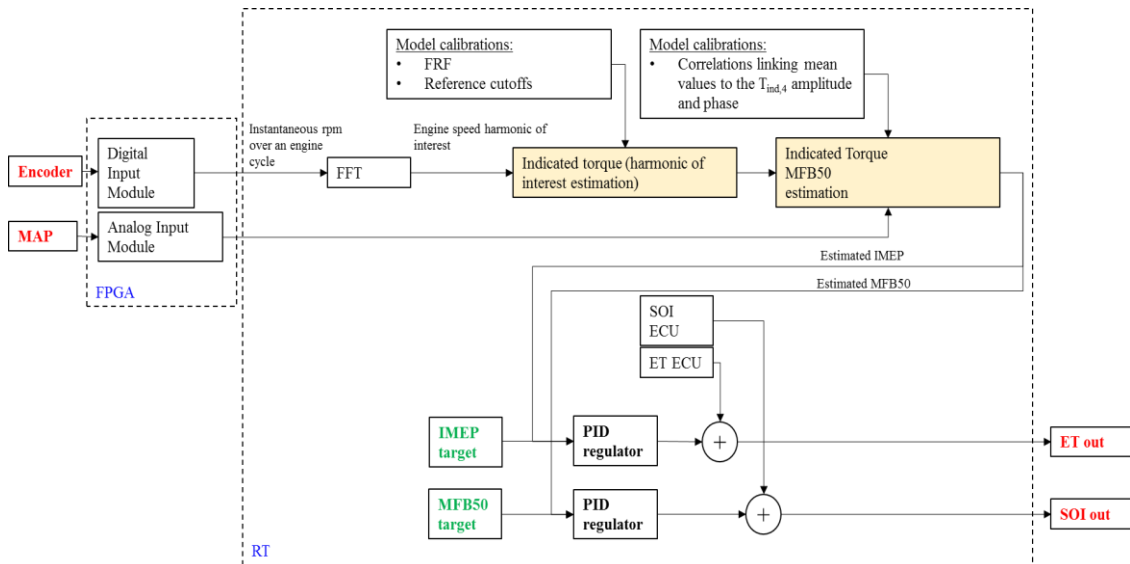
Figure 2.20: IMEP, MFB50 control scheme based on estimated data

As it can be noticed, the estimator loop triggers the combustion control loop in which two PID regulators take the estimation output as feedback to adjust the main injection energizing time as well as the entire pattern timing, in terms of start of the main injection, to accomplish specific targets in terms of delivered torque and combustion phasing.

To validate the presented structure two different kind of tests have been performed: firstly, pilot injections sweeps in order verify how the estimator loop works when the "shape" of the indicated torque over the engine cycle changes; secondly, IMEP target steps.to check how the closed loop correction behaves. Then, some critical issues are discussed.

First of all, the tests where the injection pattern is varied are reported.

Figure 2.21, Figure 2.22 show the results of the first test made at 2000rpm, where a three-injections pattern has been adopted. The quantities of both the pilot injections are varied starting from 1.2 mm^3/str to 0.3 mm^3/str, which is the value where the injectors start behaving in a not repeatable way, entering the ballistic region. The algorithm sketched in Figure 2.20 has been set to follow a constant IMEP and MFB50 target, being 4.5bar and 9degATDC respectively. The feed forward contributions (SOI ECU, ET ECU) have been kept constant throughout the entire test. Thus, while the pilot injected quantities decrease, the closed loop controller has to set the main injection parameters to increase its energizing time and moving to a more advanced SOI. This should happen because as far as the effect of the pilot injections is reduced, combustion phase tends to retard since the fuel is injected later and the charge preconditioning effect of the pilot injection vanishes.
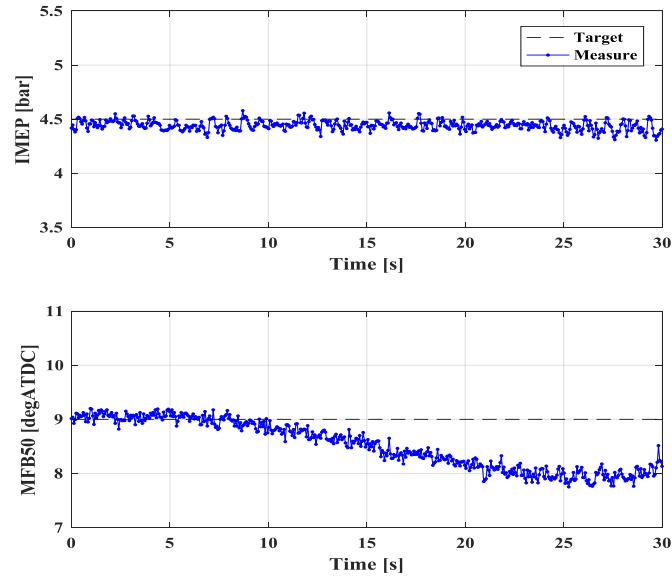
Figure 2.22: Combustion closed loop control on estimated indices, 1st test, IMEP, MFB50
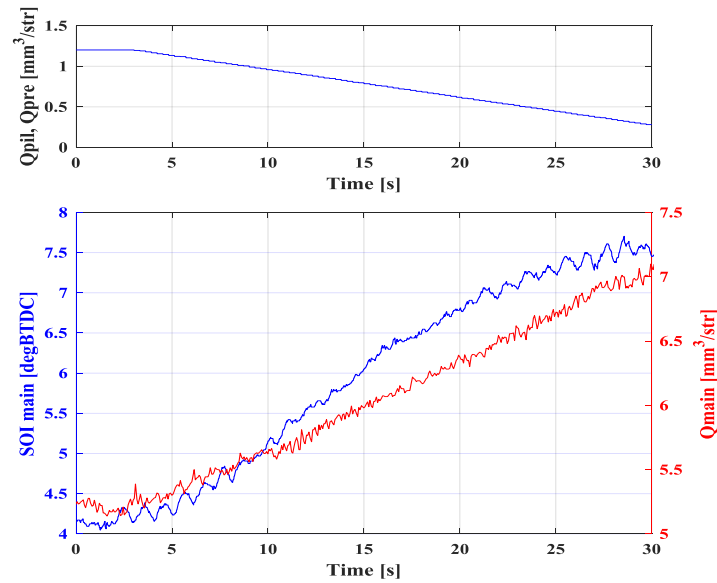
Figure 2.21: Combustion closed loop control on estimated indices, 1st test, Actuations

If IMEP is observed, a reasonably good behavior could be appreciated, since it is maintained constant even if a very little bias is present due to estimation errors. Moreover, the difference in the main injection quantity between the end of the test and the beginning is almost equal to the value that has been taken away by the pilot injections.

Concerning the MFB50, the phenomenon has been caught properly, since the controller has detected a tendency in combustion to retard, thus it has actuated SOI in the right direction. A clear drift can be seen though from second 20 to 30, when the modification in indicated torque "shape"

45

has influenced the correlations used to calibrate the model, (recalling that it has been trained when base calibration has been applied).

The second reported test is similar to the previous one, but only a pilot injection has been used and more variation has been imposed (from 2.5 mm³/str, to .0.6 mm³/str). Results can be seen in Figure 2.23 and Figure 2.24.

Here, a slightly higher bias is observed on IMEP, while MFB50 estimation is once again more influenced (long period oscillations), but it remains closer to the target.
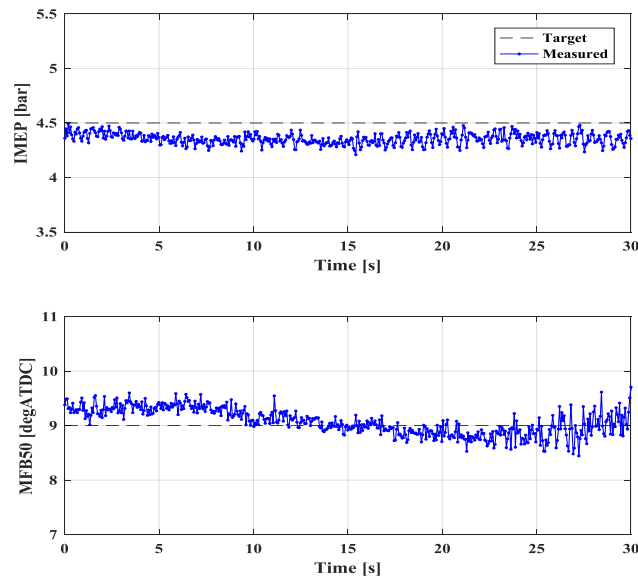
Figure 2.23: Combustion closed loop control on estimated indices, 2nd test, IMEP, MFB50
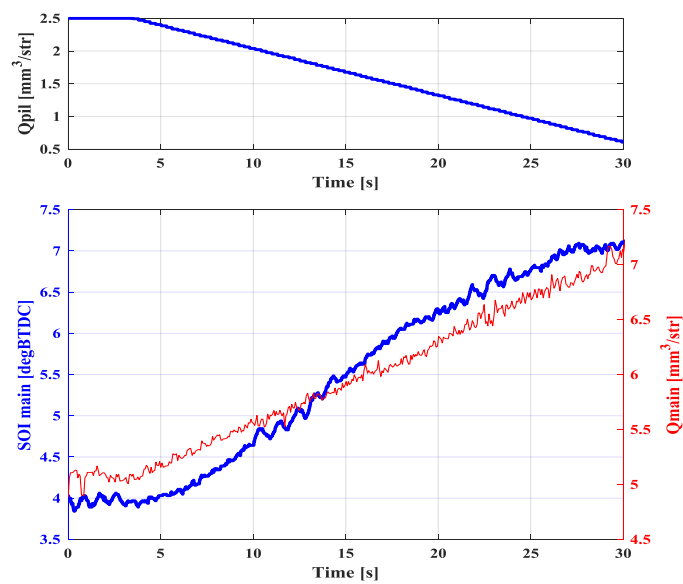
Figure 2.24: Combustion closed loop control on estimated indices, 2nd test, Actuations

46

The third test is aimed at determining how the closed loop contribution is able to respond when IMEP targets is varied through steps. The engine operating condition has been set to 2000rpm with base calibration (three injection pattern). Target IMEP has been then varied as the top two subplots show in Figure 2.25.
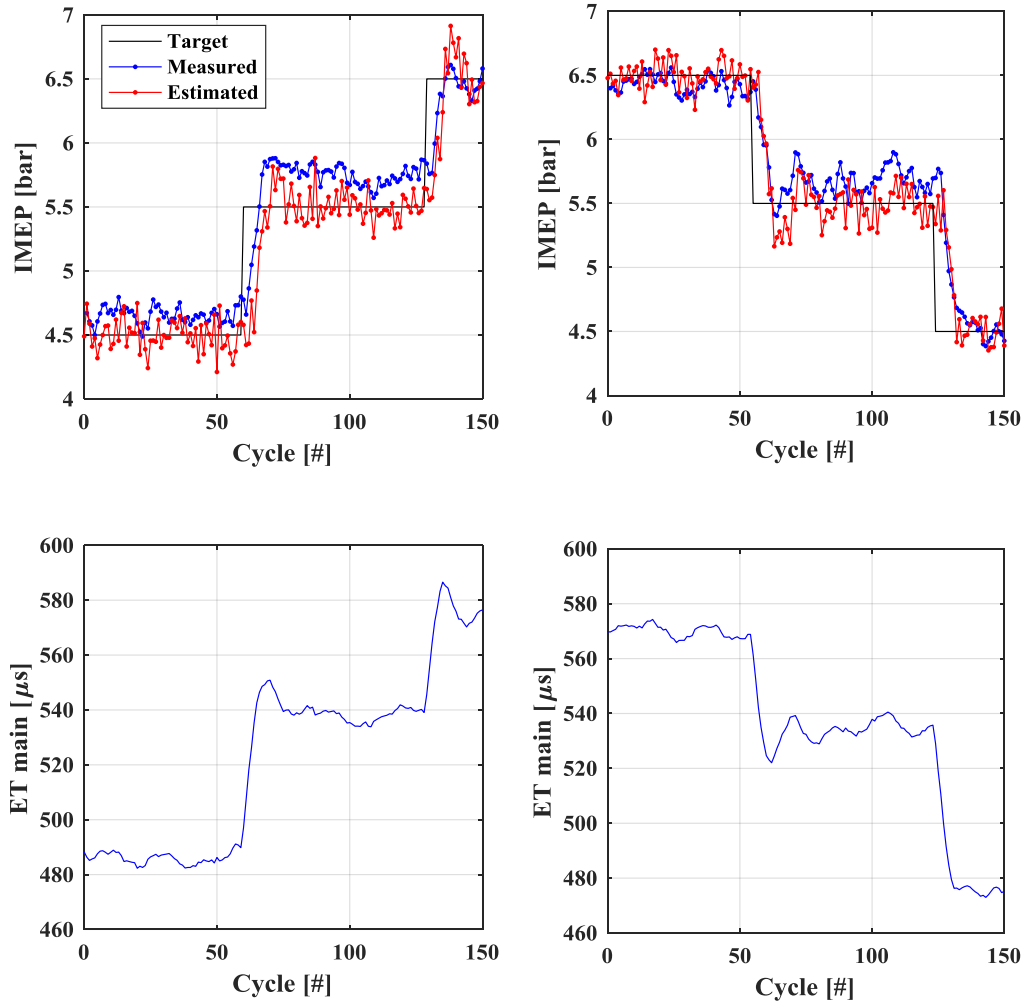
Figure 2.25: Combustion closed loop control on estimated indices, 3rd test

During these tests, the controller has demonstrated to behave in a quite satisfying way, taking into account that no open loop contribution has been varied when these target changes have been imposed. It is able to bring the processed variable to target within 10 cycles even if a slight overshoot is observed. However, a bias on the estimated IMEP is still present depending on the load conditions.

The final discussed subject related to the described methodology in estimating combustion indices by means of the analysis of engine speed fluctuations is the reliability it could guarantee over time. In particular, a driveline is composed by components that could exhibit ageing and the

47

frequency response function could be affected by these phenomena. In particular the worst case, making this approach inapplicable, is the arising of non-linearities making the FRF itself depending on the engine load. In Figure 2.26 it is shown how a slightly damaged elastic joint can affect the FRF, as it can be noticed the several engine speed ramps splits as load is varied directly implying an estimation error.
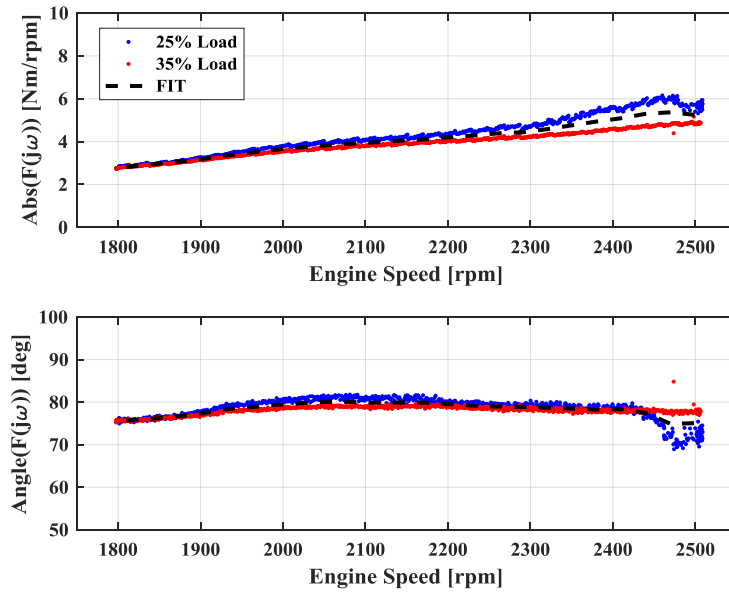
Figure 2.26: 4th harmonic FRF, elastic joint damaged

The presented approach is based on engine speed fluctuations and therefore can be used with ordinary engine equipment. Calibration effort is needed to obtain a consistent mapping of the frequency response function linking the speed harmonic components to the torque ones as well as the data related to the reference conditions involved in equation 2.4. Moreover, reliable correlations between the harmonic of interest (depending on the engine architecture) and the mean quantities over an engine cycle must be provided. Once this information is deduced, the proposed algorithm has demonstrated to be able to feed a closed loop combustion controller aimed at accomplishing determined targets in terms of IMEP and MFB50. The main issue in adopting such an approach is the possibility of a drift in the driveline characterization making the obtained calibrations inapplicable, this problem can potentially be overcome by on-line learning the FRF, exploiting cut-offs and speed ramps.

NOx estimation model based on in-cylinder pressure trace

The last topic presented, concerning the analysis on conventional diesel combustion, is a nitrogen oxides concentration estimation model based on in-cylinder pressure trace. Once again, it is focused on engine-out emissions since the central topic of the study remains combustion analysis.

Exploring literature regarding the field of pollutant species estimation models, several approaches can be found which differ because of the way they link the control parameters to the desired output [15,16]: namely several black-box models are often used, but in this case something more related to the physical phenomena responsible of NOx generation is looked for. Although black-box models can be considered quite representative of the matter of interest with the great advantage to be compatible with most of the commercial ECUs, adopting a formulation which is able to derive NOx concentration using in-cylinder pressure as main input is worthy for diesel engine, because of the many degrees of freedom allowing rate-of-heat release management. In addition, model predictive capabilities are enhanced, to some extent, and calibration effort is drastically reduced using the latter solution.

The aim of the work reported in this section is then the validation and improvement of a model found in literature [17] that has been the core of many revised solution by the same authors [18,19] and even others [20]. The formulation adopted as starting point of the present discussion is based on thermal NOx formation mechanism proposed by Zel'dovich, since this kind of reactions are the main cause of nitrogen oxides emission in a CI engine (other formation mechanisms, such as prompt NOx, are less important). As it is well known, Zel'dovich states that the nitrogen oxides generation is encouraged by high local temperature and the presence of oxygen. Thus, two fundamental quantities to be evaluated in order to get an estimation of produced NOx are the energy release rate and the adiabatic flame temperature (which depends on oxygen concentration), in this context an Arrhenius like reaction kinetic factor is used to introduce the temperature dependent term. Nevertheless, the successively discussed model cannot be identified as a fully "white-model" since reaction kinetics in not described rigorously.

In the following treatment, results are reported when the starting model structure (directly derived from literature) has been applied to experimental data collected through a DOE in steady-state conditions, secondly some modifications are proposed. Some other tests in transient condition are then used to verify the obtained model and finally the sensitivity with respect to measure uncertainties are evaluated.

Every input required to the discussed model can be deduced from sensor currently available on CI engines with the exception of in cylinder pressure.

First of all, the base model structure has to be introduced and every previously reported dependency have to be deepened.

$$NOx_m = \int_{SOC}^{EOC} k_1 \cdot ROHR(\alpha) \cdot \left(\frac{n}{2000}\right)^{k_2} \cdot e^{\left(\frac{k_3}{T_{ad}(\alpha)}\right)} d\alpha \qquad 2.6$$

Equation 2.6 reports the formulation initially adopted to express the exhaust NOx mass, here ROHR is angle resolved rate of heat release, n is the engine speed and T_{ad} is the adiabatic flame temperature.

As it can be noticed, the main idea supporting this expression is that the amount of produced NOx follows an Arrhenius-like kinetics (exponential term) which has to be weighted with the amount of energy released instantaneously. The total NOx mass is then the integral evaluated from the start of combustion (SOC) to the end (EOC). The middle term, expressing the dependence with respect to engine speed is often introduced to help the model catching the effects related to the in-chamber charge motion which change significantly when the engine speed varies. However, as it is shown later, this term has a negligible effect in this case and can be canceled out. Factors k_1, k_2, k_3, are constant tuning parameters.

Some consideration must be made on how ROHR has to be computed. In this particular application, the net heat release rate (NHRR), often used to express ROHR (Equation 2.8) would not be ideally appropriate to represent energy delivered by combustion, since from the reaction kinetics point of view, what matters is the gross heat release rate. Several methods exist, correlating some physical variables to the wall-heat losses (Annand, Woschni's) and blow-by, in our case a simple consideration is made for calibration simplicity, synthetically described by the following equations.

$$ROHR(\alpha) = NHRR(\alpha) + w \cdot T_{mean}(\alpha) \qquad 2.7$$

$$NHRR(\alpha) = \frac{\gamma}{\gamma - 1} p(\alpha) \frac{dV(\alpha)}{d\alpha} + \frac{1}{\gamma - 1} V(\alpha) \frac{dp(\alpha)}{d\alpha} \qquad 2.8$$

$$w = \frac{(LHV \cdot m_{diesel} - max(CHR))}{\int_{SOC}^{EOC} T_{mean}(\alpha) d\alpha} \qquad 2.9$$

$$CHR(\alpha) = \int_{SOC}^{EOC} NHRR(\alpha) d\alpha \qquad 2.10$$

Here, the wall heat losses are assumed to be proportional to the mean chamber temperature T_{mean} (radiative heat exchange is neglected), thus the net heat release rate is corrected by an additive

term following the shape of this quantity which is scaled to make the integral of such a contribution to be equal to the energy losses. It is known that this kind of assumption is strong, but it has helped improving model behavior, to some extent.

The last key thing to be highlighted concerning equation 2.6 is how the adiabatic flame temperature (T_{ad}) can be calculated. The procedure reported in [17] has been completely reproduced, thus details on the algorithm are not shown here. It is just interesting to recall which contributions it contains. The adiabatic flame temperature is modeled to be the sum of three terms:

- Unburnt gases temperature: temperature increment/decrement due to the compression/expansion computed using a recursive polytropic law;
- Temperature shift due to combustion: black-box modeled in function of the oxygen fraction and air/fuel ratio, fitting coefficient obtained by chemical equilibrium codes;
- Temperature drop due to dissociation effects: threshold model based on the sum of the previous terms. Once again, a black-box fitting function is applied.

The previously sketched steps suggest that air-related quantities such as the fresh air mass flow rate, EGR rate, boost pressure, play a key role in adiabatic flame temperature determination (Figure 2.27).
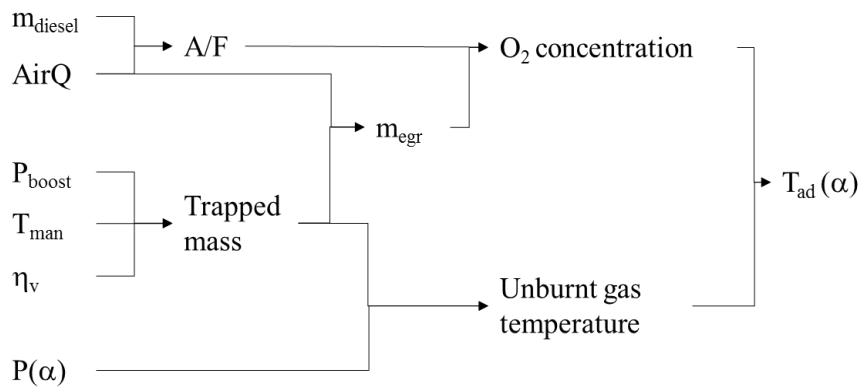
Figure 2.27: Steps to compute adiabatic flame temperature. [17]

Equation 2.6 has been tested in steady-state operating conditions by applying it to data acquired in a full-factorial DOE whose parameters have been: engine speed, load, fresh air mass flow rate (AirQ), boost pressure, start of injection (SOI). Every other control parameter has been managed through standard engine calibration. The investigated levels are reported in Table 2.2.

Engine Speed [rpm]	1800, 2200, 2600, 3000
Engine Load, BMEP [bar]	5, 8, 13
Injection Timing [ΔCA with respect to baseline]	-4, 0, 4
Boost Pressure [Δ% with respect to baseline]	-10, 0, 10
Mass Air Flow [Δ% with respect to baseline]	-10, 0, max

Table 2.2: DOE parameters ranges

Mass air flow (AirQ) and boost pressure targets have been managed independently, by controlling EGR valve and VGT position. In particular, AirQ setpoint has been imposed to the engine control system, since it includes a closed loop control using EGR as lever; boost pressure target has been set in the TBCS environment instead, which communicates to INCA and adjust directly VGT position.

It is quite reasonable that not every combination between boost pressure and AirQ can be reached in a determined operating point, however it may not be easy (and worthy) to determine a priori which are the available values, actuators saturation has been experienced. For sake of model validation, this has not been a critical issue.

Another thing to be specified, is that for each speed, load and boost pressure condition as acquisition with the maximum allowable AirQ must be performed. It means that the EGR valve is completely shut and consideration on volumetric efficiency (defined as the ratio between the actual breathed charge and the theoretic one at the measured boost pressure and temperature) can be made exploiting MAF sensor reading. Volumetric efficiency has been mapped as a function of engine speed and boost pressure and used to determine EGR effective percentage by subtracting the measured AirQ to the estimated trapped mass. Forasmuch as it is a key parameter an additional ultrasonic air flow rate sensor has been added (FEV AirRate DN100) to check the standard debimeter accuracy. Other methods based on pressure signal processing can be used to determine cylinder trapped mass [21], here the most straightforward has been chosen.

The model training dataset has been chosen as a half of the depicted experimental plan and k_1, k_2, k_3 optimization has been carried out by minimizing the root mean square error (RMSE) globally. Figure 2.28 reports how the initial formulation behaves by comparing estimated and measured NOx concentration in part per million mass.
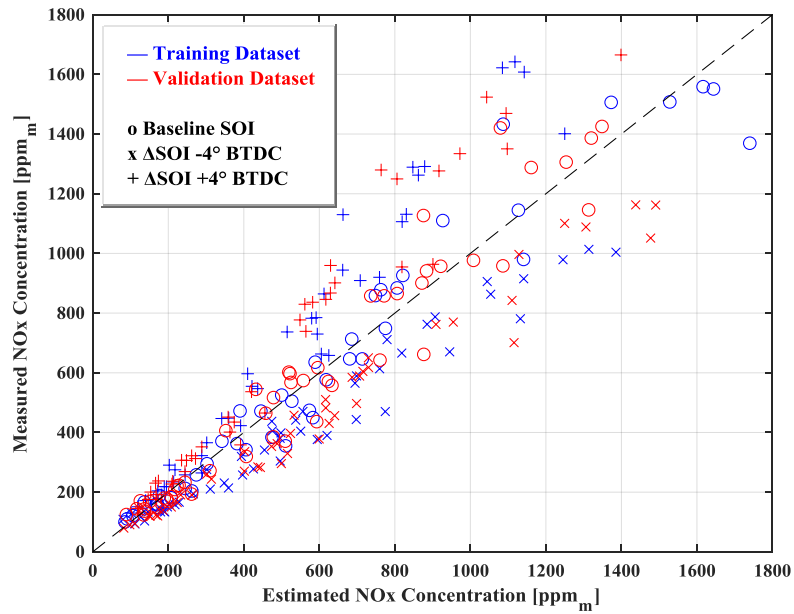
Figure 2.28: Starting model steady state response

Different colors identify the training and the validation datasets while symbols are used to group the different injection timing delta with respect to the base calibration. It can be noticed that the distribution is well-centered (a mean error of 3.5 ppmm is present) but an evident dispersion is present when NOx concentration increases.

A remarkable thing is that three sets are present sharing the same SOI variation, thus it seems the starting model expression is not able to detect combustion phase properly. A deeper analysis on the several terms composing equation 2.6 has been performed.

As previously anticipated the factor including engine speed has been found to be negligible and has been excluded.

Concerning the exponential term, the attention has been focused on k_3 coefficient. First of all, it has been verified that for each test a k_3 value bringing the estimation to match the measured value always exist. Secondly, the dependencies optimal k_3 has, with respect to some indices related to combustion phase, have been sought. It has been found a clear trend if optimal k_3 value is plotted with respect to MFB50 (Figure 2.29).

This kind of functionality, suggesting that reaction kinetics are sensitive to the angular position at which combustion take place, has been modeled through a linear fit, thus the final model formulation is shown in equations 2.11 and 2.12.

$$NOx_m = \int_{SOC}^{EOC} k_1 \cdot ROHR(\alpha) \cdot e^{\left(\frac{k_3(MFB_{50})}{T_{ad}(\alpha)}\right)} d\alpha \qquad 2.11$$

$$k_3(MFB_{50}) = b_1 \cdot MFB_{50} + b_2 \qquad 2.12$$
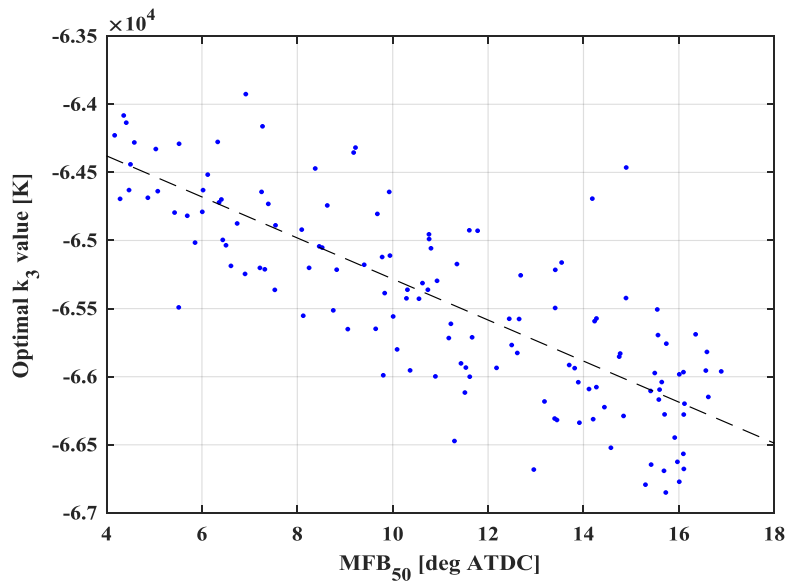
Figure 2.29: Optimal k3 tendency with respect to MFB50

The global scaling factor k_1 has been optimized once again by minimizing RMSE over the training dataset while b_1 and b_2 coefficients have been detected starting from Figure 2.29 in which, once again, only the training dataset is reported.
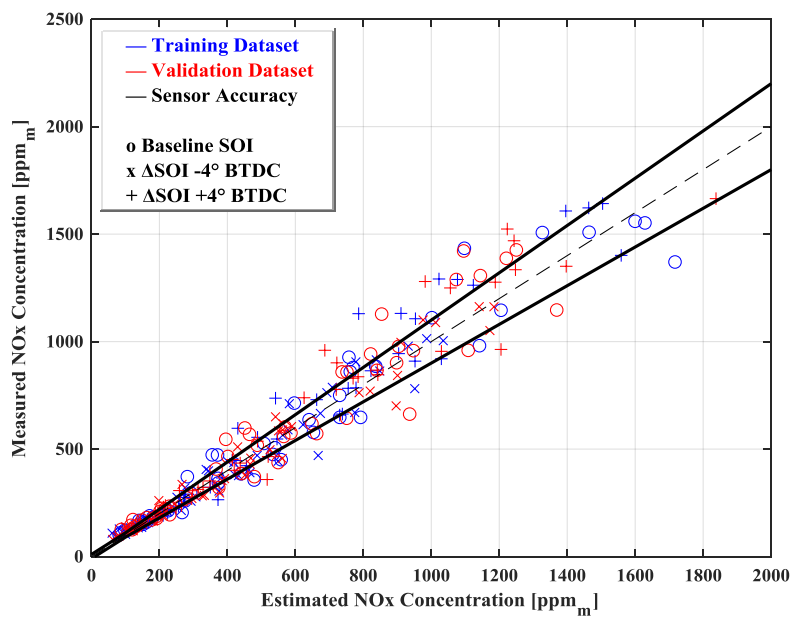
Figure 2.30: Modified formulation response in steady-state conditions

Model response improvements are shown in Figure 2.30, where NOx sensor accuracy is also displayed.

As it can be noticed, the previously observed dispersion decreases (RMSE moves from 166ppmm to 99ppmm), but most importantly, different SOI groups are overlapped.

Once the model has been tuned using steady-state tests it has been applied to data acquired in transient conditions regarding engine speed and load, injection timing and fresh air mass flow rate independently. In particular, load and SOI steps, speed and AirQ ramps have been performed. Results shown in Figure 2.31, demonstrate that the model has a consistent behavior since regime conditions are reasonably well represented, in addition, a cycle resolved approach (as the one dealt with in this section) allows a faster dynamic than the NOx probe, regardless of the estimation accuracy.

NOx sensor dominant time constant has found to be almost two seconds. Cyclic dispersion is present instead.
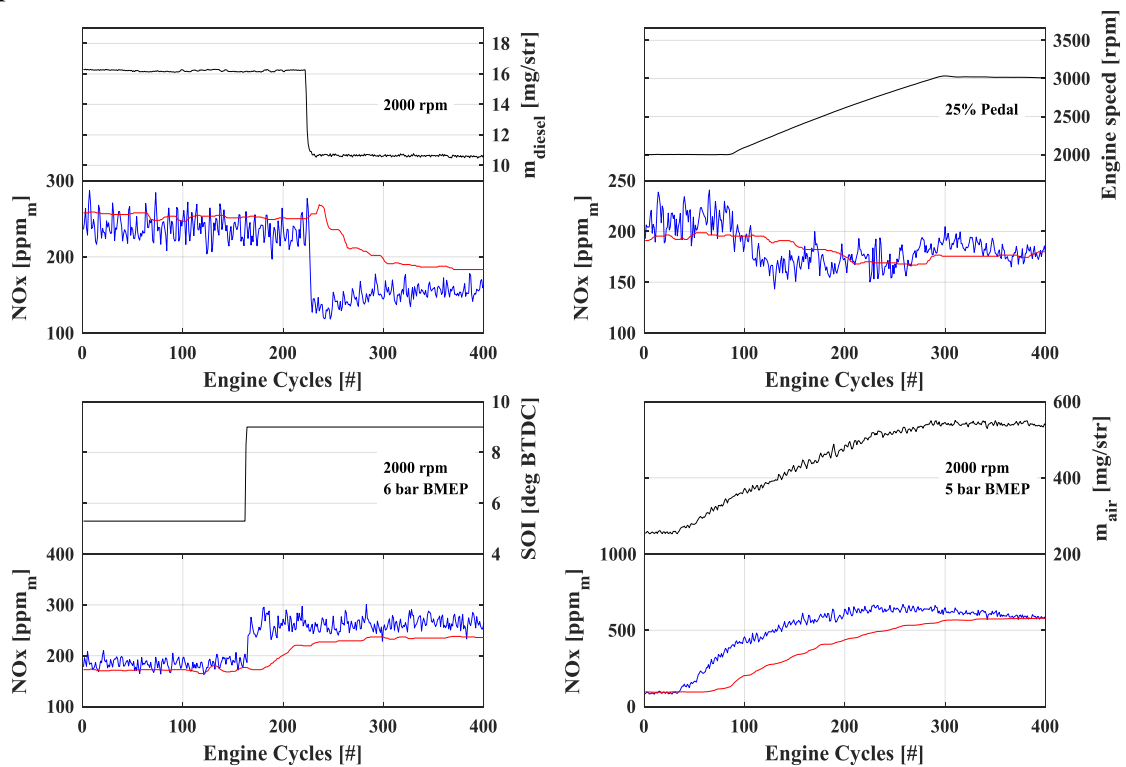
Figure 2.31: Model response in transient condition. blue line: estimation, red line: measure

Finally, since a certain dispersion is present even with the modified model structure at high nitrogen oxides emissions (Figure 2.30), an analysis on how the several measurement errors could affect the estimation has been carried on.

Volumetric efficiency, air mass flow rate, boost pressure, intake manifold temperature, fuel mass and measured exhaust oxygen fraction (UEGO) have been identified to be the key factors. A two percent variation has been imposed to each one of these variables one factor at a time, and model

estimation is evaluated in two of the steady-state points discussed above, one at low, the other at high NOx emission.

Results are shown in Figure 2.32.
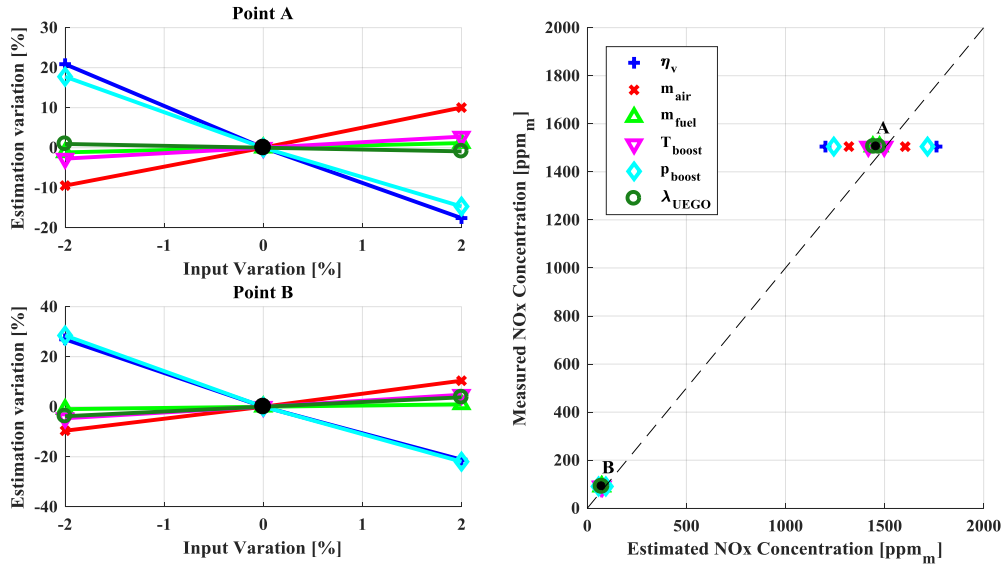
Figure 2.32: Model response to measure uncertainties

It is quite evident and relevant that the proposed formulation has a huge sensitivity with respect to every parameter concerning air (as one can expect), this happens because the oxygen fraction has a great impact on the adiabatic flame temperature. On the contrary, the model can withstand precision errors on fuel mass affected variables.

These considerations, in a way explain the previously observed dispersion, since the operating conditions where the highest nitrogen oxides concentrations have been measured are the ones where the greatest air mass flow rate has been set.

The target of this research has been to test the validity of a model traced in literature and suitable to link the nitrogen oxides production to the in-cylinder pressure evolution.

Modifications on the initial model structure have been developed in order to limit estimation dispersion when combustion phase changes. All these things considered, the proposed formulation has been found to behave convincingly because every tendency is respected and modeled in the right direction in both steady-state and transient conditions.

Concerning robustness, some issue arises when dealing with measure precision on the air-related parameters: they, notoriously hard to be quantified, can make the relative estimation error increase up to ten times the relative error on the input.

Finally, from the dynamic point of view a cycle-resolved approach can help to overcome sensor response, which is affected by gas transport delay and probe dynamic.

3. REACTIVITY CONTROLLED COMPRESSION IGNITION

The subject of reactivity-controlled compression ignition (RCCI) is dealt with, in this chapter, from the very first approach to this kind of combustion strategy to some results concerning combustion control techniques and control-oriented modeling.

The adopted methodology to deduce some of the most relevant aspects shown from now on has a strong experimental nature; every reported phenomena and considerations have been studied starting from the acquired data, which, systematically, have determined the aspects to furtherly be investigated.

RCCI operation is intended in this work as a dual-fuel combustion where the mixing of a high reactivity fuel and a low reactivity one, allows having an additional degree of freedom, being beneficial to control self-ignition of an almost homogenous charge whose aim is to avoid diffusive behavior as well as every critical aspect (from emissions point of view) linked to conventional CI combustion heterogeneities [22,23]. As low reactivity fuel gasoline (RON 95) is used, while diesel as the high reactivity one.

Concerning the injection methodology, gasoline is port injected during the intake phase exploiting the hardware facilities described in chapter 1; diesel is direct injected using the common-rail system. Direct injection pattern is always set to be a single injection whose timing is used as a control lever to obtain consistent combustion phasing.

Direct injection split is not taken into account because of the small injected quantities involved, which would make the injector behavior not repeatable unless rail pressure is decreased to values traditionally incompatible with diesel direct injection because of PM origination.

The structure of the present chapter is mainly divided in three sections:

- a preliminary experimental plan aimed at catching some tendencies belonging to the way combustion takes place with respect to the basic control parameters; the same experimental data are also used as evidences of RCCI advantages and critical points.

- considerations on which control levers are most suitable to stabilize combustion when it is found to be either excessively rough or near to misfire. A closed loop combustion control algorithm is then proposed to accomplish these tasks and helping to overcome some extreme sensitivities to environmental/intake conditions. Combustion remote sensing is discussed to compute indices able to properly feed the controller.

  In this section, also a description is made regarding the code that has been developed up to this thesis writing and making the engine functioning in full RCCI (four cylinders) mode.

- a preliminary combustion modeling phase aimed at improving control, a set of single cylinder RCCI operation data is used to this purpose.

As it can be noticed, most of the work is done to obtain a stable operating condition and make the engine functioning as robust as possible in transient conditions. In this sense this work inevitably lacks in complete engine operating field characterization, even if, it must be anticipated that by adopting RCCI combustion mode with stock engine hardware (piston and combustion chamber design, intake runners, …), obviously optimized to run the engine with conventional diesel combustion, a limit is found when increasing load, as it is explained further on. To overcome this kind of issue computational fluid dynamic is required together with the possibility to design and build complex components and it is certainly beyond the scope of this work [25,26].

Combustion sensitivity with respect to the main control parameters

In this section some initial test plan results are reported, whose aim is to clarify some basic functionalities combustion indices, emissions and efficiency have when the basic control parameters are varied. Firstly, a 2000rpm, 3bar BMEP condition is examined, then load is increased to 5bar BMEP.

RCCI: 2000rpm 3bar BMEP

This first experimental activity has been carried on at very low load. This choice has been made since every searched tendency can be obtained, and tests can be conducted without limitations caused by excessive impulsive combustion, thus the entire experimental plan can be explored.

For sake of consistency, load has not been kept constant in every tested condition, because of the substantially different levels of efficiency present in the explored region. Cumulated fuel consumption (gasoline + diesel) has been selected as the parameter to be maintained as constant as possible exploiting fuel balances measurements; here the difference in lower heating values

between the two fuels has been neglected. In particular, the target consumption value is the one guaranteeing 3bar BMEP in diesel only operation. All four cylinders have been run in RCCI mode.

The main control parameters whose effect has been looked for, are: direct injection timing (SOI), and EGR valve opening.

The following figures reports some of the most interesting outputs concerning engine performances when gasoline to total mass ratio is kept equal to 70%, all values with the exception of MFB50 are normalized by the reference value obtained with the baseline engine calibration in CDC functioning.

Concerning the way adopted to perform this first experimental activity, it must be specified that the VGT position has been kept constant, meaning that a forced variation in the EGR valve position has had an effect on boost pressure since the exhaust mass flow rate travelling through the turbine changes.
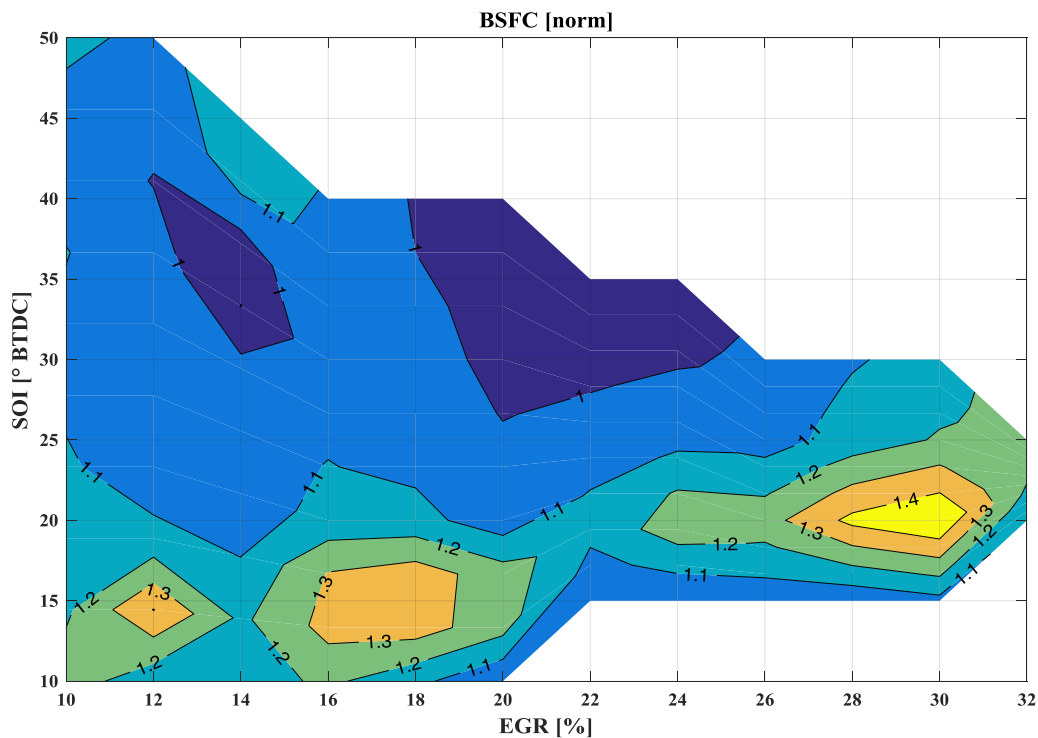
Figure 3.1: RCCI 2000rpm 3bar BMEP 70% gasoline, BSFC variation with respect to reference CDC operating condition
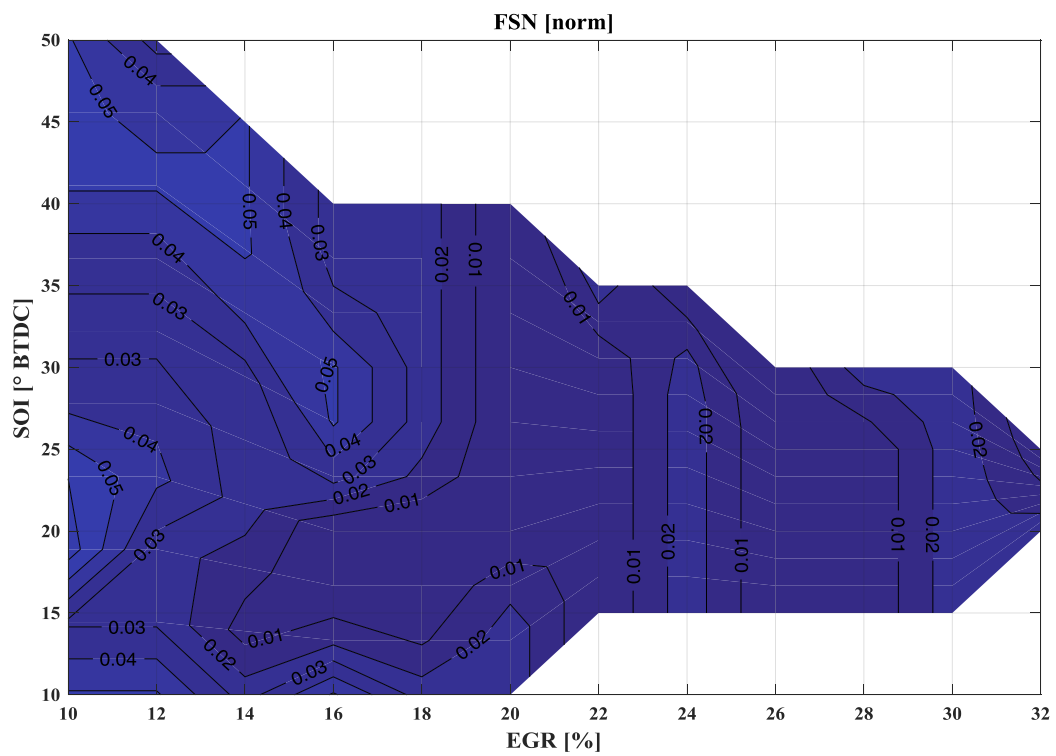
Figure 3.2: RCCI 2000rpm 3bar BMEP 70% gasoline, FSN variation with respect to reference CDC operating condition
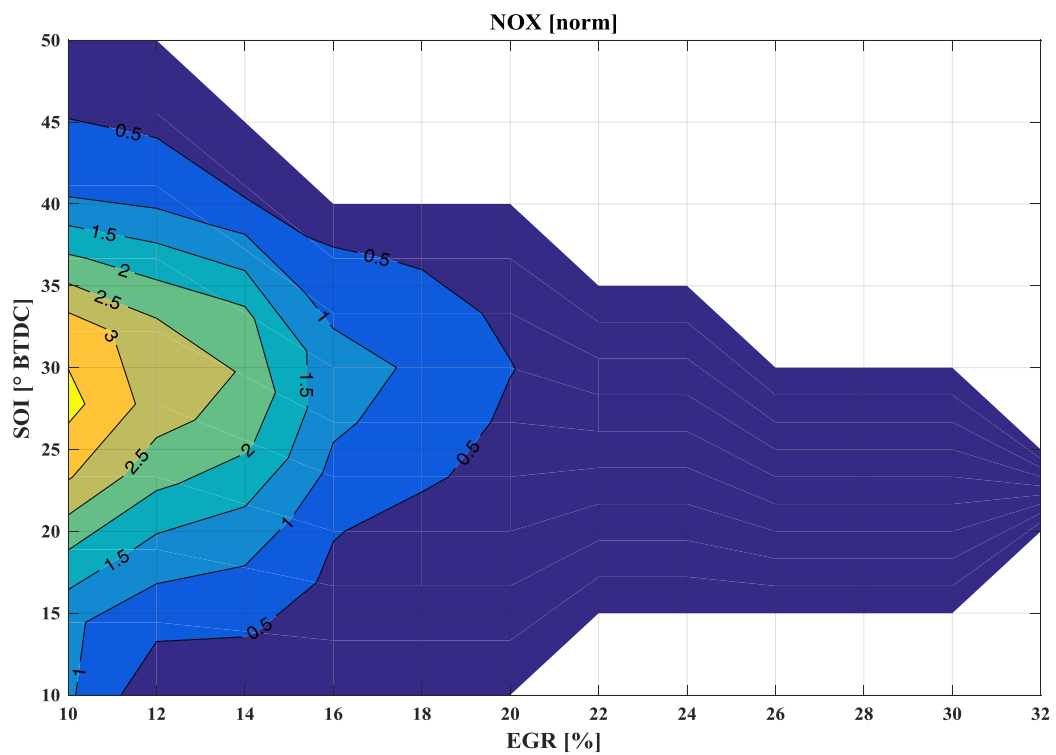
Figure 3.3: RCCI 2000rpm 3bar BMEP 70% gasoline, NOx variation with respect to reference CDC operating condition
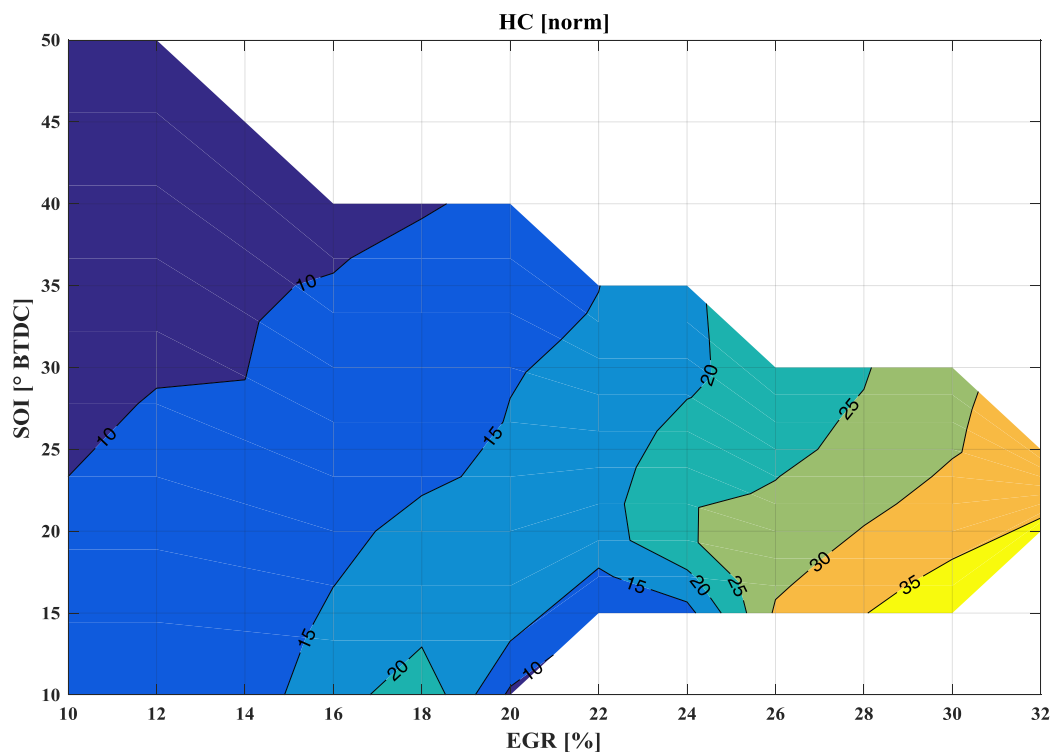
Figure 3.4: RCCI 2000rpm 3bar BMEP 70% gasoline, HC variation with respect to reference CDC operating condition
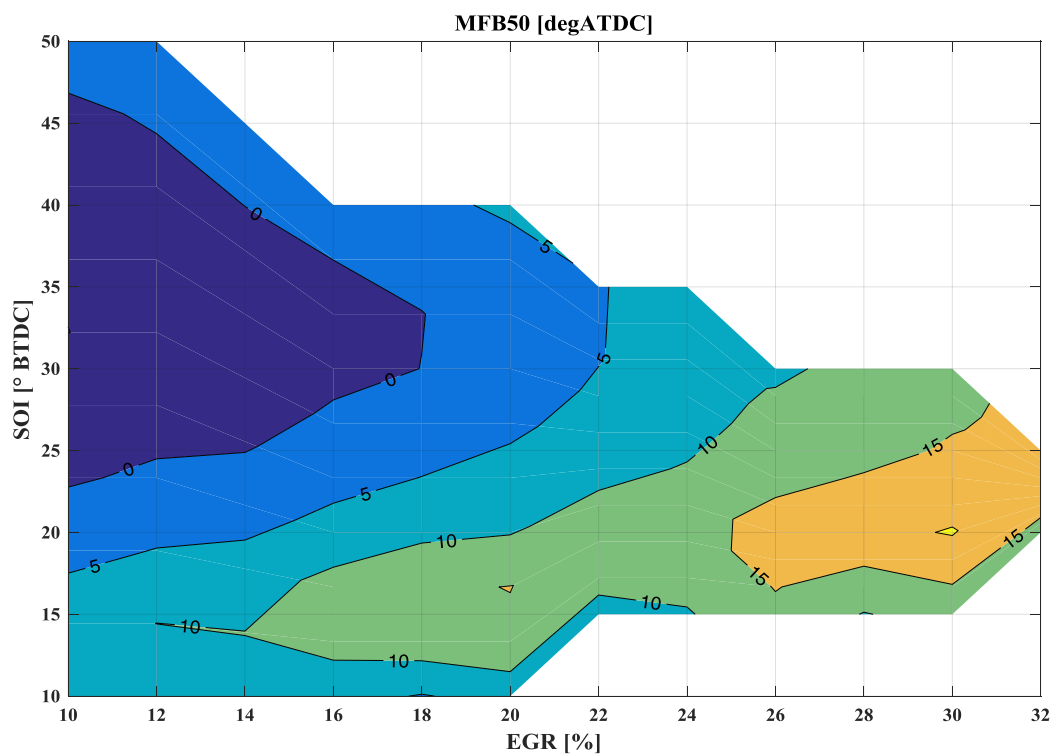
Figure 3.5: RCCI 2000rpm 3bar BMEP 70% gasoline, MFB50

63

Figures 3.1 to 3.5 provide an initial idea of which are the benefits using an RCCI injection strategy. It is quite remarkable that some regions exist where brake specific fuel consumption resembles the one obtained with conventional diesel combustion but with a great gain on the critical diesel pollutant emissions such as nitrogen oxides and PM which almost vanishes (namely FSN is reported, but literature evidences the good correlation occurring between FSN and PM). However, a huge increase in unburnt hydrocarbon (HC) concentration is detected (here measured with a compact exhaust gas diagnosis system, AVL DiTest Gas 1000). When interpreting these results, it has to be taken into account that conventional diesel combustion produces ultra-low HC emission, thus when this value is used as a term of comparison a twenty-times greater measure can be considered as not worrying. In addition, the environment is globally lean, so the HC part in exhaust gases could be easily abated with an oxidation catalyst to be fit in the exhaust pipe.

Combining the data shown by Figure 3.1 Figure 3.3 and Figure 3.5 an interesting phenomenon can be observed: first of all NOx concentration is quite well-correlated with the combustion phase as it will be investigated later on, secondly the behavior of MFB50 itself splits the investigated field in two parts. In the first one, bottom part of the above graphs, MFB50 "follows" the direct injection timing, then it reaches a minimum value, depending on the EGR valve opening, and begin to move in the opposite direction as SOI is furtherly advanced. This inversion zone determines a more efficient combustion as the upper part in Figure 3.1 proves. All these things considered, a convenient region can be highlighted (Figure 3.6).
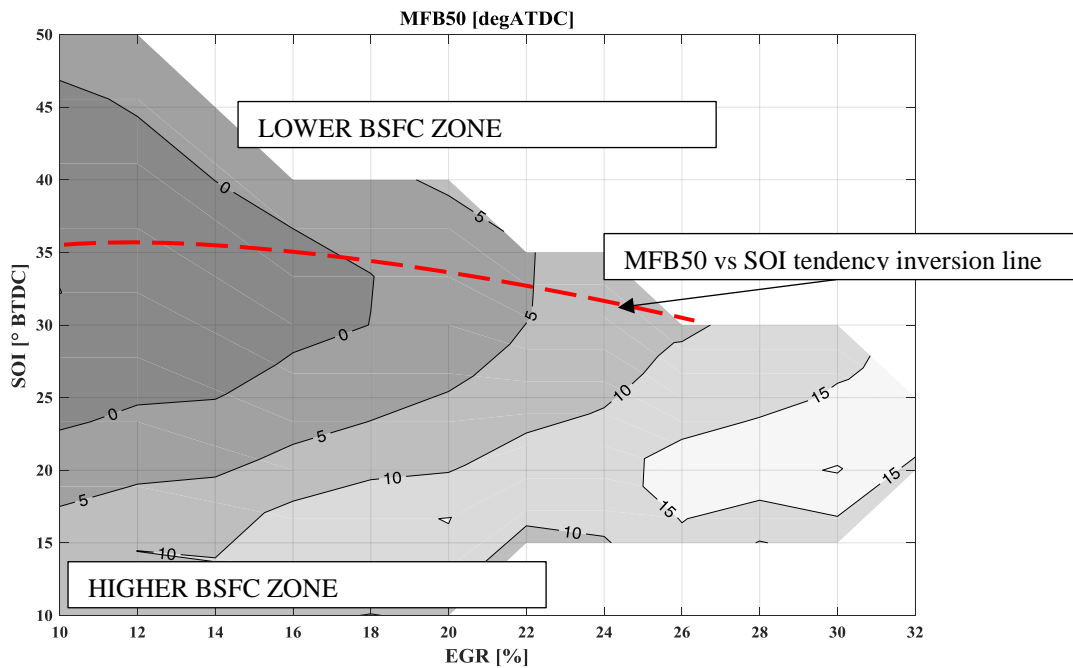
Figure 3.6: Operating regions

To put in evidence the changes combustion undergoes while SOI is varied, Figure 3.7 reports in-chamber pressure and rate of heat release (curves are an ensemble average over 150 cycles) when EGR is maintained at 10%.
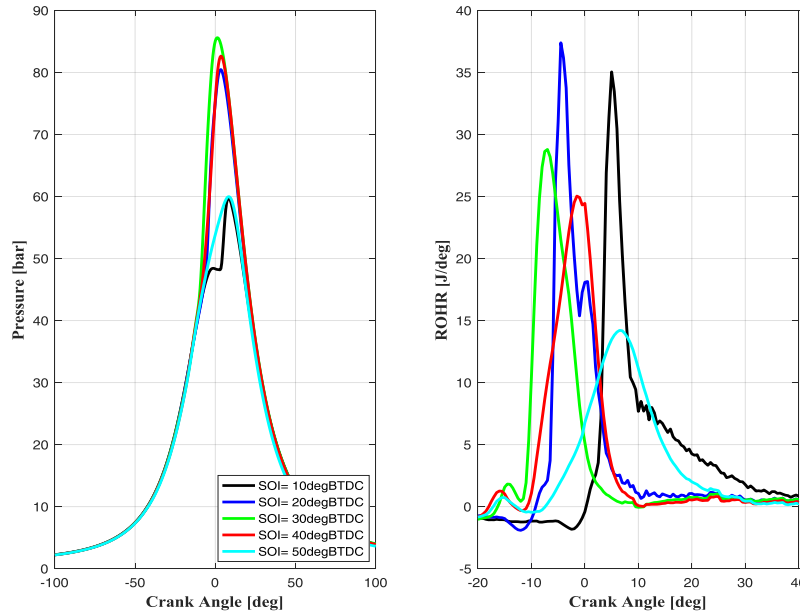
Figure 3.7: SOI influence on heat release, EGR 10%

Observing the right section of the figure it is clear that comparing ROHR before and after the inversion in MFB50 combustion behaves differently even if combustion phase reaches the same value. Regarding the effects of increasing the amount of EGR a retard on combustion center is detected, as the combustion velocity tends to slow down (Figure 3.8).
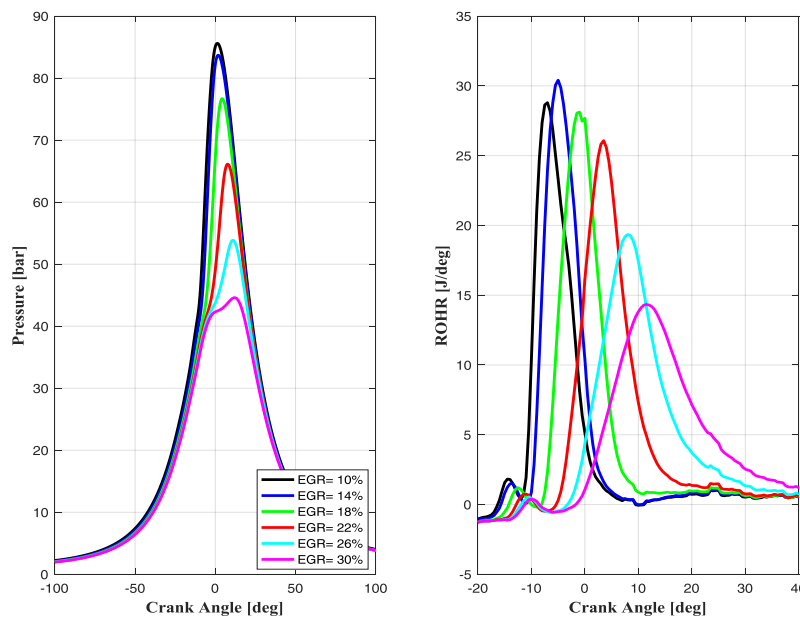
Figure 3.8: EGR influence on heat release, SOI 30 degBTDC

This last consideration has to be interpreted by taking into account that VGT position has been always kept constant, though EGR reduction determines not only a growth in the fresh air breathed (AirQ) but also an increase in boost pressure (which certainly affects mixture reactivity) as Figure 3.9 testifies.
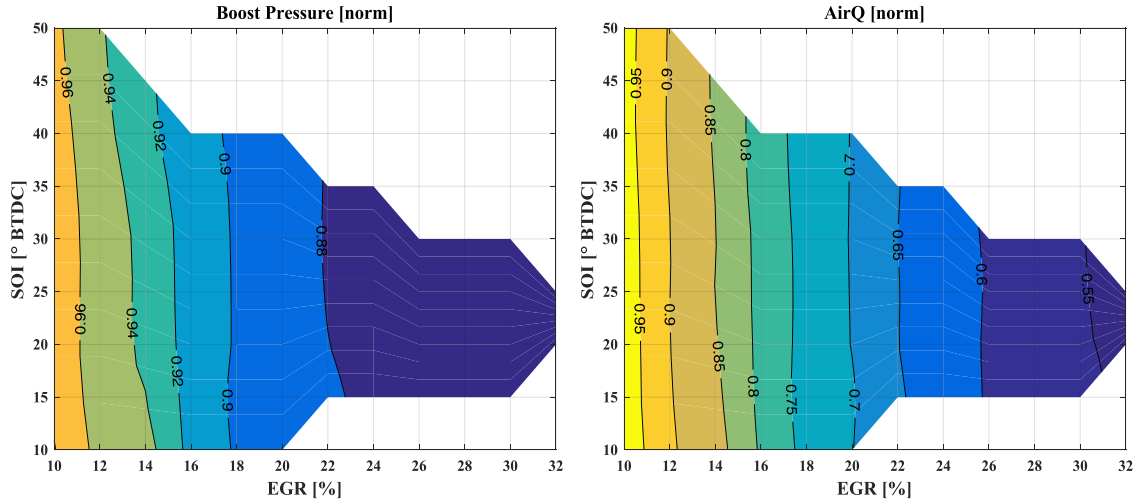
Figure 3.9: RCCI 2000rpm 3bar BMEP, Boost pressure and fresh air mass flow rate normalized by reference CDC values

In order to complete the analysis of this operating condition two more parameters have to be observed being potentially useful to quantify combustion stability from one side and its knocking tendency from the other. IMEP coefficient of variation (CoV) defined as the ratio between the standard deviation and the mean value over a 150 cycles buffer is reported in Figure 3.10 while peak pressure rise rate (PPRR) is shown in Figure 3.11.
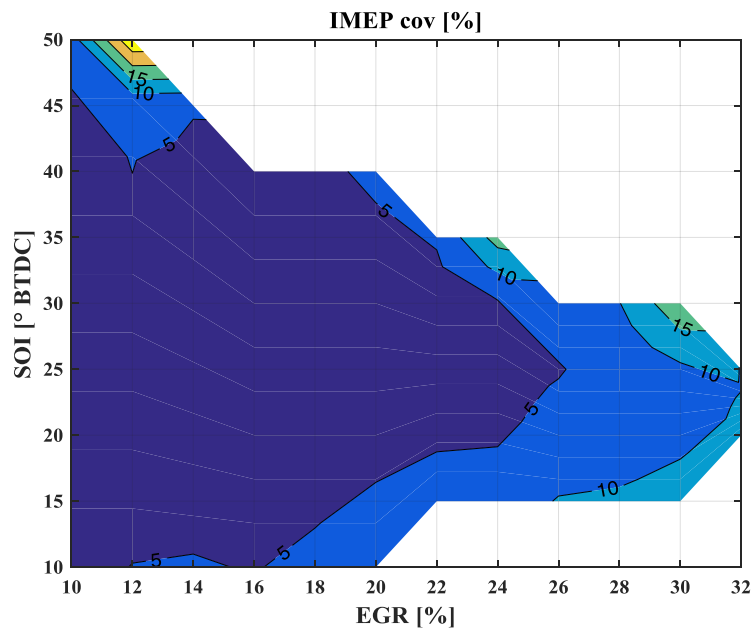
Figure 3.10: RCCI 2000rpm 3bar BMEP 70% gasoline, IMEP coefficient of variation
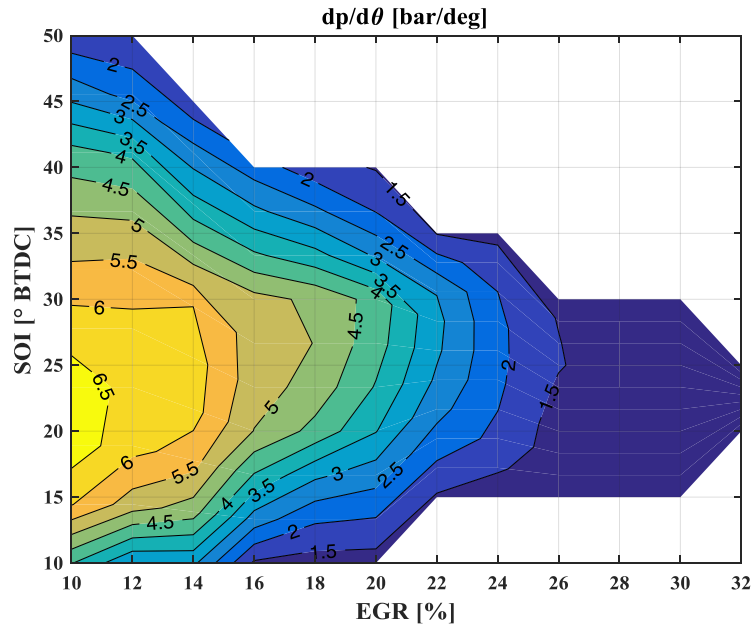
Figure 3.11: RCCI 2000rpm 3bar BMEP 70% gasoline, PPRR

These variables are shown in their respective absolute value (not normalized with respect reference CDC value) since it could be more significant. However, it has to be considered that IMEP CoV in CDC operating condition is equal to 5% and PPRR almost 2.5 bar/deg, thus every region where PPRR exceeds 5 bar/deg can be identified as potentially worrying, recalling that load is very low in this functioning point. Analyzing the information provided by the last reported indices, in the region of interest starts becoming definite a zone where the combustion is stable (IMEP CoV resembling CDC value) and not problematic from the PPRR point of view. Both these indices exhibit a good correlation with respect to MFB50 (Figure 3.5), thus combustion phase assumes a key role as a synthetic index to describe combustion stability (as well as combustion efficiency). Moreover, PPRR can explain the link existing between MFB50 and the amount of NOx produced, since a more impulsive combustion is expected to generate higher local temperature directly implying nitrogen oxides origination according to Zel'dovich mechanism.

Until now, data related to a single injected mass split (70% gasoline) have been discussed. To examine the effects of a different energy repartition between the high reactivity fuel and the low reactivity one an analogous experimental activity has been carried on but keeping the amount of gasoline equal to the 80% of the total fuel mass. Results are shown in the following figures.

67
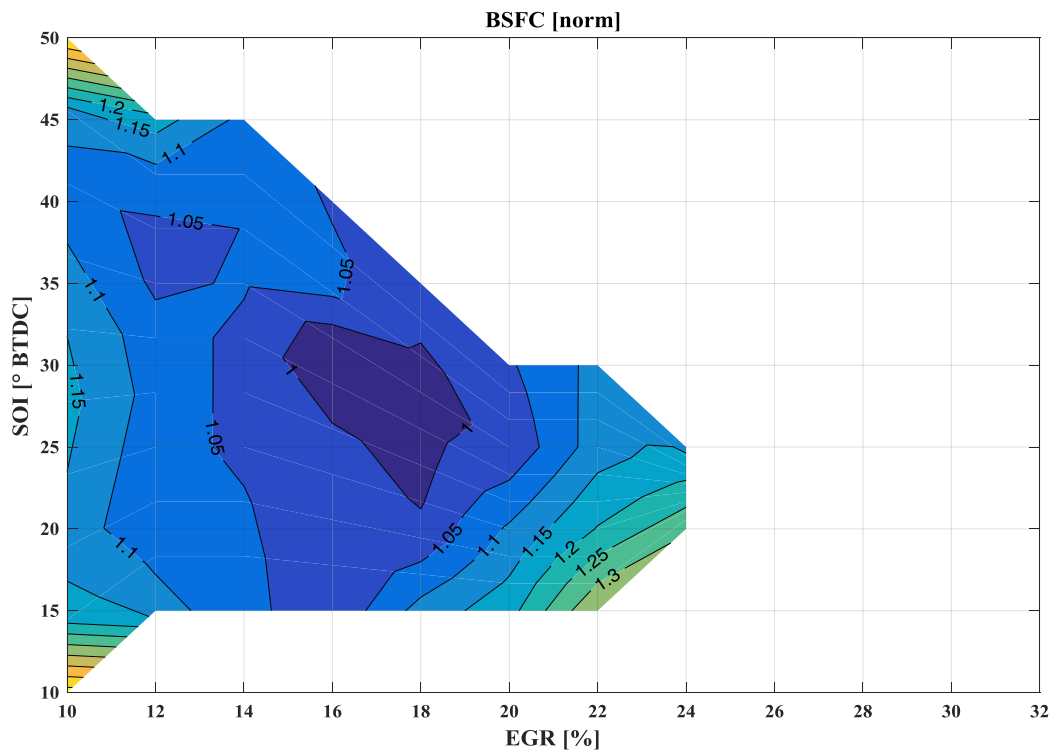
Figure 3.12: RCCI 2000rpm 3bar BMEP 80% gasoline, BSFC variation with respect to reference CDC operating condition
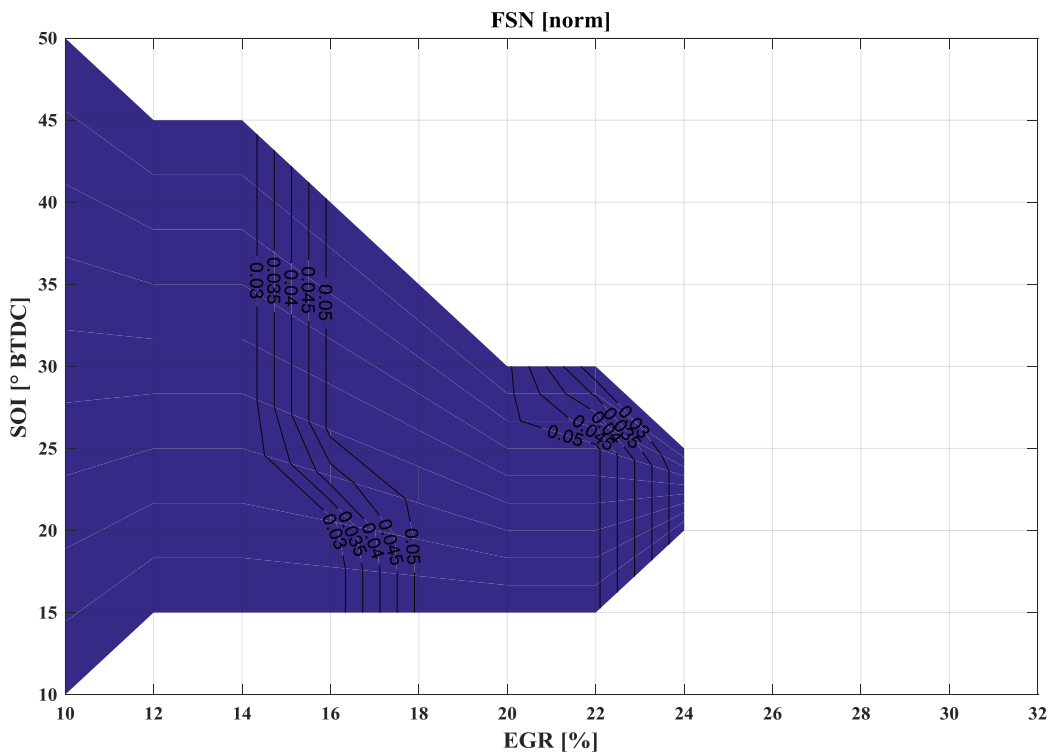
Figure 3.13: RCCI 2000rpm 3bar BMEP 80% gasoline, FSN variation with respect to reference CDC operating condition
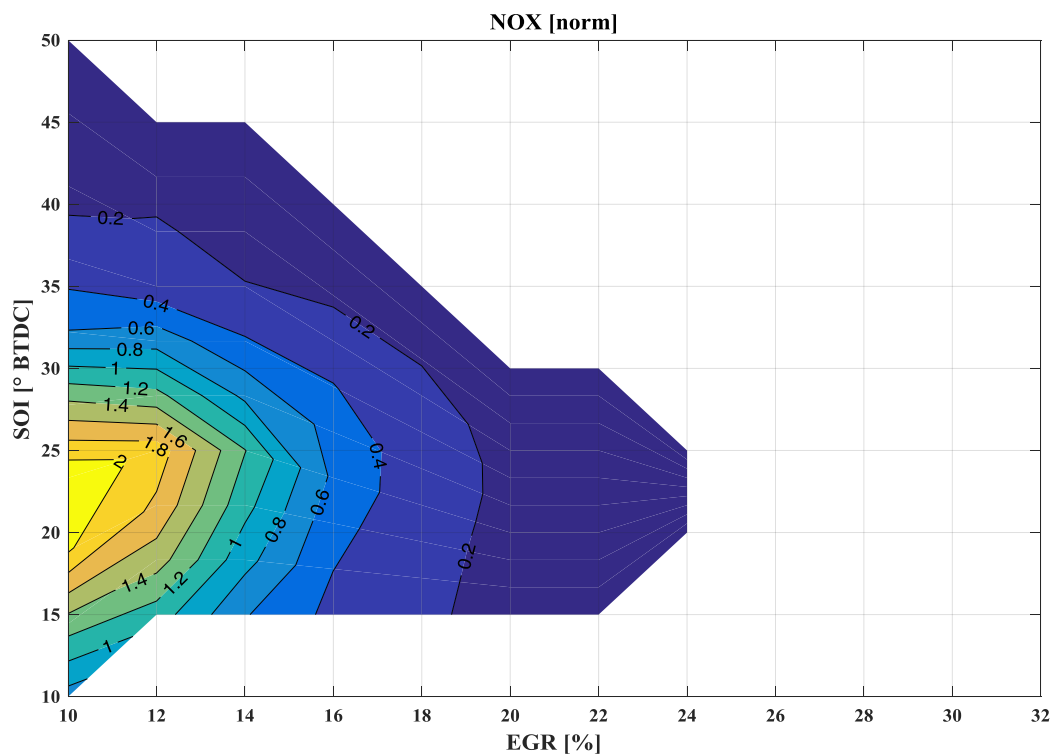
Figure 3.14: RCCI 2000rpm 3bar BMEP 80% gasoline, NOx variation with respect to reference CDC operating condition
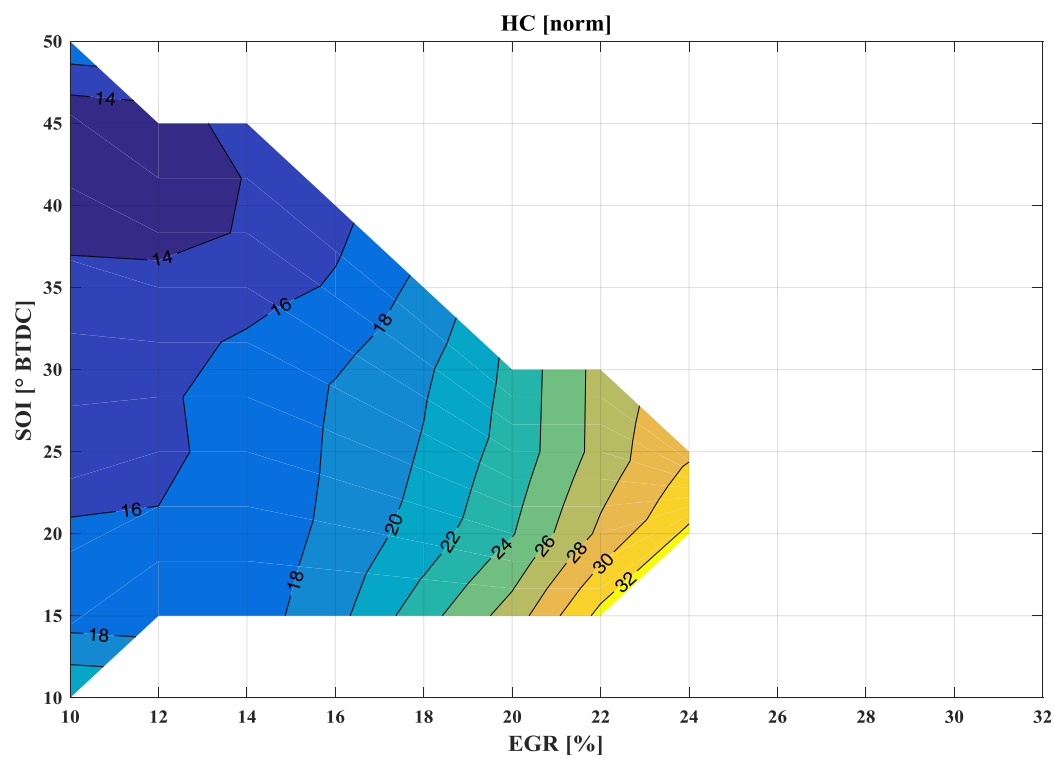
Figure 3.15:RCCI 2000rpm 3bar BMEP 80% gasoline, HC variation with respect to reference CDC operating condition
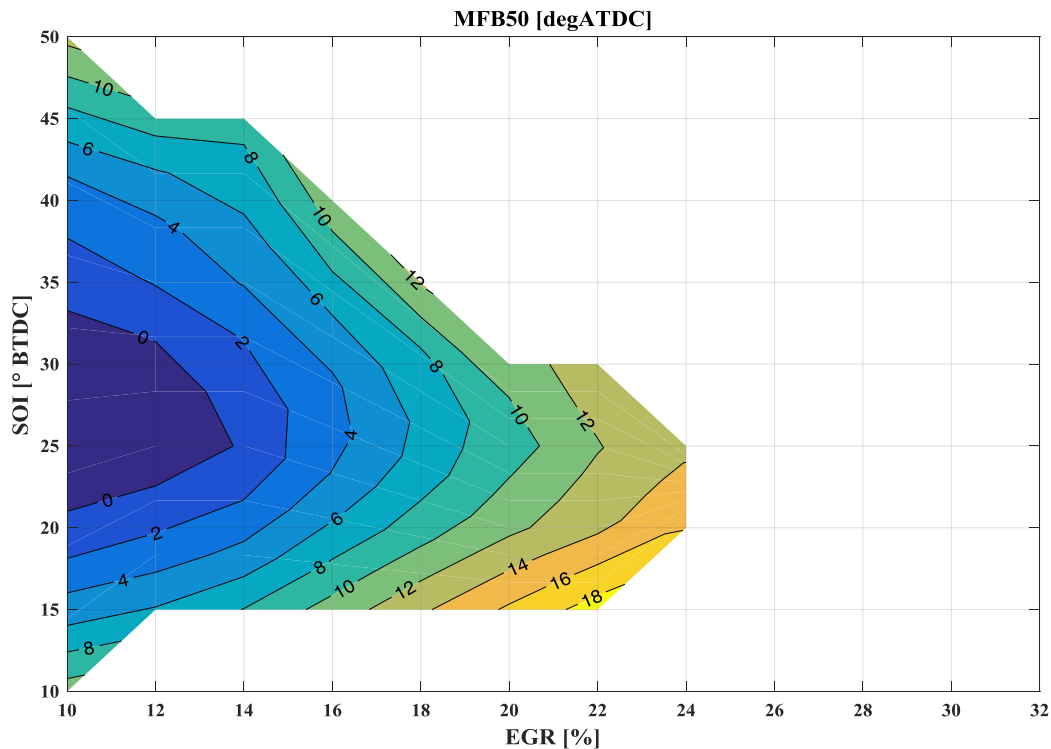
Figure 3.16: RCCI 2000rpm 3bar BMEP 80% gasoline, MFB50

The same trends seen in the 70% gasoline tests are confirmed, but the effects gasoline has on pollutant emissions is enhanced, as expected: lower NOx and higher HC concentration are observed. MFB50 "dual" behavior is as well detected.

The key thing to be noticed, comparing the two sets of tests with different amount of gasoline to diesel ratio, is the extension of the region of stability in the SOI, EGR plane. In the latter condition, the introduced EGR mass cannot be forced to be as high as the one reached in the 70% gasoline experimental plan, since the lower injected diesel mass tends to decrease mixture reactivity, thus a greater level of combustion dispersion is present (Figure 3.18).

The effects of combustion velocity decrease when mixture is less reactive, at even air-related variable condition, can be seen also by analyzing peak pressure rise rate (Figure 3.17), whose values are lower with respect to the previous case.

These considerations show how the quantity split between the two fuels is an effective control parameter, because relatively small changes (10%) have a significant effect on combustion, in general, adding gasoline makes combustion velocity lower independently of combustion phase, because of the fewer ignition sources. This is a good manner to control PPRR, but the increased cyclic dispersion has to be taken into account.
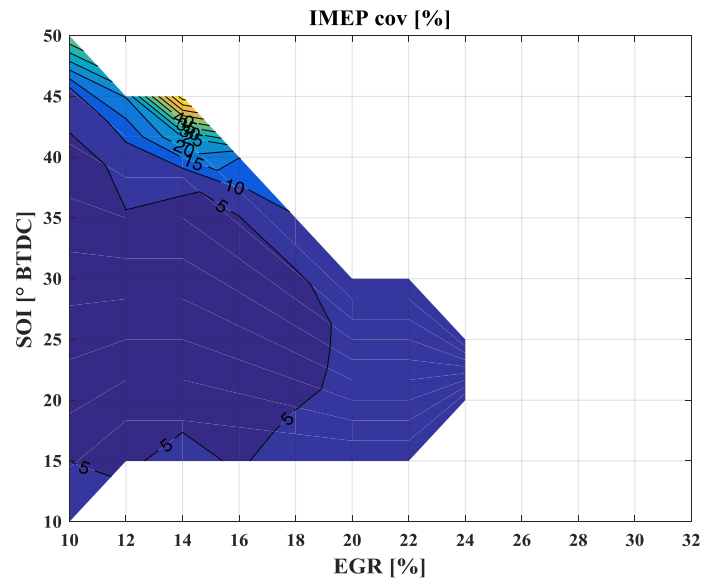
Figure 3.18: RCCI 2000rpm 3bar BMEP 80% gasoline, IMEP coefficient of variation
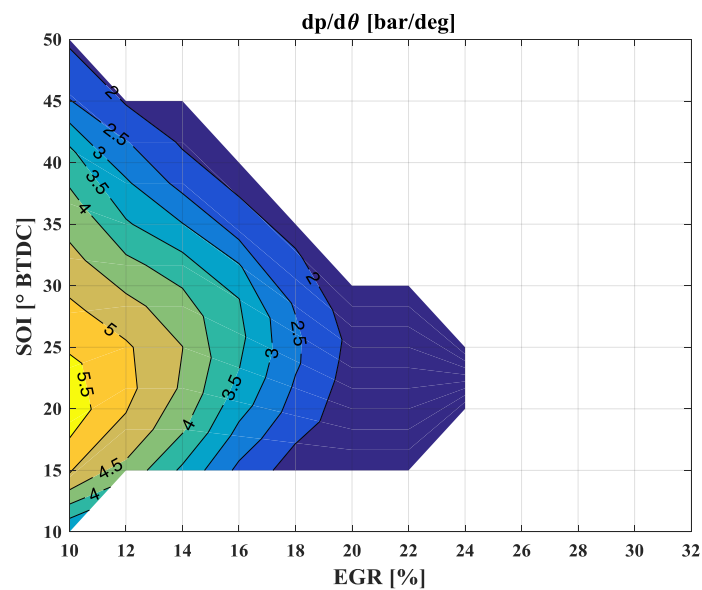
Figure 3.17: RCCI 2000rpm 3barBMEP 80% gasoline, PPRR

Concerning the first analysis related to the 2000rpm 3bar BMEP operating point the following conclusions can be stated:

- The presence of a low reactivity fuel, which is port injected, allows the formation of a homogeneous mixture whose ignition is guaranteed by a small diesel injection has proven to provide significant advantages on the pollutant species typical of a CI engine.
- Hydrocarbon component has been acquired to be significantly higher with respect to the standard diesel combustion, but it is a less critical specie because of the way it can be reduced in a lean environment.

71

- Brake specific fuel consumption has found to be very influenced by combustion phase, as one can expect, but advantages are present if the target MFB50 is reached by actuating an advance injection, implying higher ignition delays thus diesel premixing.

- Increasing gasoline percentage is useful to obtain performances nearer to a homogeneous, fully premixed, combustion as a higher gain on NOx has been detected. From a combustion control point of view, a larger amount of gasoline moves the combustion phase to larger MFB50 values and worsen the IMEP standard deviation.

- The same tendency in retarding MFB50 is present if the amount of EGR is increased when the VGT position is kept constant, causes are to be identified in the lower boost pressure and oxygen presence, decreasing mixture reactivity even if warmer charge is breathed.

- The minimum level of the acquired BSFC can be compared to a conventional diesel combustion mode and are obtained with an EGR percentage being a trade-off between the excessively retarded combustion and a useless boost pressure. Higher BSFC levels when EGR valve has been kept to 10% are due to the efficiency losses of a greater pumping cycle.

- Peak pressure rise rate is quite well correlated with NOx, as previously discussed. Although IMEP CoV exhibits a drastic decrease if PPRR is higher, the values that have been reached may be worrying if load is increased, placing this variable as a possible limiting issue. A potential combustion phase control should take into account these phenomena.

- SOI has demonstrated to be an efficient control lever to manage MFB50, however the optimal SOI value (namely the one guaranteeing the optimal combustion phase) is very sensitive with respect to the surrounding conditions (air quantity, boost pressure, gasoline/diesel split).

RCCI: 2000rpm 5bar BMEP

In the second engine operating point examined, the total injected mass has been increased, then, the same dependencies have been searched. From the test conduction point of view, it has not been possible to perform systematic acquisitions in the whole experimental plane (EGR, SOI) as the ones reported above for the 3bar case. The reasons limiting the investigation are the insurgence of excessive PPRR or knocking conditions in the advanced MFB50 zones and the very high sensitivity of combustion with respect to surrounding conditions in the high ignition delay region. Therefore, the two regions where MFB50 has shown to behave in the opposite way while SOI is varied, have been analyzed separately.
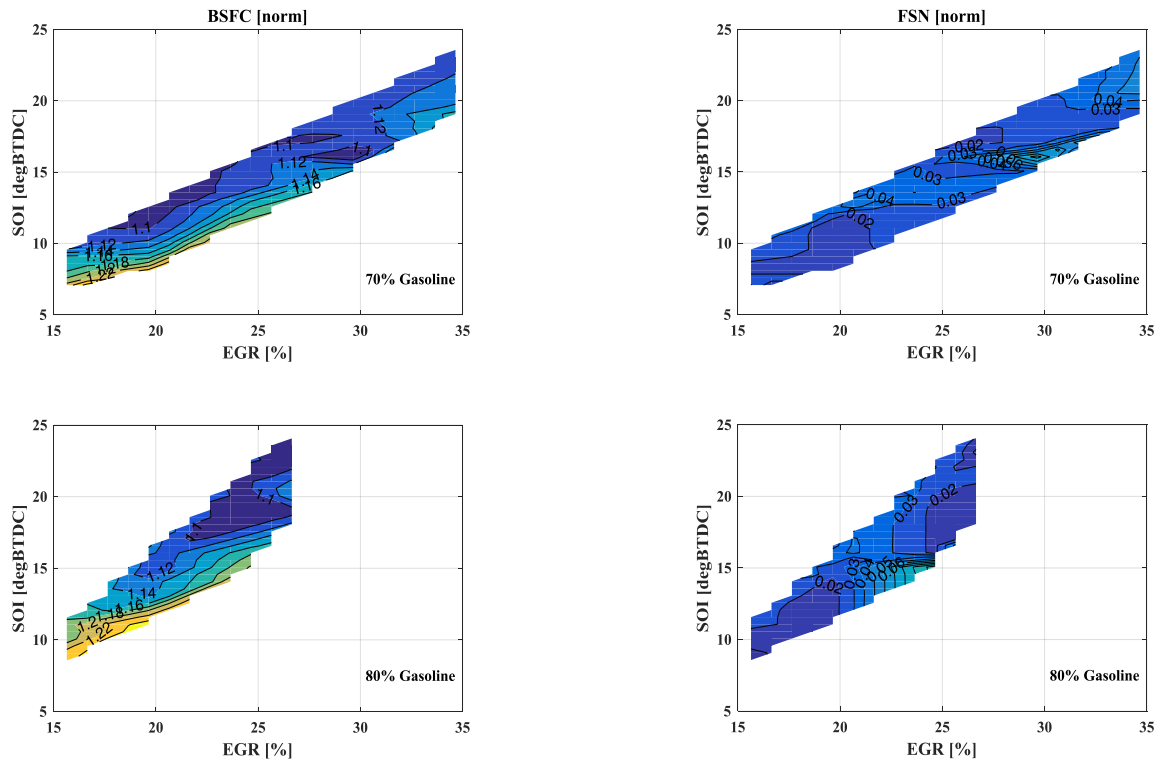
Figure 3.19: RCCI 2000rpm 5bar BMEP, BSFC and FSN norm wrt CDC
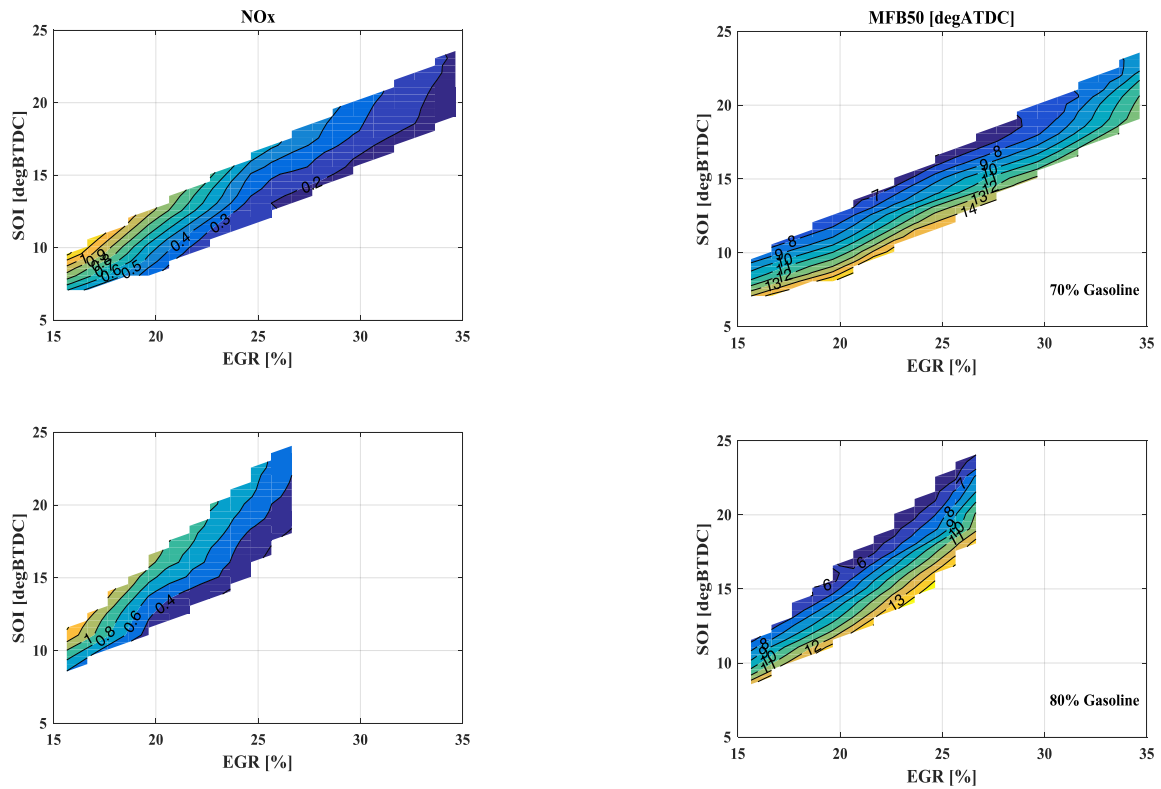
Figure 3.20: RCCI 2000rpm 5bar BMEP, NOx norm wrt CDC and MFB50
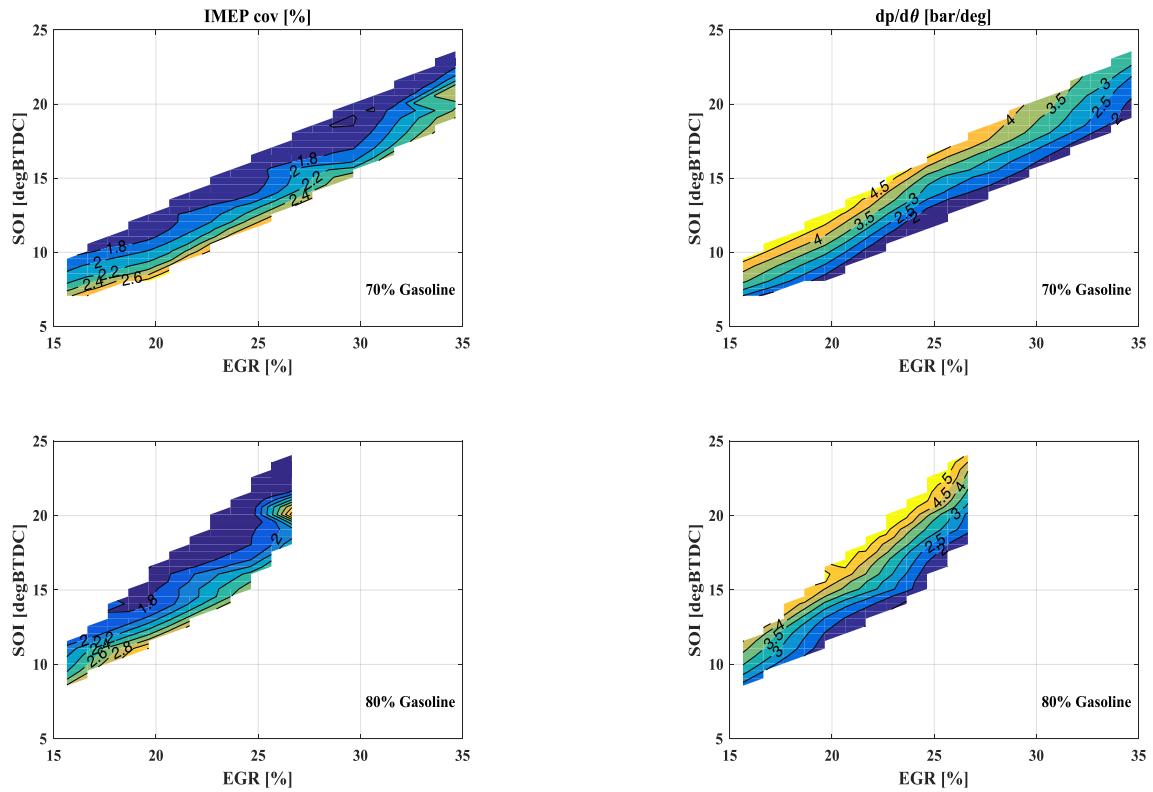
Figure 3.21: RCCI 2000rpm 5bar BMEP, IMEP CoV and PPRR

Figures from 3.19 to 3.21 reports the main variables of interest tendencies in the low ignition delay zone, which is the one exhibiting a conventional correlation between SOI and MFB50. Two combination of energy split between the two fuels have been tested (70% and 80% gasoline to total mass ratio). Results are similar to the ones obtained in the previous treated case, since an advantage is present concerning the pollutant emissions, but BSFC is considerably higher with respect to the standard diesel combustion delivering the same amount of torque, even in the optimal combustion phase conditions. Increasing the amount of gasoline improves this aspect, but not as much as it would be required to reach CDC performances. However, in this region a desirable comportment of combustion phase is detected, since it can be easily controlled with SOI: a very repeatable and consistent behavior of MFB50 has been observed while the direct injection timing is varied. The optimal SOI value, namely the one guaranteeing the MFB50 at which the BSFC is at its minimum, is very influenced by EGR. A consideration has to be made regarding the independent effects that could be achieved by varying EGR and SOI. This analysis shows that every potential target on synthetic combustion indices can be accomplished by moving only one of the parameters under study, in this sense it is much preferable controlling combustion using SOI because of its higher determinism and precision deriving from the common-rail system as well as the possibility to perform cycle-to-cycle corrections, improving control dynamic. The

only effect on which EGR can be considered independent from SOI is NOx concentration, as a greater EGR valve opening tends to reduce NOx regardless of the adopted SOI. Finally, as the previous test at lower load has shown, moving to a higher gasoline percentage is beneficial from the BSFC point of view, but makes the available operating plane smaller, because combustion stability worsening.

As an example, on how heat release and combustion indices are influenced by SOI variations, Figure 3.22 shows in cylinder pressure and ROHR for each SOI value tested at 25% EGR and 80% gasoline (being the optimal conditions for BSFC). On the right-hand side, it could also be noticed the dependencies linking IMEP and PPRR to MFB50. Indicated mean effective pressure, in particular, has demonstrated a behavior that can be considered similar to a spark-ignited (SI) engine, here the optimal MFB50 value can be easily identified to be almost 7.5deg ATDC.
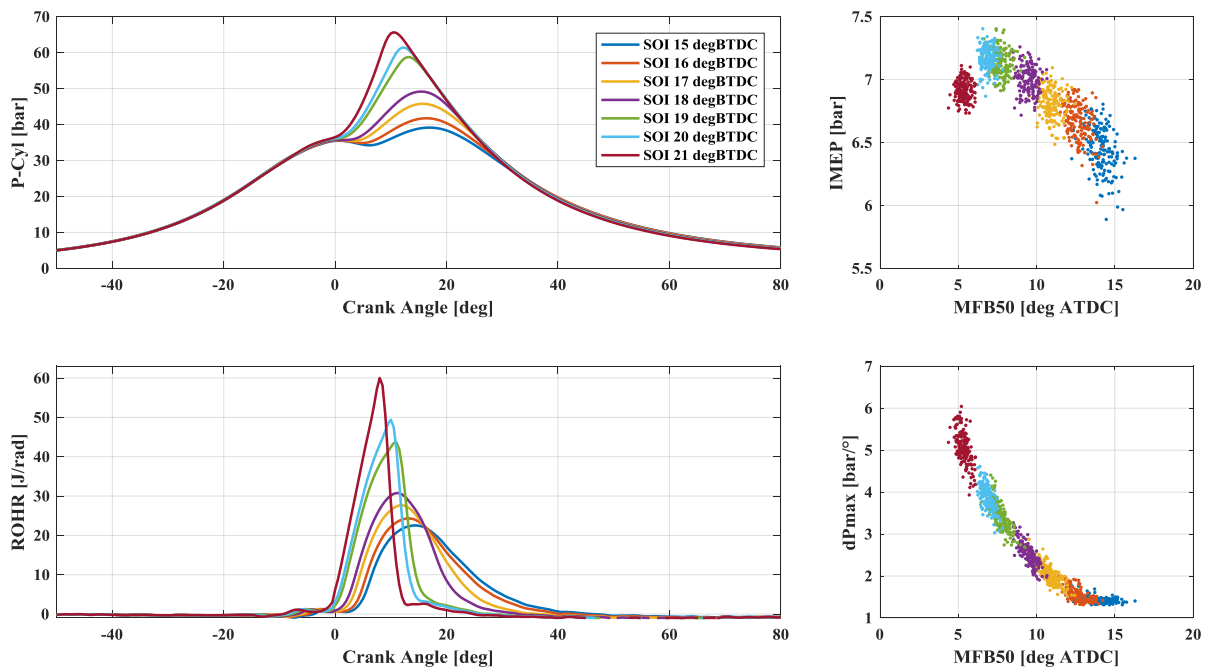
Figure 3.22: RCCI 2000rpm 5bar BMEP 80% gasoline 25% EGR, heat release comparison

The analysis of the high ignition delay zone (the region in which MFB50 has shown an inverted correlation with respect to SOI) is more critical: in this operating condition it has been harder to obtain a stable combustion on all the four cylinders than in the 3bar BMEP case, thus the acquired points are not sufficient to build a 2D map as the ones reported above.

Here, the 80% gasoline case only is reported, because the previous tests have suggested trying to keep gasoline percentage as high as possible, as long as combustion can be maintained stable. Investigated EGR values are 0% and 15%, but in this case VGT position has been changed to lower the turbine inlet pressure while EGR valve has been forced to close, because it would have

generated unnecessary boost (which is costly from the pumping cycle point of view in this operating condition).

Variables of interest are reported in Figure 3.23 and Figure 3.24.
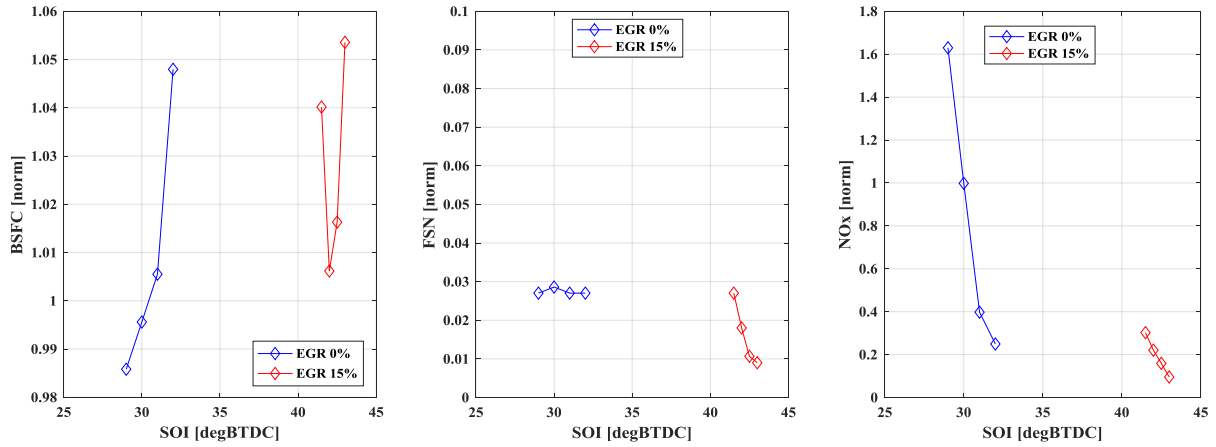
Figure 3.23: RCCI 2000rpm 5bar BMEP 80% gasoline, efficiency and emissions in the high ignition delay zone
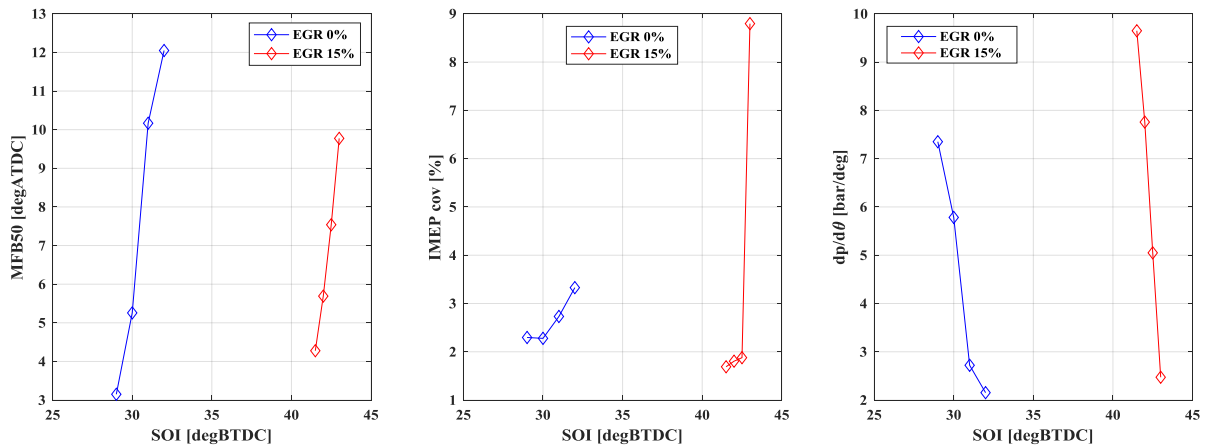
Figure 3.24: RCCI 2000rpm 5bar BMEP 80% gasoline, combustion indices in the high ignition delay zone

The first thing to be noticed is how BSFC behaves, which, in this case, reaches values comparable with conventional diesel combustion. At the same time, the advantages on FSN and NOx are still present, even if NOx emission are similar to CDC in the 0% EGR case if PPRR is not properly controlled. These two effects allow identifying this region in the EGR, SOI plane as the convenient one, providing significant improvements over conventional diesel combustion, considering that the same result has been obtained in the lower load condition.

Nevertheless, the 5bar BMEP points highlights a very critical issue when load increases, being the narrowing of the combustion stability region existing between excessive PPRR and undesired CoV which is even worsened by the introduction of EGR.

Figure 3.24 reports very significant indices of the critical aspects subsisting in this operating point:

- Very high sensitivity of MFB50 with respect to SOI;
- Great SOI variations to get the optimal MFB50 while EGR is varied;
- Narrow SOI range taking knocking combustion to misfire (particularly evident in the red curve, in rightmost plots).

The first two points are the reasons why a base calibration of this kind of combustion is hardly obtainable: the optimal SOI values are strongly influenced by the surrounding conditions and potentially hazardous events can occur if the desired SOI is missed by few crank angle degrees.

The third point represents the load limit existing by running the engine in RCCI mode, since the cited range tends to become smaller as the injected mass is increased. It must be recalled that no combustion chamber design optimization has been done, and it could beneficially affect this phenomenon.

In Figure 3.25, in-chamber pressure and heat-release curves shows the effects of four degCA SOI variation in the 0% EGR condition, here considered as optimal because of stability reasons, even if the 15% one is better performing on NOx concentration.
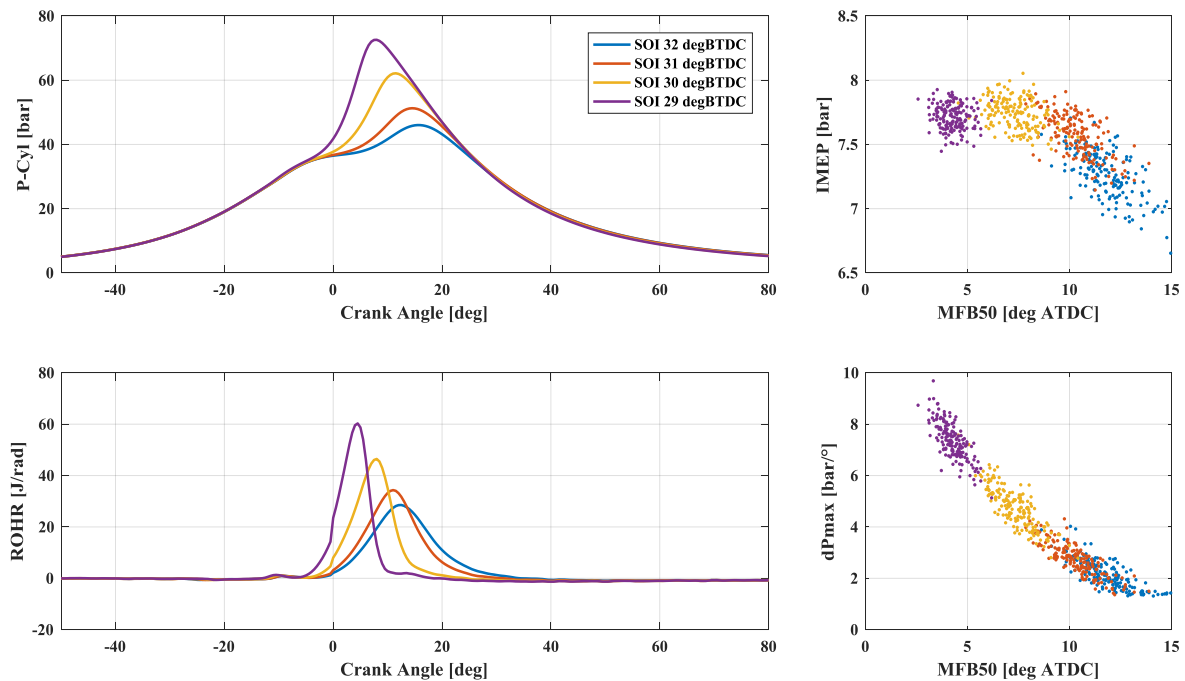
Figure 3.25: RCCI 2000rpm 5bar BMEP 80% gasoline 0% EGR high ignition delay zone, heat release comparison

In order to conclude the analysis of the sensitivities RCCI combustion has shown with respect to the main control parameters, it has to be stated that the 5bar BMEP operating point has confirmed every consideration listed at the end of the previous subsection, dealing with the 3bar BMEP one.

In addition, as just discussed, load is critical from the combustion stability point of view in the SOI zone where the RCCI combustion has proven the best performances (high ignition delay).

Qualitative speaking, Figure 3.26 sketches how combustion phase behaves while EGR and SOI are varied and gasoline to total mass ratio is fixed.
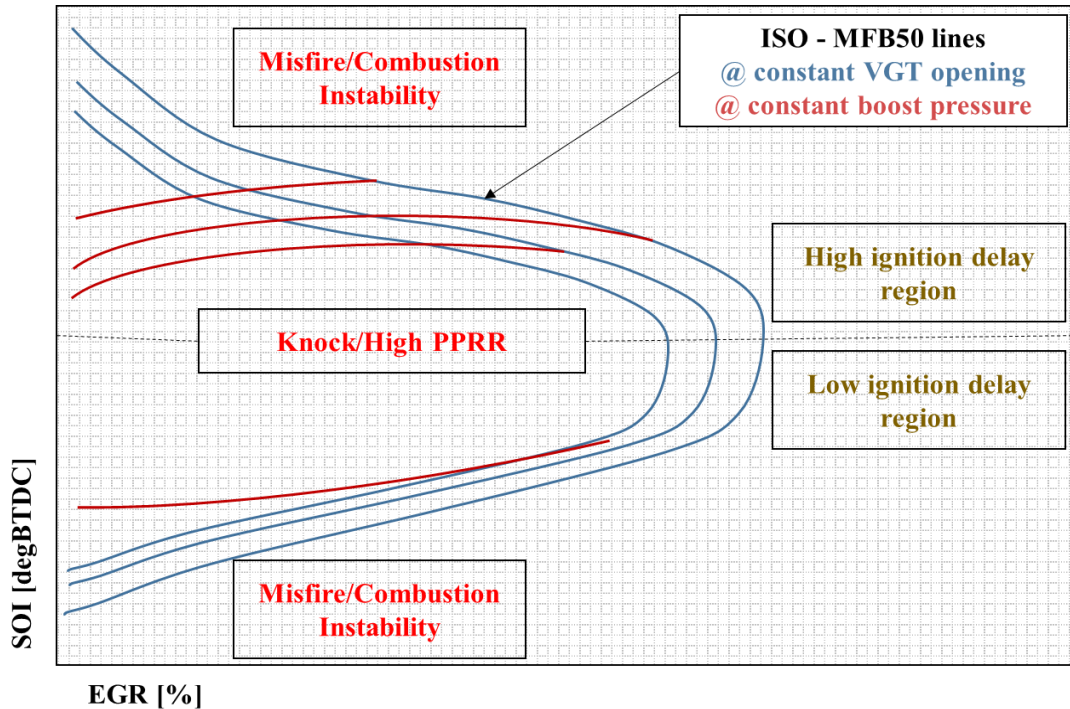
Figure 3.26: RCCI qualitative operating (SOI, EGR) plane

In particular, lines represent the points locus where the combustion phase remains at the same value. Blue ones depict an experiment plane similar to the one seen in the description of the 3bar BMEP case (constant VGT position), red ones illustrate what happen if the VGT system is set to generate lower turbine inlet pressure while EGR valve is closed, in order to maintain a constant boost pressure. This solution is valid because of the gain on BSFC previously discussed.

Considering the tendency in getting tighter of the stability region present between the high PPRR zone and misfire one in the high ignition delay region, the next step that has been performed, has regarded the development of a closed loop combustion phase controller, aimed at making RCCI functioning more robust, by adjusting DI SOI in order to follow a MFB50 target. This solution has allowed a further improvement also on the crucial aspects of balancing cylinders, since the controller works independently for each cylinder. Details are discussed in the next section.

RCCI closed loop combustion phase control

Previous section has highlighted the most critical characteristics of a RCCI combustion, mainly regarding combustion instability and over-sensitivity to environmental conditions. To overcome

these issues, the adopted approach has been the construction of a closed loop combustion controller, since the test bed facilities allow the real-time processing of indicating feedbacks as already seen for the conventional diesel combustion case [26,27].

In this section, a global description of the code allowing RCCI operation and its interface with engine standard ECU is firstly reported, then the structure of the implemented MFB50 controller is presented, finally considerations on remote combustion sensing are made, in order to feed the controller with data whose source is independent from in-cylinder pressure sensors [28,29,30].

Global RCCI control algorithm description

The interface between the RCP system and the engine ECU is illustrated in the first chapter, in this context the variables exchanged between the two real-time targets during RCCI operation are the whole dataset schematized in Table 1.3. In fact, the code running inside the RCP system has to be aware of the reference CDC actuations in a determined operating condition to manage the CDC to RCCI transition and vice versa. At the same time, it must be able to completely overwrite the injection pattern as well as the commands related to the EGR valve and VGT position. While the direct injection parameters can be forced via CAN protocol, EGR and VGT position are managed exploiting the ASAM/ASAP communication linking the TBCS and the INCA software: the RCP commands an air mass flow target and a VGT position (or boost pressure target) to the TBCS system that forward the requests to the ECU (via INCA).

The control architecture in RCCI operating mode relies on a base structure based on feed-forward contributions mapping of the main engine control parameters in function of engine speed and load. In particular, air related quantities and rail pressure are time-based computed at 100 Hz while the direct injection timing and energizing time as well as the port fuel injectors energizing time (thus the energy split) is calculated cycle by cycle for all the four cylinders. PFI rail pressure and injection timing are kept constant since negligible sensitivity has been noticed with respect to these factors.

Diesel SOI, which has been identified as one of the key parameters to control the RCCI combustion is furtherly corrected by a closed loop contribution which could either be fed by the indicating data or an estimation algorithm and includes protection from both knocking combustions and misfire/inefficient combustions. An adaptive look-up table is present to store closed loop contribution history and learn an improved open loop value.

The complete representation of the algorithm can be seen in Figure 3.27.
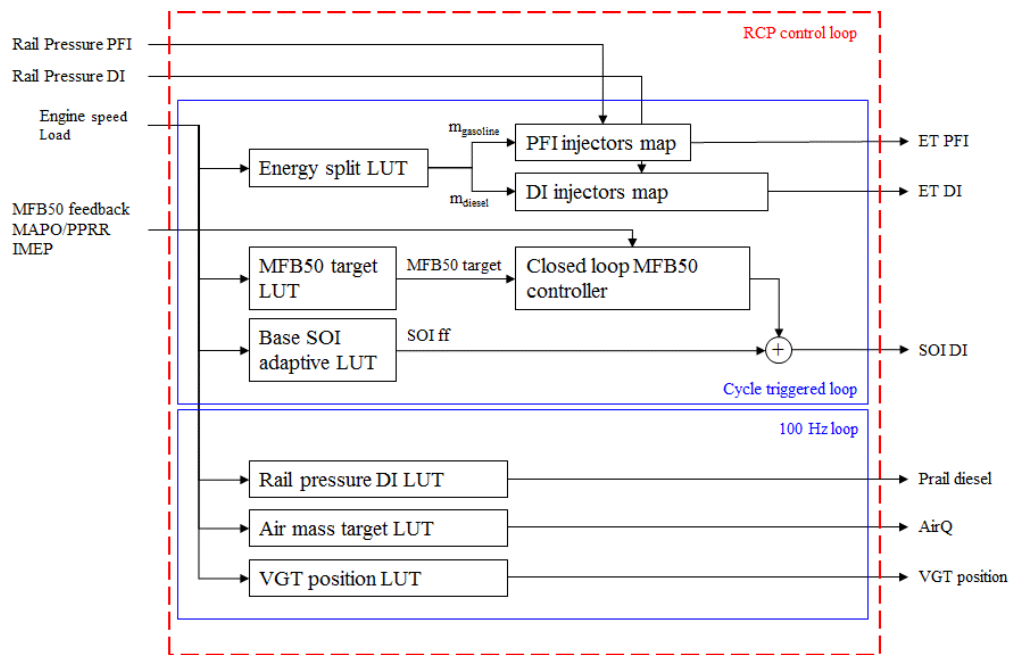
Figure 3.27: RCP control loop in RCCI operating condition

In order to manage the transition between CDC and RCCI mode a parallel loop has been added including a Simulink model which allows performing the right sequence of operations to smoothly reach the specific actuations target defined by the main control loop. In CDC operating mode parameters read by ECU are simply sent back to it.

Closed loop MFB50 control

As already discussed, an efficient combustion phase management is crucial because every parameters of interest regarding performances and stability is strongly related to MFB50. In addition, Figure 3.24 reports an example on how steep are the tendencies linking the combustion indices and the control variable, making an open-loop only approach a hardly applicable approach.

Figure 3.28 reports an example of which is the available operating range in terms of MFB50 for a 2000rpm, 5bar BMEP 70% gasoline operating condition.

The natural solution to this issue is the adoption of indicating data as feedbacks to accomplish a specific target in terms of MFB50. The following diagram represents, more in detail how SOI is managed to reach a stable operating condition.

Figure 3.29 shows the structure of the discussed algorithm. As it can be noticed the core of the closed loop correction is a PID regulator, which targets a MFB50 (which is calibrated in function
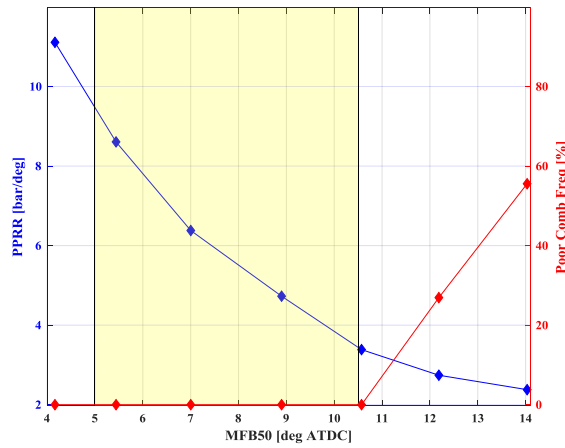
Figure 3.28: example of the RCCI available operating range in terms of MFB50, 2000rpm 5bar BMEP

od engine speed and load). The feedback of the regulator is the average of the measured MFB50 values over a determined buffer including normally 20 to 50 cycles. MFB50 is measured and published on CAN bus cycle by cycle, the control algorithm thus includes in the buffer only cycles considered as "valid" (not affected by very poor combustion making MFB50 value not significant).
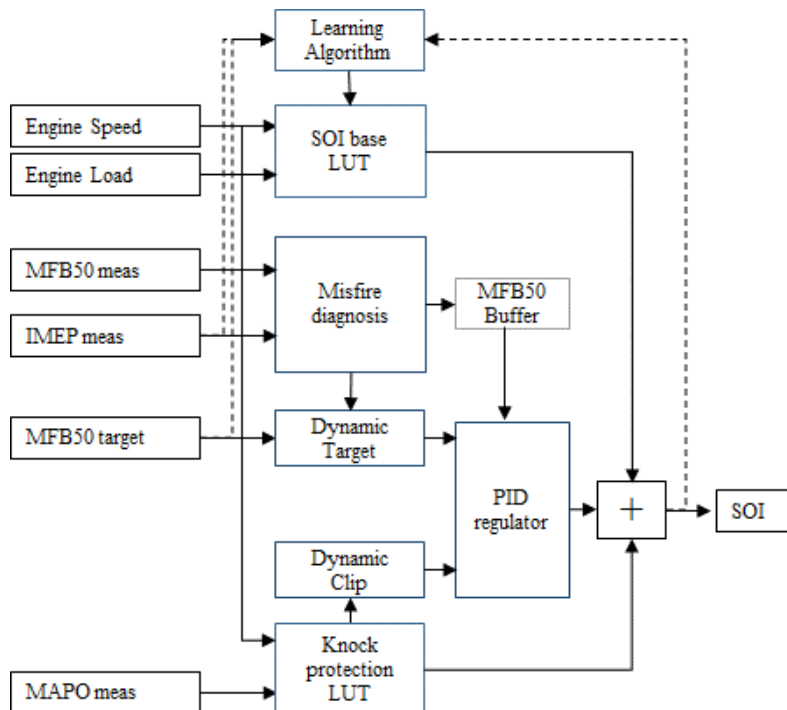
Figure 3.29: SOI management algorithm

As previously noticed, in the region of interest (high ignition delay) the PID gains must be calibrated in order to obtain an advance of SOI when the combustion is wanted to retard.

81

Two dynamic corrections on PID parameters are present aimed at protecting the engine from dangerous conditions, namely knock and misfire.

- Concerning knock, a dynamic lower clip has been developed limiting PID output to values greater than a threshold deriving from the interpolation of a look-up table depending on a knock index and engine speed (recall that the lower SOI, expressed in deg BTDC, mean more advanced MFB50 and impulsive combustion). Here MAPO is used, but it can be substituted by other kind of indices well correlated with combustion impulsivity or knock as shown later. The dynamic clip acts as a "saw-tooth" profile triggered by a knock event and gradually brought back to its original constant value. The necessity to force a variation on the PID clip and not on its output directly arises because it must be "informed" of the constraint the controller set on SOI, since the anti-windup block can properly work without making an uncontrolled growth of the integral contribution.

- Regarding misfire, an analogous approach would have made the two protections to possibly conflict. This could happen because the stability region becomes narrower as load increases. In order to avoid such a behavior, the correction depending on the detection of poor combustions acts on the PID target. This solution makes the knock protection predominant. In details, the PID target is corrected taking into account the number of misfires or poor combustions within a predetermined buffer, as well as the occurring sequence (consecutive misfires trigger the correction even if the threshold percentage inside the buffer is not yet reached). The correction criterion is based on making MFB50 target advance by an additive contribution depending on the misfire percentage in the buffer. If this target protection intervenes iteratively in an "oscillatory way" in a determined operating condition, it means that the MFB50 target which has been set cannot be accomplished without losing efficiency and possibly falling into dangerous conditions. Misfire diagnosis is based on the observation of the delivered indicated torque, by comparing it with an expected value obtained as a function of engine speed and load.

The last block that needs to be discussed is the one governing the self-update of the base SOI LUT. It is based on a three-dimensional matrix, basically defined as the SOI base map where on the third dimension is set to obtain a circular SOI buffer for each operating point discretized in terms of speed and load. When the MFB50 is stable within a certain error band with respect to the target value, a single element of the described buffer is written and the feed forward SOI contribution is computed as the average of the buffer itself. The described algorithm is replicated

for each cylinder. Following figures shows how the closed loop controller behaves while MFB50 target steps are performed.
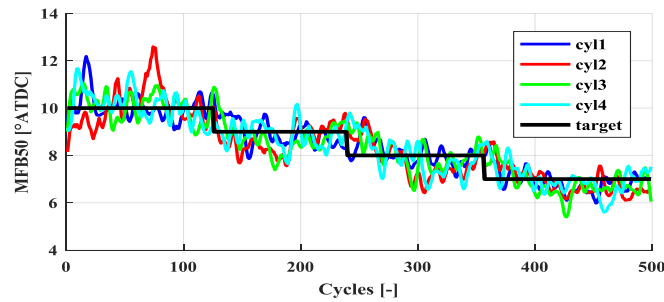
Figure 3.31: closed loop MFB50 controller example, target steps

Figure 3.31 illustrates how the closed loop controller is able to balance the four cylinders and make them follow the imposed target, the test has been carried on at 2000rpm, 5bar BMEP, 70% gasoline without any feed forward contribution variation. Figure 3.30 is aimed at showing the behavior of the discussed protection function the test is once again performed at 2000rpm, 5bar BMEP, 70% gasoline. As it can be noticed when poor combustions occur (MFB50 target 10 degATDC) the PID is fed with a corrected, more advanced, target. While knock protection is evident when MFB50 target drops to 6.5 degATDC, it makes the target impossible to be reached
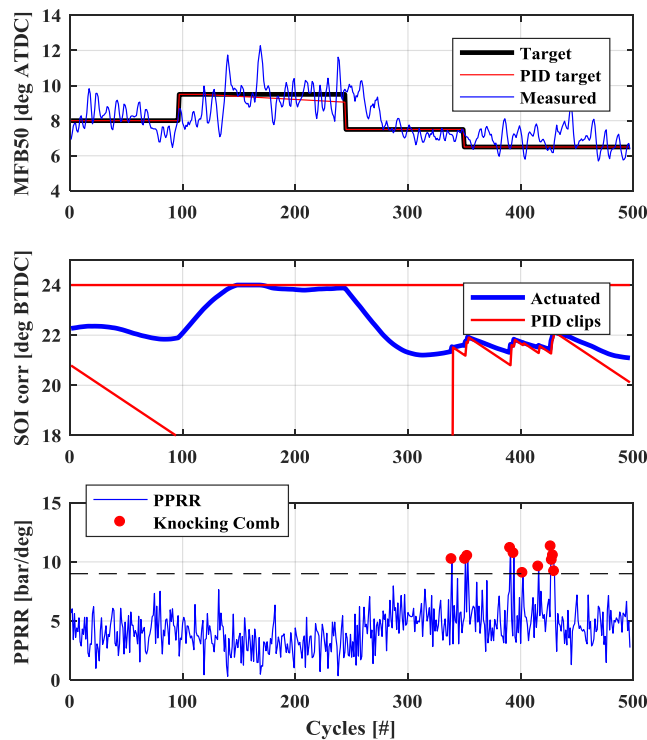
Figure 3.30: closed loop MFB50 controller example, PPRR and misfire protection functioning

83

as the saw-tooth profile keeps on limiting PID correction. In this test, PPRR is used to identify excessive rough combustions.

A closed loop control on MFB50 also helps to keep the engine stable in critical operating condition.

An example is reported below where the engine is maintained at 2000rpm 7bar BMEP 80% gasoline 0% EGR (Figure 3.32).
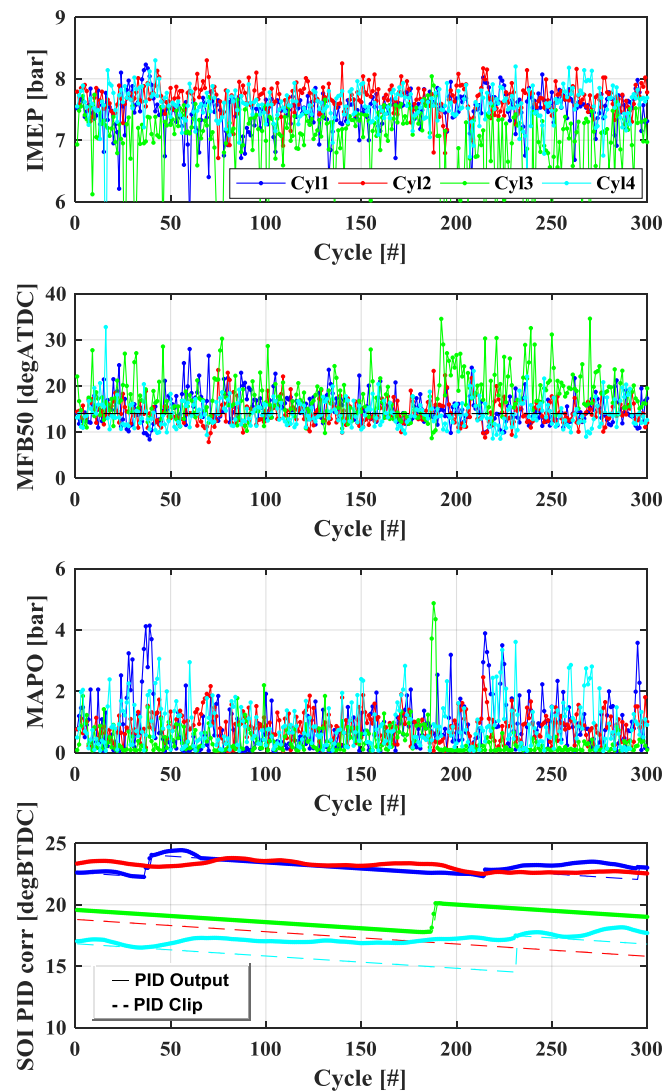
Figure 3.32: RCCI, 2000rpm 7bar BMEP, MFB50 control example

When load is increased to almost 7bar BMEP, the available operating range in terms of MFB50 is centered at 14 degATDC (which is far from optimal IMEP, Figure 3.33), but small fluctuations lead easily to either high PPRR or misfiring, thus the target MFB50 can be hardly accomplished. Cylinder three (green curve) suffers of a remarkably high instability.

In Figure 3.32, MAPO is reported, since it has been used as knock index (PPRR was not available real-time) to feed the controller protections. It is an acceptable choice because it includes a high pass filter, it is sensitive to pressure derivative indeed. Another key aspect is the differences in SOI values to meet the target MFB50 among the four cylinders: a possible interpretation can be made recalling that the air flow courses the intake manifold from cylinder four to cylinder one it can be assumed that cylinder one and two breathe a warmer charge with respect to cylinder four and three.
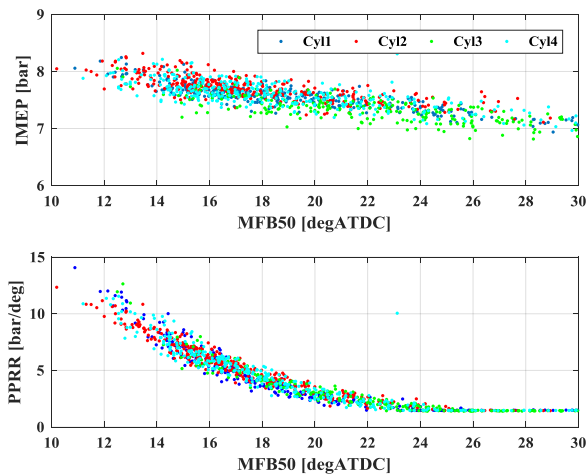
Figure 3.33: RCCI 2000rpm 7bar BMEP indicated indices

Figure 3.34 provides an example of which is the cyclic dispersion by showing the cylinder pressure curves related to cylinder one. On one side such a dispersion is present because target MFB50 equal to 14degATDC can be considered quite retarded and non-optimal for IMEP CoV as discussed below for this kind of combustion, at the same time though PPRR strongly limits the available operating range.
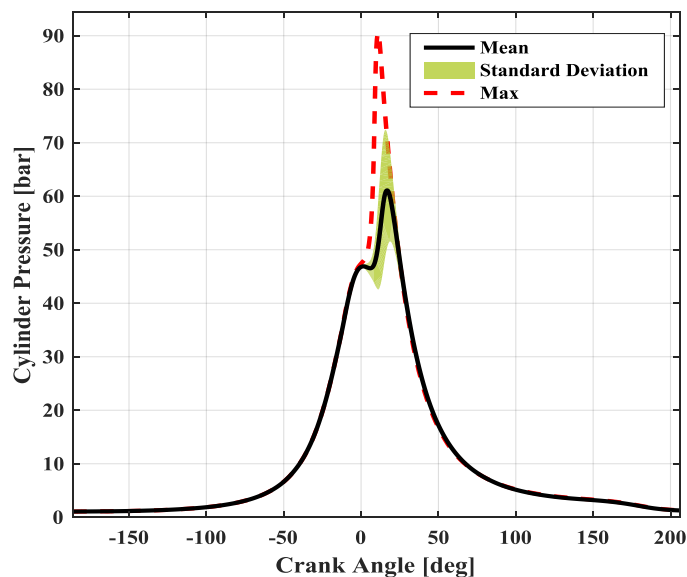
Figure 3.34: RCCI, 2000rpm 7bar BMEP, Cylinder pressure 1

Remote combustion sensing

Until now, the proposed control algorithm has been seen when fed by indicated data deriving from the measurement and processing chain linked to in-cylinder pressure measurement. However, it is known that this kind of technique is hardly applicable outside a research or development environment (i.e. production) because of the sensors cost. At the same time, it has been widely discussed that a closed loop combustion phase control would be very beneficial applied to RCCI combustion.

In this section some algorithms are treated whose goal is to obtain indices capable to describe combustion in a reasonably reliable manner starting from signal currently available on an engine, engine speed sensor, accelerometers, for instance.

The first approach which is dealt with, is the application of the same concept shown in section 2.2 for conventional diesel combustion: a frequency response function, describing how instantaneous indicated torque is translated into driveline speed oscillations, has been determined. Successively, harmonic content is correlated to the mean quantities of interest, namely mean indicated torque and MFB50 over a single engine cycle. To be more precise, as FRF, the same results obtained for conventional diesel combustion is used, since the torsional behavior of the crankshaft-brake system is independent of the combustion by which the engine is run. Coefficients, which allow obtaining mean indices, have been updated instead. Following figures describe how the estimation behaves in a 2000rpm 5bar BMEP, RCCI operating conditions at different SOI and EGR percentage. Every tested condition has been concatenated in the following plots.
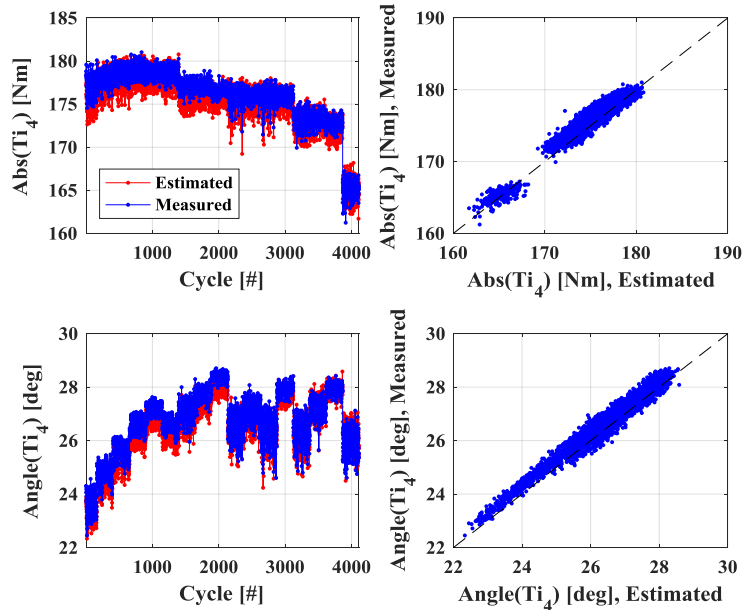
Figure 3.35: RCCI, Indicated torque 4th harmonic estimation

86
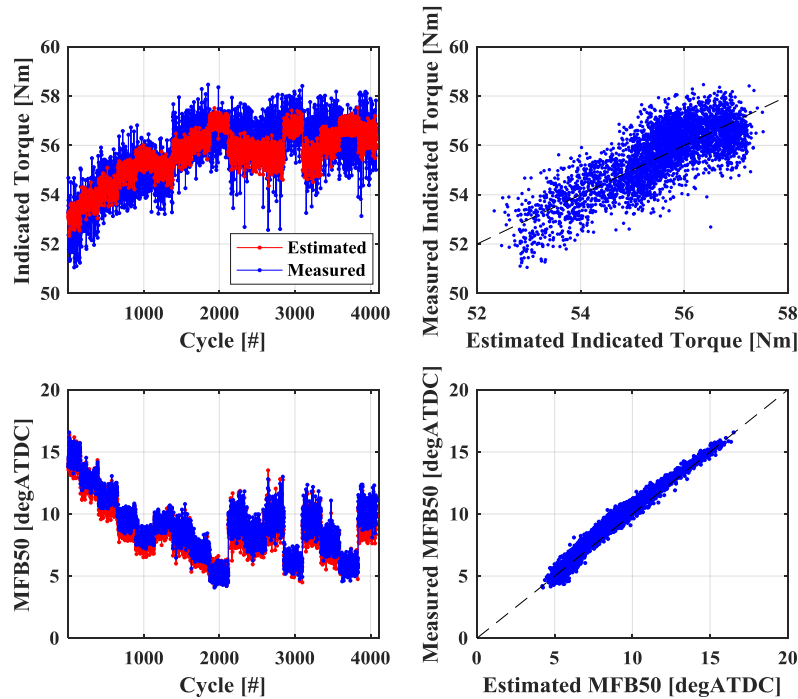
Figure 3.36: RCCI, Indicated torque and MFB50 estimation

Figure 3.36 illustrates that the goodness of the estimation can be considered acceptable: root mean square errors are 0.8Nm and 0.6deg for indicated torque and MFB50 respectively. Torque does not vary in a significant way actually (in this case the engine load has been kept constant), thus the estimation procedure must be tested on a wider load range. Here, a single load condition has been verified because the engine operating field is very limited in RCCI operating condition and 5bar BMEP is one of the key functioning conditions to be investigated. Nevertheless, it can be appreciated that the small variation in indicated torque can be detected.

MFB50 estimation, which is the one to be interested in, for combustion phase control purposes, is reasonably reliable, but a great issue is present due to the fact that this algorithm outputs the average MFB50 of the four cylinders in a single cycle. As it will be discussed in detail in the next section, RCCI combustion is strongly influenced by in cylinder thermal conditions, which are subjected to non-negligible heterogeneities among the four cylinders. This is the reason why the injection timing in is sensibly different for each cylinder (Figure 3.32). These things considered, it is widely more useful to obtain an independent MFB50 estimation.

The approach that is described below make use of an accelerometer signal whose processing is aimed at obtaining a cylinder by cylinder MFB50 estimation.

The basic idea is to evaluate accelerometer signal in time domain in order to obtain information on the instant at which pressure peak occurs.

First of all, it is worthy to highlight the used sensor and its installation. A PCB 352C33 accelerometer has been glued to engine head with epoxy resin between cylinders two and three, as shown in Figure 3.37.

Figure 3.37: Accelerometer installation

If the accelerometer signal is examined in a single engine cycle the signature of combustion clearly arises by applying a proper band-pass filter between 500 and 2300 Hz as depicted in Figure 3.38.
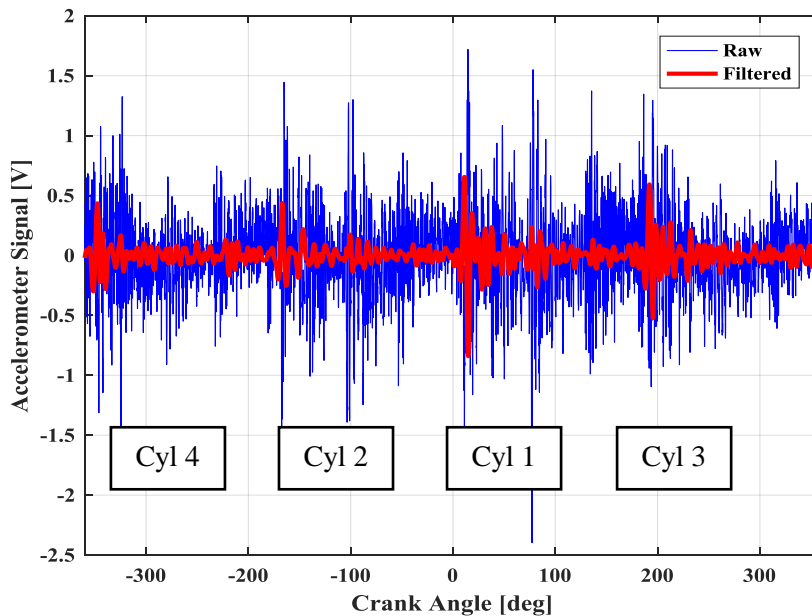
Figure 3.38: Accelerometer signal

Moving into a deeper analysis, it can be seen that by shifting the signal of a fixed time quantity (in the order of milliseconds tenth), representing the propagation delay of the waveform leaving

combustion chamber and reaching the sensor, it is very well correlated with the behavior of the in chamber pressure derivative (Figure 3.39). The value of such a delay has been learned for each cylinder by processing a training dataset and then it is set to a fixed value for all the results shown from now on.
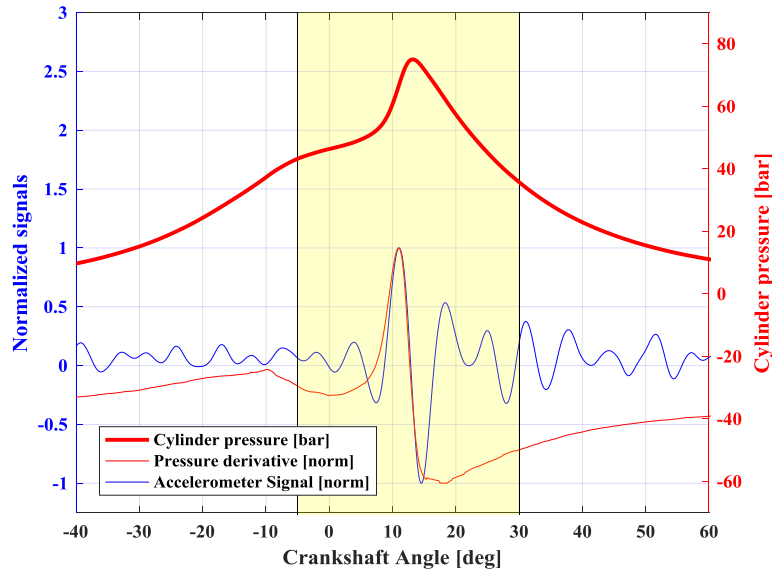
Figure 3.39: Correlation between in cylinder pressure derivative and accelerometer signal

An investigation window has to be set in order not to be influenced by irrelevant events from combustion analysis point of view. It has been imposed from -5 to 30degATDC in the illustrated example. Inside this window the peak acceleration is searched, and the successive zero-crossing represents the positon at which the pressure peak is reached. Finally, pressure peak position is converted into a value of MFB50 by a mapped correlation.

The entire procedure is schematized in Figure 3.40.
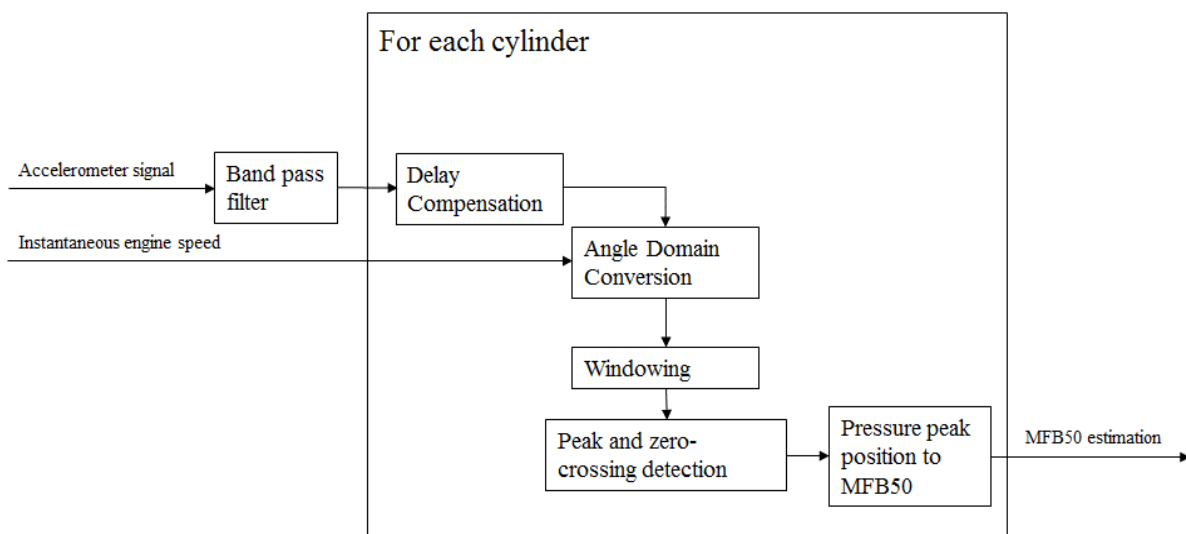
Figure 3.40: MFB50 estimation procedure by accelerometer signal processing

Results obtained for a 2000rpm 5bar BMEP operating condition, where a SOI sweep has been performed, are shown in Figure 3.41 in terms of pressure peak position estimation, while Figure 3.42 illustrates the correlation between pressure peak position and MFB50, which is mainly a offset.
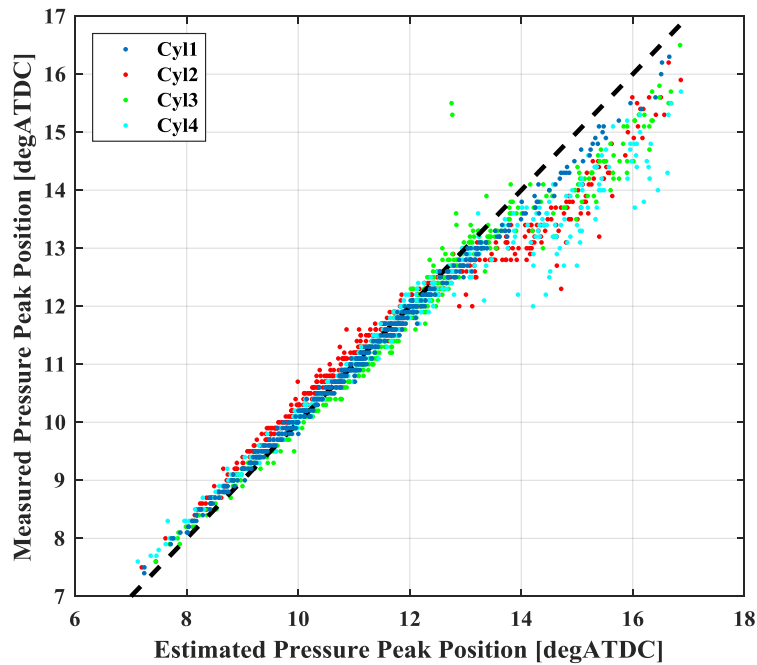
Figure 3.41: Pressure peak position estimation
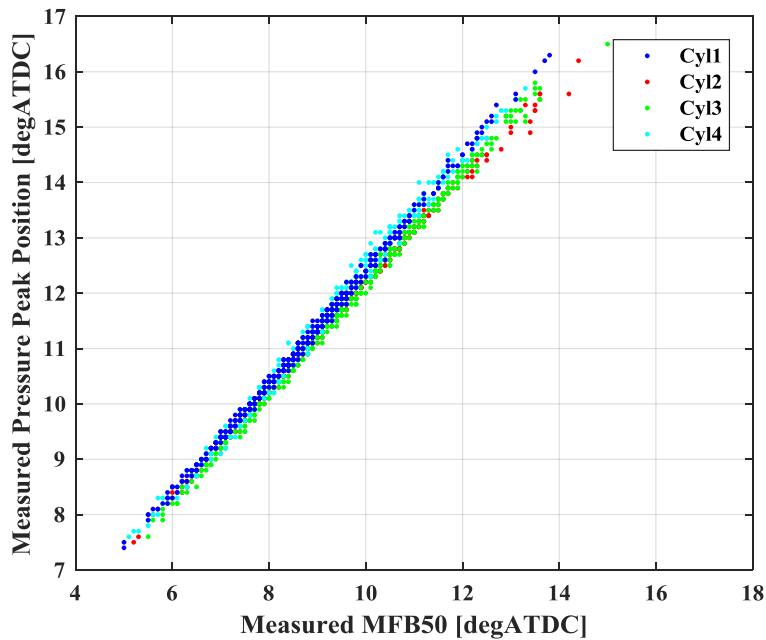
Figure 3.42: Correlation between MFB50 and pressure peak position

The estimation is to be considered reliable when MFB50 is close its optimal value (8degATDC) or more advanced, since in these conditions combustion is impulsive enough to produce a reliable

mark on accelerometer signal. If MFB50 is retarded, estimation becomes unprecise, but at the same time combustion is less efficient and proximal to misfire, those conditions have to be avoided indeed.

However, the MFB50 estimation procedure is not sufficient to completely feed the closed loop combustion controller because it needs some indices reflecting the knocking tendency and misfiring combustion as well.

Exploiting an accelerometer signal, the simplest processing to obtain information concerning knock or PPRR is to develop an integral index in determined frequency band and angular window. In particular, Figure 3.43 reports the correlations obtained between the accelerometer index and PPRR where the same filtering used for MFB50 estimation is used and a -15 - 5 deg window
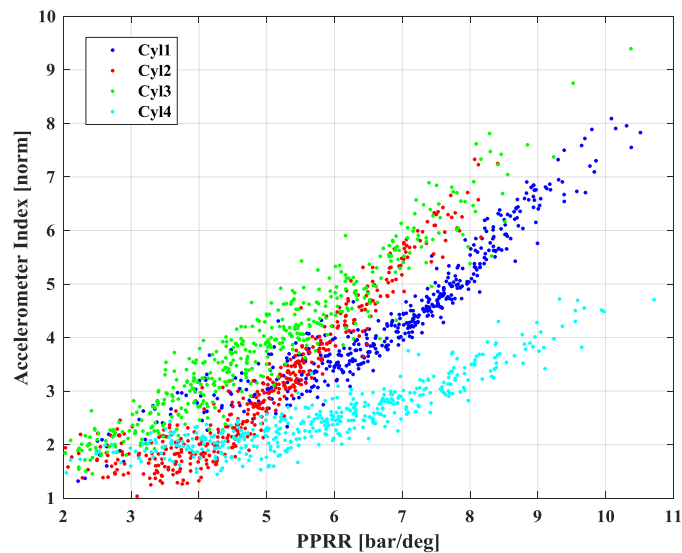
Figure 3.43: Accelerometer integral index

centered in the estimated pressure peak position is chosen. The frequency range is far from ordinary knock indices because as already discussed the most critical thing in this kind of combustion is the peak pressure rise rate: the example reported above concerning the 2000rpm 7bar BMEP operating condition shows how the MAPO values are relatively low but PPRR is quite aggressive. The dispersion seen between the several cylinders in Figure 3.43 is due to the accelerometer position: in fact, cylinder four and one imply a less sensitivity while the index behaves at its best for cylinder three. The nonlinear correlation present for low PPRR values can be explained with the surrounding noise.

The last thing to be taken into account to make the controller independent from in cylinder pressure sensor is the capability to identify weak combustions and misfires. Firstly, a modified approach involving engine speed fluctuations has been tested resembling the one used to determine mean indicated torque and MFB50. The modifications made, regard the window in

which the engine speed is analyzed, since a more restricted angular range, namely the one related to a single cylinder combustion (180 deg) is used to determine the FRF and evaluate torque produced by each cylinder. The comparison between the obtained individual torque and an expected one makes the combustion to be considered a misfire or a valid cycle.
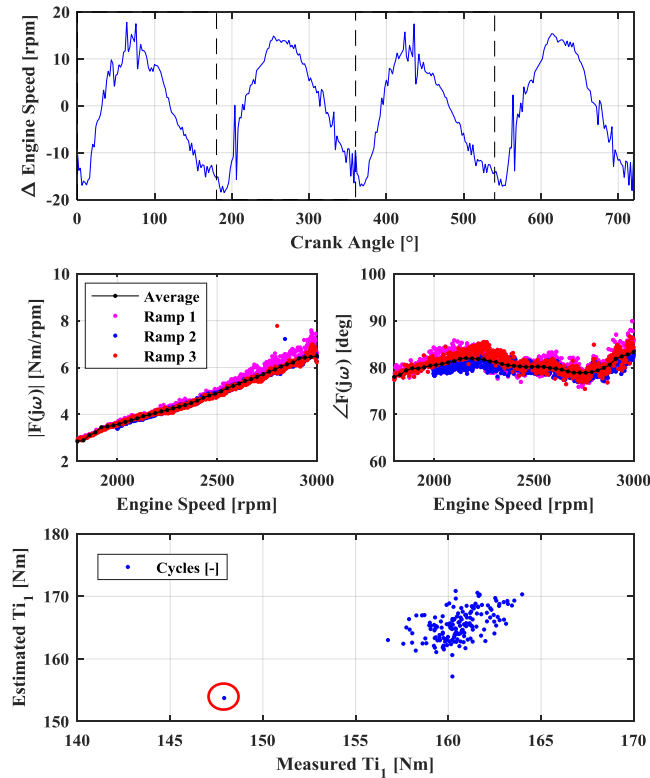
Figure 3.44: weak combustions identification example using engine speed signal

Figure 3.44, shows how the starting engine speed signal over an engine cycle is windowed to get the portion related to a single combustion stroke, then a FRF is used to move from the first harmonic of the windowed engine speed signal to the related torque harmonic (named $T_{i,1}$ in the figure). To determine the FRF the same approach shown in chapter 2.2 based on engine speed ramp at different loads is used as shown in the middle row. In the bottom plot it is clear how the critical weak combustion can be identified by observing the amplitude of the examined harmonic content.

This procedure has a precarious issue though, when a cylinder misses a combustion, it could influence the engine speed not only in the 180deg associated to its stroke, but also the neighbor combustion estimation.

For this reason, the weak combustions identification has been implemented as a threshold model based on an accelerometer index, similar to the one used to determine PPRR. This solution has an additional advantage because, if the integral index is low, the MFB50 estimation could easily

fail even if combustion delivers sufficient torque. Thus, avoiding inserting in MFB50 buffer every combustion which could make the estimation not reliable is a more robust (even if limiting) technique to feed the closed loop controller.

Every discussed algorithm has been implemented in the RCP system and linked to the closed loop controller previously illustrated.

Results are shown in following figures for a 2000rpm 5bar BMEP operating condition.
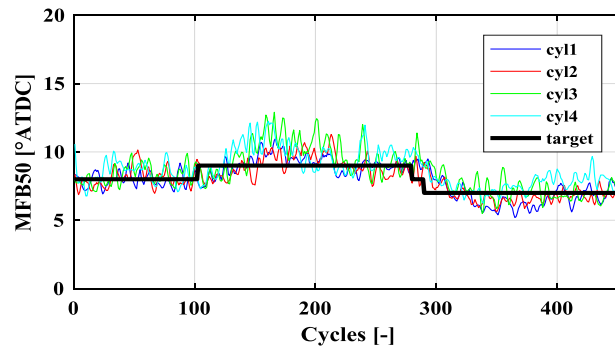
Figure 3.45: closed loop MFB50 controller example based on accelerometer estimation, target steps

Figure 3.45 proves how the four cylinders combustion phase is controlled with a single accelerometer, feed forward contribution is kept unchanged throughout the test.
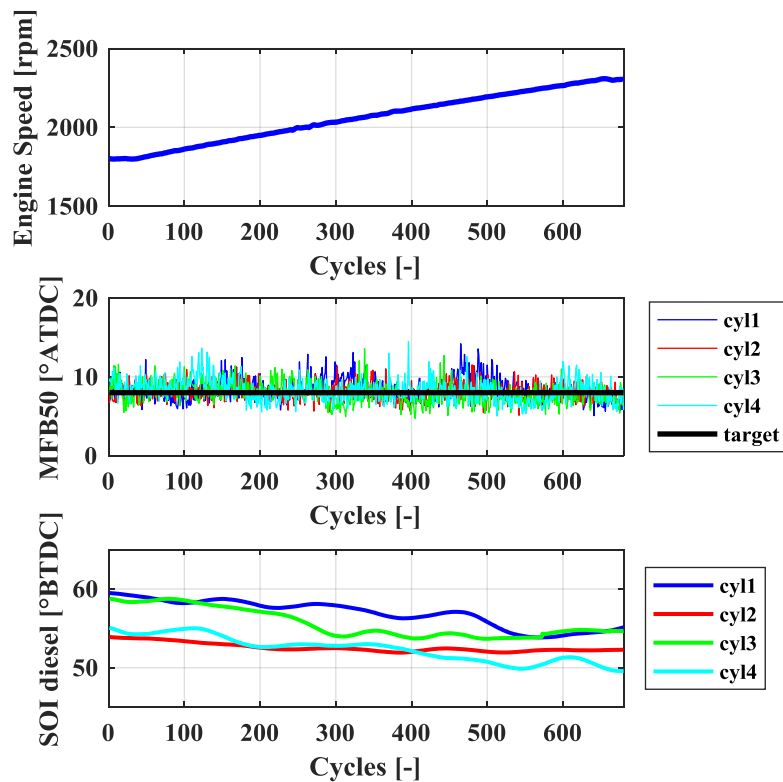
Figure 3.46: closed loop MFB50 controller example based on accelerometer estimation, engine speed ramp

93

Moreover, Figure 3.46, reports how the controller behaves in engine speed transient conditions, once again the feed forward contribution is kept constant to evaluate the performance of the controller.

Figure 3.47 reports the same test shown in Figure 3.30 but performed closing the loop on accelerometer estimations (the test has been carried on by controlling a cylinder using in-chamber pressure sensors, and another one with accelerometer). As it can be noticed the knocking events and the poor combustions are evaluated on the same integral index, when a poor combustion is detected the target is automatically advanced to prevent the controller to fall in a zone where the estimation fails (which is near to misfire). When high PPRR combustions occur, the protection impedes the PID regulator to bring the MFB50 to the set target.
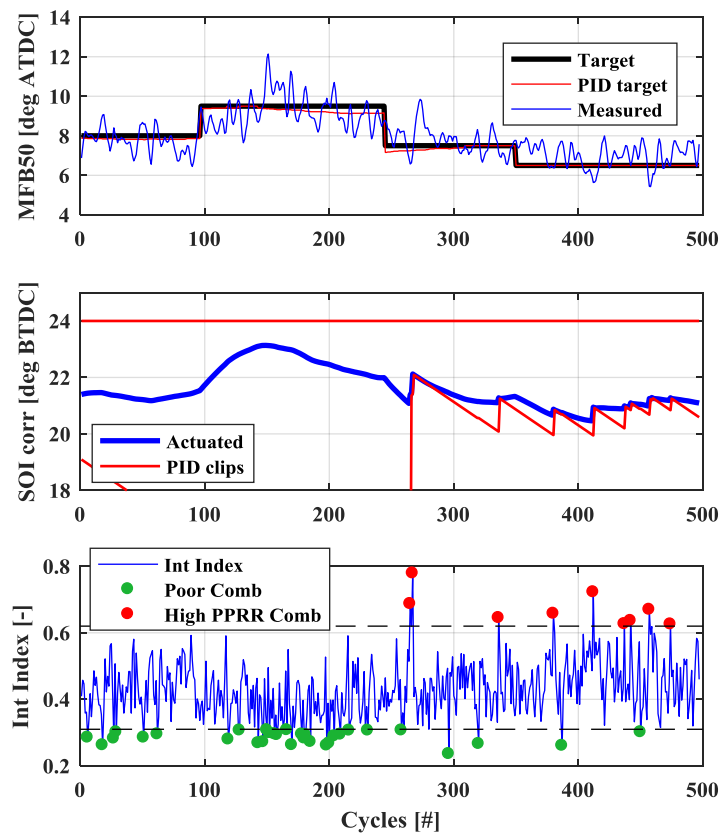
Figure 3.47: closed loop MFB50 controller example based on accelerometer estimation, PPRR and misfire protection functioning

In this section, methodologies to control RCCI combustion in hardly stable conditions have been presented which can be based either on in cylinder pressure measurement or on proper accelerometer signal processing. It is easy to realize that even if the discussed procedures are able to keep the engine stable, the whole control system cannot rely only on closed loop contributions because they do not act sufficiently fast on transients. The next section reports an analysis on the ignition mechanism aimed at providing accurate open loop values to the controller.

94

Heat release experimental analysis of ignition mechanism

The last section focused on RCCI combustion, reports an experimental analysis on the way heat is released when some key control parameters are varied. The ultimate goal is to provide a model-based feed forward contribution to the combustion phase controller in order to improve stability and better handle transient conditions by a reduced necessity to rely on the PID regulator.

The following data have been obtained by running the engine with CDC on three cylinders while the fourth one has been used as a "laboratory" cylinder to investigate combustion without risking engine operation instability (which has been guaranteed by the other three cylinders). Mutual interactions have been discouraged by keeping a null EGR rate and low boost levels.

Getting back to the initial investigation on RCCI combustion it has already discussed that MFB50 shows a dual behavior with respect to SOI variations, and it has been highlighted that the very sensible benefits can be achieved in the so-called "high ignition delay" region.
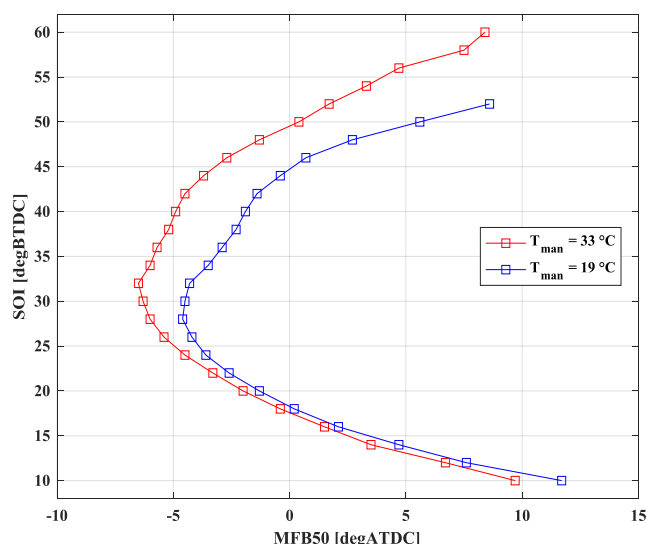
Figure 3.48: SOI vs MFB50 tendency sensitivity with respect to intake temperature

Figure 3.48 shows that in the region of interest a huge sensitivity to surrounding conditions is present (here intake temperature is varied by changing intercooler operation) which is one of the most relevant contribution to the necessity to correct the SOI base look-up table. The tests are conducted at 2000rpm by keeping constant the amount of fuel injected: 7.5mg/str gasoline, 3.3 mg/str diesel. Recalling that the stability region in terms of MFB50 is limited, it is clear how a base LUT corrected only by a PID can bring the engine to an undesired operating condition being either misfire or knock.

These are the motivations to the following analysis of ignition mechanism.

One of the most significant metrics on which combustion phase depends is the start of combustion (SOC). Examining RCCI heat release rate it can be observed that if SOI is maintained in the high ignition delay region a little amount of energy (named low temperature heat release, LTHR) is delivered before the main combustion occurs which is due to chemical reactions braking high reactivity fuel (mainly) hydrocarbon chains as literature explain [31,32]. If SOI is kept to lower values, than this kind of reactions are englobed in the main heat release as Figure 3.49 testify. The reported ROHRs are taken from the red curve in the previous figure and computed by subtracting to the standard ROHR calculation a reference curve obtained in cut-off conditions in order to limit distortions due to wall-heat losses and blow-by.
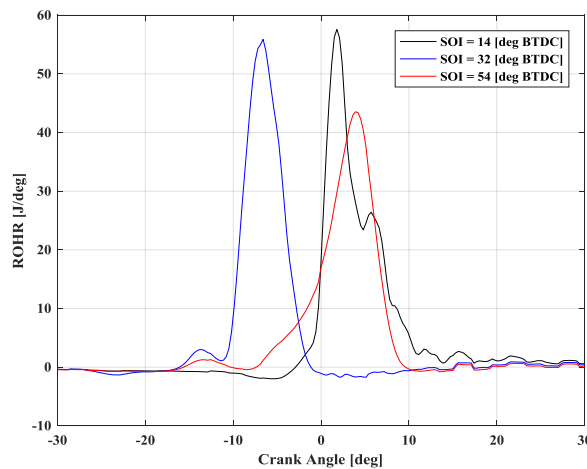
Figure 3.49: RCCI heat release rates at different SOI

If low temperature heat release SOC is compared to the high temperature one (Figure 3.50) it can be seen that the MFB50 start to behaves in the opposite way as soon as LTHR SOC stops to advance, and the two curves in Figure 3.50 begin to diverge. SOC is computed as the position at which a fixed amount of energy is released being in the order of Joule fraction for LTHR SOC and approximatively 25J for main heat release SOC.
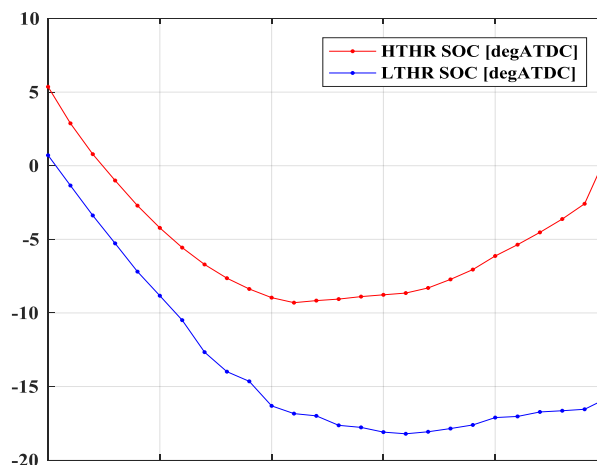
Figure 3.50: HTHR and LTHR SOC vs SOI

However, LTHR SOC (thus HTHR SOC) strongly depends on cylinder thermal conditions as well as on the mixture composition. To find this functionality, some tests have been performed where SOI has been kept fixed at significant values being 10degBTDC, 48degBTDC and 56degBTDC because representative of a low ignition delay zone, a high ignition delay zone and a near misfiring condition respectively. For each SOI examined a gasoline mass sweep has been performed. The whole procedure has been repeated for two levels of injected diesel.
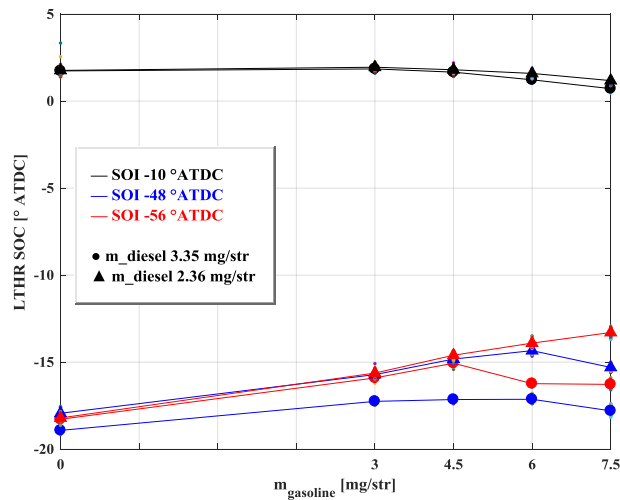
Figure 3.51: LTHR SOC vs injected gasoline mass

Figure 3.51 shows non-monotonic tendencies in LTHR SOC when SOI is maintained constant. These results can be interpreted as two contributions are present and influencing ignition delay:

- the first one is linked to the increasing amount of gasoline which, being a low reactivity fuel, tends to make combustion retard;
- the second one is the thermal state of trapped residual gases, since a higher exhaust temperature encourage a more advanced SOC in the next cycle.

Black curve does not show this dual-behavior because its SOI guarantees a sufficiently energetic combustion to make the second contribution prevail. The red and blue curves start from a near misfiring condition, so the first contribution is only present until at a certain point (amount of injected gasoline) combustion is able to self-sustain and a step to a more advanced SOC is done.

These tests have allowed to develop a simple model to express ignition delay, in particular what seems important is the in-cylinder temperature at the moment of the direct injection which has to take into account the intake charge temperature as well as the previous cycle residual gases.

Following expressions are used to determine the synthetic parameter describing cylinder thermal state.

$$T_{EVO} = \frac{p_{EVO}V_{EVO}}{Rm_{tot}} \qquad\qquad 3.1$$

$$V_{\%EGR} = \frac{V_{cc}\left(\frac{p_{exh}}{p_{man}}\right)^{\frac{1}{\gamma}}}{V_{cc} + V_d} \sim M_{\%EGR} \qquad\qquad 3.2$$

$$T_{IVC} = \frac{T_{man}m_{air} + T_{EVO}M_{\%EGR}m_{tot}}{m_{air} + M_{\%EGR}m_{tot}} \qquad\qquad 3.3$$

$$T_{SOI} = T_{IVC}\left(\frac{V_{IVC}}{V_{SOI}}\right)^{\gamma-1} \qquad\qquad 3.4$$

As it can be noticed temperature at SOI (T_{SOI}) is computed as the weighted average of intake temperature and residual gas temperature. If Figure 3.51 data are rearranged expressing the ignition delay in function of T_{SOI}, the diagrams shown below are obtained (Figure 3.52).
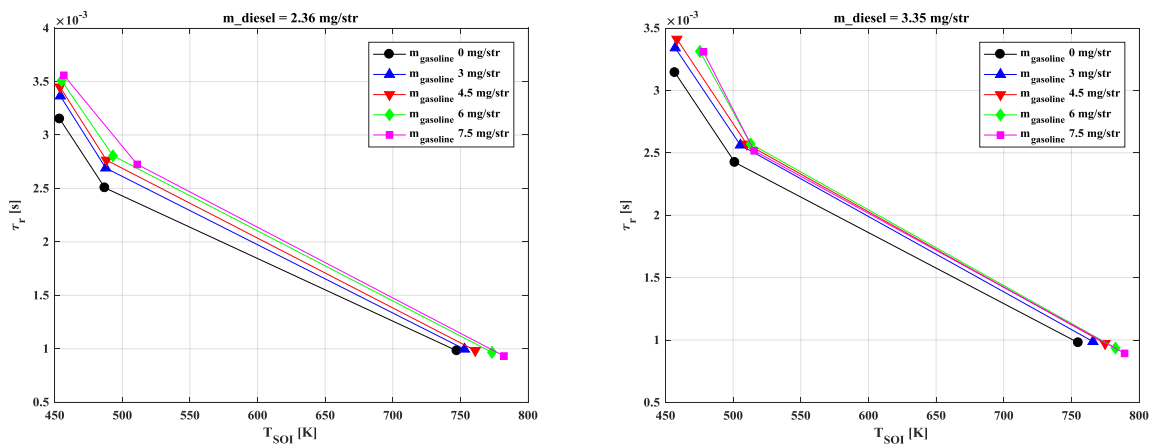
Figure 3.52: Ignition delay vs TSOI and gasoline percentage

Ignition delay can be thus assumed depending on T_{SOI} and gasoline percentage. Intuitively, these dependencies are not the ones uniquely affecting ignition delay, since every other factor whose impact is reflected on charge temperature (coolant temperature, oil temperature, cylinder walls temperature…) should be taken into account. However, the remarkable thing when dealing with RCCI, is that combustion is sensitive to its own history.

For sake of completeness, the data presented in Figure 3.48 are used to verify the consistency of the adopted model formulation. In Figure 3.53, they are inserted in the previously discussed dataset in order to show the complete trend the ignition delay undergoes while temperature at SOI changes. The curves at different manifold temperature are overlapped when τ_r is displayed against T_{SOI}.
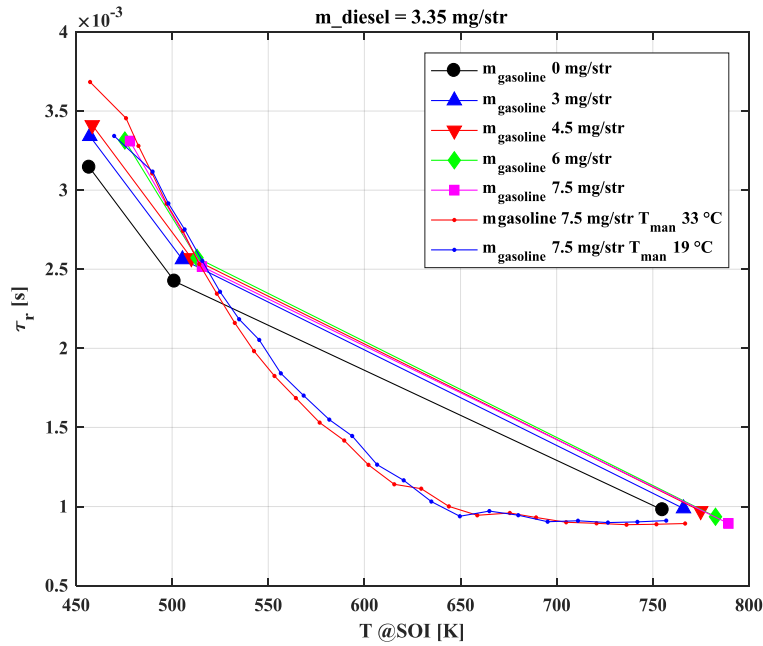
Figure 3.53: Ignition delay vs TSOI and gasoline percentage (2)

The Ignition delay assumes an important role, as it represents how diesel is dispersed in the combustion chamber (certainly influencing combustion phase): the more ignition delay is present the more diesel can be considered homogeneous. From combustion control point of view, this tendency can be used to correct injection timing when environmental conditions are different from the ones to whom the base SOI look-up table is referred to. These things considered, the SOI correction has to be based on the target ignition delay obtaining both a reasonable start of combustion and a mixture homogeneity making combustion velocity to be in a valid range. Additional corrections to center precisely the combustion phase can be performed by the closed loop controller.

The following tests show how a correction based on T_{SOI} re-centering helps controlling combustion phase.

Figure 3.54 reports a test in steady state conditions at 2000rpm 70% gasoline, where the intake temperature has been kept 10K cooler with respect to temperature used for base calibrations. It can be seen (red line) that if no feed-forward correction is made, the PID regulator has to perform a great effort to keep combustion stable: when it is switched-off, combustion almost drops to zero IMEP values. If feed forward contribution is corrected, taking into account T_{SOI} the PID regulator makes only slight adjustment to SOI.

This example is particularly "fortunate" as the T$_{SOI}$ based correction brings the combustion to its target phase. This fact is not rigorously guaranteed by the discussed assumptions, but the objective here is to demonstrate that taking into account an index describing in-cylinder thermal conditions is a great step in order to properly control MFB50 and improve combustion stability characteristics.
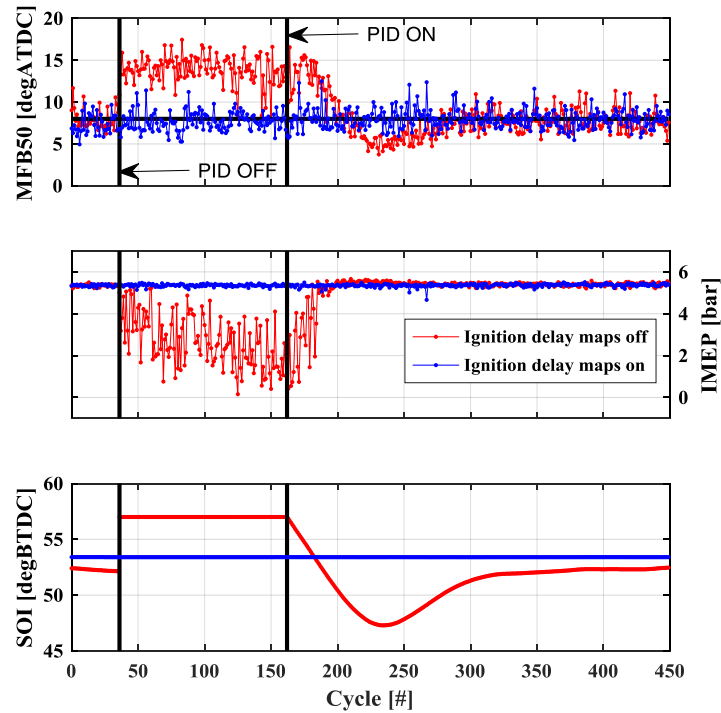
Figure 3.54: Ignition delay maps based SOI correction example

In Figure 3.54 it can be also noticed the influence combustion has on the successive cycles, namely the one modeled by equations 3.1 to 3.4: observing the red line, when SOI is set to values far from optimal by switching off the PID regulator, combustion tends to misfire gradually, since cylinder thermal state progressively cool down.

CONCLUSIONS

The present thesis work is focused on experimentation in the field of compression-ignited engines. Several aspects have been dealt with concerning conventional diesel combustion, which in different ways try to offer points of interest in managing some crucial issues, typical of how a modern diesel engine combustion is controlled. On the other hand, RCCI injection strategy has been investigated to test which advantages it could demonstrate over the ordinary diesel combustion and which kind algorithms it needs to be run without the arisen of potentially threatening events for the engine itself.

Noise handling through non-ordinary calibrations and closed loop control has been presented, demonstrating that some advantages could be obtained in pollutant emissions, efficiency and noise radiation itself. Then, some remote combustion sensing algorithms based on engine speed signal processing, already developed through years, have been used to feed a closed loop combustion phase and torque controller which in some applications is certainly a way to accomplish specific emissions and efficiency targets because of their strong link with the identified combustion indices. Finally, a study on how nitrogen oxides are linked to the rate of heat release has been illustrated, because managing this quantity is relatively easy, thus, understanding physics on which NOx formation mechanisms are based can help avoiding black-box calibrations which are time consuming and hardly reliable when surrounding conditions are changed.

Concerning the study on low temperature combustions, reactivity-controlled compression ignition combustion has been analyzed, since, theoretically speaking it is the one providing the more extended operating range because of the additional control parameter, being the gasoline to diesel ratio. The benefits of adopting a homogenous combustion on a compression-ignited engine have been observed, but the limited stability has made the treatment of RCCI combustion to be more focused on finding a way to control this kind of combustion to obtain better performing operating conditions and cylinders balancing. Two ways to perform closed loop combustion control have

been presented, one of which has the particularity to avoid the usage of in cylinder pressure measurements. Finally, some considerations have been carried on mixture ignition mechanism aimed at overcoming the issue of the over-sensitivity of combustion to the surrounding conditions.

NOMENCLATURE

A/F	[-]	air fuel ratio
AirQ:	[mg/str]	fresh air mass flow rate
APmax:	[degATDC]	angle at which the peak pressure is detected
ATDC:		after top dead center
BMEP:	[bar]	brake mean effective pressure
BSFC:	[g/kWh]	brake specific fuel consumption
BTDC:		before top dead center
CAN:		controller area network
CDC:		conventional diesel combustion
CHR:	[J]	cumulative heat release
CI:		compression – ignition
COV:	[%]	coefficient of variation
DOE:		design of experiment
DPF:		diesel particulate filter
DT:	[us]	dwell time
ECU:		electronic control unit
EGR:		exhaust gas recirculation
EOC:	[degCA]	end of combustion
ET:	[us]	energizing time
F(jω)	[Nm/rpm]	driveline speed to torque transfer function
FPGA:		field programmable gate array
FRF:		frequency response function
FSN:	[-]	filter smoke number
HC:		unburnt hydrocarbon
HTHR:		high temperature heat release
IMEP:	[bar]	indicated mean effective pressure

ISFC:	[g/kWh]	indicated specific fuel consumption
LHV:	[J/kg]	lower heating value
LTC:		low temperature combustion
LTHR:		low temperature heat release
LUT:		look-up table
$M_{\%EGR}$:	[-]	mass percentage of trapped residual gases
MAF:		mass air flow
MAPO:	[bar]	maximum amplitude pressure oscillation
MFB50:	[degATDC]	angular position at which the 50% of energy is delivered
NHRR:	[J/degCA]	net heat release rate
NOx:		nitrogen oxides
NOx_m:	[mg]	nitrogen oxides mass
PID:		proportional-integral-derivative regulator
PM:		particulate matter
PPRR:	[bar/degCA]	peak pressure rise rate
R:	[J/(kg K)]	specific gas constant
RCCI:		reactivity controlled compression ignition
RCP:		rapid control prototyping
RMSE:		root mean square error
ROHR:	[J/degCA]	rate of heat release
RON:	[-]	research octane number
RT:		real-time (PC)
SCR:		selective catalytic reductor
SDU:		smart driving unit
SI:		spark – ignition
SOC:	[degCA]	start of combustion
SOI:	[degBTDC]	start of injection
SW:		software
UEGO:		universal exhaust gas oxygen sensor
T_{ad}:	[K]	adiabatic flame temperature
T_{eng}:	[Nm]	torque applied to the engine
T_{EVO}:	[K]	in-cylinder temperature at exhaust valve opening
T_{ind}:	[Nm]	indicated torque
$T_{ind\ est}$:	[Nm]	estimated indicated torque
$T_{ind\ est,i}$	[Nm]	estimated i-th indicated torque harmonic
$T_{ind,i}$:	[Nm]	i-th indicated torque harmonic
$T_{ind\ ref,i}$:	[Nm]	i-th indicated torque harmonic in reference condition

T_{IVC}:	[K]	in-cylinder temperature at intake valve closing
T_{load}:	[Nm]	torque applied to load
T_{man}:	[K]	intake temperature
T_{mean}:	[K]	mean in-chamber temperature
T_{SOI}:	[K]	in-cylinder temperature at SOI
TBCS:		test bed control system
TDC		top dead center
TVA:		throttle valve actuator
V:	[m^3]	angle resolved combustion chamber volume
$V_{\%EGR}$:	[-]	volume percentage of trapped residual gases
V_{cc}:	[m^3]	combustion chamber volume at TDC
V_d:	[m^3]	cylinder displacement
V_{EVO}:	[m^3]	cylinder volume at exhaust valve opening
V_{IVC}:	[m^3]	cylinder volume at intake valve closing
V_{SOI}:	[m^3]	cylinder volume at SOI
VGT:		variable geometry turbine
WI:		water injection

m_{diesel}:	[mg/str]	diesel injected mass
m_{egr}:	[mg/str]	EGR mass
$m_{gasoline}$:	[mg/str]	gasoline injected mass
m_{tot}:	[mg/str]	total cylinder trapped mass
n:	[rpm]	engine speed
p:	[Pa]	angle resolved in-chamber pressure
p_{EVO}:	[Pa]	in-cylinder pressure at exhaust valve opening
p_{exh}:	[Pa]	exhaust pressure
p_{IVC}:	[Pa]	in-cylinder pressure at intake valve closing
p_{man}:	[Pa]	intake pressure

α:	[degCA]	crank angle coordinate
γ:	[-]	specific heat ratio
η_v:	[-]	volumetric efficiency
θ_{eng}:	[degCA]	crankshaft angular position
$\dot{\theta}_{eng}$:	[degCA/s]	crankshaft angular position derivative
$\ddot{\theta}_{eng}$:	[degCA/s^2]	crankshaft angular position 2nd order derivative
$\dot{\theta}_{eng,i}$:	[degCA/s]	crankshaft angular speed i-th harmonic
θ_{load}:	[degCA]	engine load angular position

$\dot{\theta}_{load}$:	[degCA/s]	engine load angular position derivative
$\ddot{\theta}_{load}$:	[degCA/s^2]	engine load angular position 2nd order derivative
λ:	[-]	dimensionless air fuel ratio
τ_r:	[s]	ignition delay
ω:	[1/s]	pulsation

REFERENCES

1. Dürnholz, M., Endres, H., and Frisse, P., "Preinjection A Measure to Optimize the Emission Behavior of DI-Diesel Engine," SAE Technical Paper 940674, 1994, doi:10.4271/940674.

2. Hanho Yun, Reitz Rolf D., "Combustion Optimization in the Low-Temperature Diesel Combustion Regime," *Int. Journal of Engine Research*, 2005.

3. Carlucci, P., Ficarella, A., and Laforgia, D., "Study of the Influence of the Injection Parameters on Combustion Noise in a Common Rail Diesel Engine Using ANOVA and Neural Networks," SAE Technical Paper 2001-01-2011, 2001, doi:10.4271/2001-01-2011.

4. Busch, S., Zha, K., Miles, P., Warey, A., "Experimental and Numerical Investigations of Close-Coupled Pilot Injections to Reduce Combustion Noise in a Small-Bore Diesel Engine," SAE Int. J. Engines 8(2):660–678, 2015, doi:10.4271/2015-01-0796.

5. Shahlari, A., Hocking, C., Kurtz, E., and Ghandhi, J., "Comparison of Compression Ignition Engine Noise Metrics in Low-Temperature Combustion Regimes," SAE Int. J. Engines 6(1):541–552, 2013, doi:10.4271/2013-01-1659.

6. Schnorbus, T., Pischinger, S., Körfer, T., Lamping, M. et al., "Diesel Combustion Control with Closed-Loop Control of the Injection Strategy," SAE Technical Paper 2008-01-0651, 2008, doi:10.4271/2008-01-0651.

7. Jörg, C., Schnorbus, T., Jarvis, S., Neaves, B. et al., "Feedforward Control Approach for Digital Combustion Rate Shaping Realizing Predefined Combustion Processes," SAE Int. J. Engines 8(3):1041-1054, 2015, doi:10.4271/2015-01-0876

8. Sellerbeck, P., Nettelbeck, C., Heinrichs, R., and Abels, T., "Improving Diesel Sound Quality on Engine Level and Vehicle Level - A Holistic Approach," SAE Technical Paper 2007-01-2372, 2007, doi:10.4271/2007-01-2372.

9. Iida, K., Akishino, K., Kido, K., IMEP Estimation from Instantaneous Crankshaft Torque Variation, SAE Technical Paper 900617.

10. J. J. Moskwa, W. Wang, D. J. Bucheger, A New Methodology for Engine Diagnostics and Control Utilizing "Synthetic" Engine Variables: Theoretical and Experimental Results, DSC-Vol. 64, Proceedings of the ASME, Dynamic Systems and Control Division, ASME 1998.

11. Ponti, F., Indicated Torque Estimation Using a Torsional Behavior Model of the Engine, SAE Powertrain & Fuel Systems Conference & Exhibition, Paper 2005-01-3761, San Antonio, Texas October 2005.

12. Ravaglioli, Vittorio & Ponti, Fabrizio & Stola, Federico. (2011). Torsional Analysis of Different Powertrain Configurations for Torque and Combustion Phase Evaluation. 10.4271/2011-01-1544.

13. Ponti, Fabrizio & Ravaglioli, Vittorio & Moro, Davide & Serra, Gabriele. (2010). Common Rail Multi-Jet Diesel Engine Combustion Development Investigation for MFB50 On-board Estimation. SAE Technical Papers. 10.4271/2010-01-2211.

14. Ponti, F., Ravaglioli, V., Serra, G., and Stola, F., "Instantaneous Engine Speed Measurement and Processing for MFB50 Evaluation," SAE Int. J. Engines 2(2):235-244, 2010, doi:10.4271/2009-01-2747.

15. Quérel, C., Grondin, O., and Letellier, C., "State of the Art and Analysis of Control Oriented NOx Models," SAE Technical Paper 2012-01-0723, 2012, https://doi.org/10.4271/2012-01-0723.

16. Kihas, D. and Uchanski, M., "Engine-Out NOx Models for on-ECU Implementation: A Brief Overview," SAE Technical Paper 2015-01-1638, 2015, doi:10.4271/2015-01-1638.

17. Arrègle, J., López, J., Guardiola, C., and Monin, C., "Sensitivity Study of a NOx Estimation Model for On-Board Applications," SAE Technical Paper 2008-01-0640, 2008, https://doi.org/10.4271/2008-01-0640.

18. C. Guardiola, J. Martín, B. Pla, P. Bares, Cycle by cycle NOx model for diesel engine control, Applied Thermal Engineering, Volume 110, 2017, Pages 1011-1020.

19. C. Guardiola, J.J. López, J. Martín, D. García-Sarmiento, Semiempirical in-cylinder pressure based model for NOX prediction oriented to control applications, Applied Thermal Engineering, Volume 31, Issue 16, 2011, Pages 3275-3286.

20. Carlucci, A., Benegiamo, M., Camporeale, S., and Ingrosso, D., "Improvement of the Control-Oriented Model for the Engine-Out NOX Estimation Based on In-Cylinder Pressure Measurement," SAE Technical Paper 2017-24-0130, 2017, doi:10.4271/2017-24-0130.

21. Guardiola, C., Pla, B., Blanco-Rodriguez, D., and Bares, P., "Cycle by Cycle Trapped Mass Estimation for Diagnosis and Control," SAE Int. J. Engines 7(3):2014, doi:10.4271/2014-01-1702.

22. Scott J Curran, Reed M Hanson, Robert M Wagner, "Reactivity controlled compression ignition combustion on a multi-cylinder light-duty diesel engine", International Journal of Engine Research, Vol 13, Issue 3, pp. 216 – 225, First published date: April-26-2012.

23. Gross, C. and Reitz, R., "Investigation of Steady-State RCCI Operation in a Light-Duty Multi-Cylinder Engine Using "Dieseline"," SAE Technical Paper 2017-01-0761, 2017, doi:10.4271/2017-01-0761.

24. Curran, S., Hanson, R., Wagner, R., and Reitz, R., "Efficiency and Emissions Mapping of RCCI in a Light-Duty Diesel Engine," SAE Technical Paper 2013-01-0289, 2013, doi:10.4271/2013-01-0289.

25. S L Kokjohn, R M Hanson, D ASplitter, R D Reitz, "Fuel reactivity controlled compression ignition (RCCI): a pathway to controlled high-efficiency clean combustion", International Journal of Engine Research, Vol 12, Issue 3, pp. 209 – 226, First published date: June-22-2011.

26. DelVescovo, D., Kokjohn, S., and Reitz, R., "The Effects of Charge Preparation, Fuel Stratification, and Premixed Fuel Chemistry on Reactivity Controlled Compression Ignition (RCCI) Combustion," SAE Int. J. Engines10(4):2017, doi:10.4271/2017-01-0773.

27. Wu Y, Hanson R, Reitz RD. "Investigation of Combustion Phasing Control Strategy During Reactivity Controlled Compression Ignition (RCCI) Multicylinder Engine Load Transitions". ASME. J. Eng. Gas Turbines Power. 2014;136(9):091511-091511-10.

28. Arnone, L., Boni, M., Manelli, S., Chiavola, O. et al., "Block Vibration Measurements for Combustion Diagnosis in Multi-Cylinder Common Rail Diesel Engine," SAE Technical Paper 2009-01-0646, 2009, doi:10.4271/2009-01-0646.

29. Andrea Businaro, Nicolò Cavina, Enrico Corti, Giorgio Mancini, Davide Moro, Fabrizio Ponti, Vittorio Ravaglioli, Accelerometer Based Methodology for Combustion Parameters Estimation, In Energy Procedia, Volume 81, 2015, Pages 950-959, ISSN 1876-6102.

30. Azzoni, P.M., Moro, D., Porceddu-Cilione, C.M., Rizzoni, G., "Misfire detection in a high-performance engine by the principal component analysis approach", 1996, SAE Technical Paper 960622, DOI: 10.4271/960622.

31. Mark P.B. Musculus, Paul C. Miles, Lyle M. Pickett, Conceptual models for partially premixed low-temperature diesel combustion, Progress in Energy and Combustion Science, Volume 39, Issues 2–3, 2013, Pages 246-283, ISSN 0360-1285, https://doi.org/10.1016/j.pecs.2012.09.001. (http://www.sciencedirect.com/science/article/pii/S0360128512000548) Keywords: Diesel engine; Emissions; Low-temperature combustion; Optical diagnostics; Conceptual model

32. Samveg Saxena, Iván D. Bedoya, Fundamental phenomena affecting low temperature combustion and HCCI engines, high load limits and strategies for extending these limits, Progress in Energy and Combustion Science, Volume 39, Issue 5, 2013, Pages 457-488, ISSN 0360-1285, https://doi.org/10.1016/j.pecs.2013.05.002. (http://www.sciencedirect.com/science/article/pii/S0360128513000257) Keywords: Homogeneous charge compression ignition; Low temperature combustion; High load; Power output; Energy conversion; Spark-assisted compression ignition

ACKNOWLEDGMENTS

Three years have almost passed since the moment I received the test bed keys, when I was still a bit confused on the differences between a CAN database (.DBC) and a BNC cable. The PhD experience has allowed me to develop an incisive approach in analyzing data and writing code, as well as a global vision on experimentation issues (days spent tightening bolts and sensors have contributed).

For these reasons, I would like to thank research group bosses: professors Ponti, Corti, Moro and Cavina.

My special gratitude to Ing. Vittorio Ravaglioli who has been both a "source of knowledge" and a good beer-mate.

Every colleague must be mentioned here, since a very desirable working environment has been present for all the time I have spent in the lab: Ing. Michele Taccioli (who's shared nights at the office trying to finish the thesis work within the upload deadline...... an hour left), Ing. Stefano Mini, Ing. Marco Cangini, Ing. Marco Abbondanza, Ing. Andrea Businaro, Ing. Francesco Ranuzzi.

I also make recommendations to Ing. Giacomo Silvagni, who should keep the tireless multijet engine alive for a long time.

Finally, I have to thank laboratory technicians for their patience (ironic content).

Leaving the work context, I certainly thank my family for every possible kind of support.

I express huge gratitude to Cecilia, who has definitely improved my existence (hope it is mutual influence).

Last but not least, I must thank every friend which I have shared time (and many dinners) with: Nicola, Elia, Monica, Giorgia, Gianluca, Ilaria and many other I won't mention for conciseness.